U.S. DEPARTMENT OF COMMERCE
National Technical Information Service

PB-252 835

Numerical Models of Lake Currents

Case Western Reserve Univ.

Prepared For
Environmental Research Lab.

April 1976

147044

PB 252 835

EPA-600/3-76-020
April 1976

Ecological Research Series

NUMERICAL MODELS OF LAKE CURRENTS

REPRODUCED BY
NATIONAL TECHNICAL
INFORMATION SERVICE
U. S. DEPARTMENT OF COMMERCE
SPRINGFIELD, VA. 22161

Environmental Research Laboratory
Office of Research and Development
U.S. Environmental Protection Agency
Duluth, Minnesota 55804

KEEP UP TO DATE

Between the time you ordered this report—which is only one of the hundreds of thousands in the NTIS information collection available to you—and the time you are reading this message, several *new* reports relevant to your interests probably have entered the collection.

Subscribe to the **Weekly Government Abstracts** series that will bring you summaries of new reports *as soon as they are received by NTIS* from the originators of the research. The WGA's are an NTIS weekly newsletter service covering the most recent research findings in 25 areas of industrial, technological, and sociological interest—invaluable information for executives and professionals who must keep up to date.

The executive and professional information service provided by NTIS in the **Weekly Government Abstracts** newsletters will give you thorough and comprehensive coverage of government-conducted or sponsored research activities. And you'll get this important information within two weeks of the time it's released by originating agencies.

WGA newsletters are computer produced and electronically photocomposed to slash the time gap between the release of a report and its availability. You can learn about technical innovations immediately—and use them in the most meaningful and productive ways possible for your organization. Please request NTIS-PR-205/PCW for more information.

The weekly newsletter series will keep you current. But *learn what you have missed in the past* by ordering a computer **NTISearch** of all the research reports in your area of interest, dating as far back as 1964, if you wish. Please request NTIS-PR-186/PCN for more information.

WRITE: Managing Editor
5285 Port Royal Road
Springfield, VA 22161

Keep Up To Date With SRIM

SRIM (Selected Research in Microfiche) provides you with regular, automatic distribution of the complete texts of NTIS research reports *only* in the subject areas you select. SRIM covers almost all Government research reports by subject area and/or the originating Federal or local government agency. You may subscribe by any category or subcategory of our WGA **(Weekly Government Abstracts)** or **Government Reports Announcements and Index** categories, or to the reports issued by a particular agency such as the Department of Defense, Federal Energy Administration, or Environmental Protection Agency. Other options that will give you greater selectivity are available on request.

The cost of SRIM service is only 45¢ domestic (60¢ foreign) for each complete microfiched report. Your SRIM service begins as soon as your order is received and processed and you will receive biweekly shipments thereafter. If you wish, your service will be backdated to furnish you microfiche of reports issued earlier.

Because of contractual arrangements with several Special Technology Groups, not all NTIS reports are distributed in the SRIM program. You will receive a notice in your microfiche shipments identifying the exceptionally priced reports not available through SRIM.

A deposit account with NTIS is required before this service can be initiated. If you have specific questions concerning this service, please call (703) 451-1558, or write NTIS, attention SRIM Product Manager.

This information product distributed by

NTIS U.S. DEPARTMENT OF COMMERCE
National Technical Information Service
5285 Port Royal Road
Springfield, Virginia 22161

TECHNICAL REPORT DATA
(Please read Instructions on the reverse before completing)

1. REPORT NO. EPA-600/3-76-020	2.	3. RECIPIENT'S ACCESSION NO.
4. TITLE AND SUBTITLE NUMERICAL MODELS OF LAKE CURRENTS		5. REPORT DATE April 1976 (Issuing Date) 6. PERFORMING ORGANIZATION CODE
7. AUTHOR(S) Wilbert Lick		8. PERFORMING ORGANIZATION REPORT NO.
9. PERFORMING ORGANIZATION NAME AND ADDRESS Department of Earth Sciences Case Western Reserve University 2040 Adelbert Road Cleveland, Ohio 44106		10. PROGRAM ELEMENT NO. 1BA026 11. CONTRACT/GRANT NO. R802359
12. SPONSORING AGENCY NAME AND ADDRESS Environmental Research Laboratory Office of Research and Development U.S. Environmental Protection Agency Duluth, Minnesota 55804		13. TYPE OF REPORT AND PERIOD COVERED FINAL 14. SPONSORING AGENCY CODE EPA-ORD

15. SUPPLEMENTARY NOTES

the author

16. ABSTRACT

As part of a research effort sponsored by the U.S. Environmental Protection Agency to study the dispersion of contaminants in near-shore areas of large lakes, ~~we have~~ developed numerical models which are capable of realistically describing the currents throughout large lakes and, in particular, in the near-shore regions of these lakes. This report summarizes our work to date on these hydrodynamic models.

In our work, the emphasis has been on the development and use of three-dimensional models. Three basic models and applications of these models are presented here. The models are: (1) a steady-state, constant-density model; (2) a time-dependent, constant-density model; and (3) a time-dependent, variable-density model. Each model has its own limitations and has certain advantages over the others. Applications of each model, especially to flows in near-shore regions, have been made and are discussed. Vertically averaged models have also been used by us, usually in parametric studies, and a brief summary of these models is also given.

A list of all publications by us resulting from or pertinent to this project is given in Section X of this report.

17. KEY WORDS AND DOCUMENT ANALYSIS **PRICES SUBJECT TO CHANGE**

a. DESCRIPTORS	b. IDENTIFIERS/OPEN ENDED TERMS	c. COSATI Field/Group
Hydrodynamics Circulation Mathematical Models Lakes	Wind Driven Circulation Models Thermal Plume Models Lake Erie Lake Michigan	08H
18. DISTRIBUTION STATEMENT RELEASE TO PUBLIC	19. SECURITY CLASS *(This Report)* Unclassified	21. NO. OF PAGES 153
	20. SECURITY CLASS *(This page)* Unclassified	22. PRICE $6.75 - 2.25

EPA Form 2220-1 (9-73)

U.S. GOVERNMENT PRINTING OFFICE: 1976 - 657-695/5402

EPA-600/3-76-020
April 1976

NUMERICAL MODELS OF LAKE CURRENTS

by

Wilbert Lick
Case Western Reserve University
Cleveland, Ohio 44106

Grant No. R-802359

Project Officer

William L. Richardson
Large Lakes Research Station
Environmental Research Laboratory--Duluth
Grosse Ile, Michigan 48138

U.S. ENVIRONMENTAL PROTECTION AGENCY
OFFICE OF RESEARCH AND DEVELOPMENT
ENVIRONMENTAL RESEARCH LABORATORY
DULUTH, MINNESOTA 55804

DISCLAIMER

This report has been reviewed by the Environmental Research Laboratory, U.S. Environmental Protection Agency, and approved for publication. Approval does not sighify that the contents necessarily reflect the views and policies of the U.S. Environmental Protection Agency, nor does mention of trade names or commercial products constitute endorsement or recommendation for use.

ABSTRACT

As part of a research effort sponsored by the U.S. Environmental Protection Agency to study the dispersion of contaminants in near-shore areas of large lakes, we have developed numerical models which are capable of realistically describing the currents throughout large lakes and, in particular, in the near-shore regions of these lakes. This report summarizes our work to date on these hydrodynamic models.

In our work, the emphasis has been on the development and use of three-dimensional models. Three basic models and applications of these models are presented here. The models are: (1) a steady-state, constant-density model; (2) a time-dependent, constant-density model; and (3) a time-dependent, variable-density model. Each model has its own limitations and has certain advantages over the others. Applications of each model, especially to flows in near-shore regions, have been made and are discussed. Vertically averaged models have also been used by us, usually in parametric studies, and a brief summary of these models is also given.

A list of all publications by us resulting from or pertinent to this project is given in Section X of this report.

This report was submitted in fulfillment of Project No. R 802359 by Case Western Reserve University, Cleveland, Ohio under the sponsorship of the Environmental Protection Agency. Work was completed as of September, 1975.

RESEARCH REPORTING SERIES

Research reports of the Office of Research and Development, U.S. Environmental Protection Agency, have been grouped into five series. These five broad categories were established to facilitate further development and application of environmental technology. Elimination of traditional grouping was consciously planned to foster technology transfer and a maximum interface in related fields. The five series are:

1. Environmental Health Effects Research
2. Environmental Protection Technology
3. Ecological Research
4. Environmental Monitoring
5. Socioeconomic Environmental Studies

This report has been assigned to the ECOLOGICAL RESEARCH series. This series describes research on the effects of pollution on humans, plant and animal species, and materials. Problems are assessed for their long- and short-term influences. Investigations include formation, transport, and pathway studies to determine the fate of pollutants and their effects. This work provides the technical basis for setting standards to minimize undesirable changes in living organisms in the aquatic, terrestrial, and atmospheric environments.

This document is available to the public through the National Technical Information Service, Springfield, Virginia 22161.

CONTENTS

Sections		Page
I	Conclusions	1
II	Recommendations	3
III	Introduction	5
IV	General Considerations in Modeling of Currents	9
	4.1 Characteristics of Lake Currents	9
	4.2 Basic Equations, Boundary Conditions, and Important Parameters	13
V	Vertically Averaged Models	22
VI	Steady-State Models	32
	6.1 The Wind-Driven Circulation in Lake Erie	33
	6.2 Effects of Partial Ice Cover	48
	6.3 A Near-Shore Model	50
	6.4 A Two-Layer, Stratified Lake	60
VII	Time-Dependent, Constant-Density Models	68
	7.1 An Overall Lake Erie Circulation Model	68
	7.2 The Near-Shore	91
	7.3 Analytic Results	94
VIII	Time-Dependent, Variable Density Models	103
	8.1 River Discharges and Thermal Plumes	104
	8.2 Lake Circulation Models	122
IX	References	132
X	Publications	138

Preceding page blank

FIGURES

No.		Page
1	Lake Erie bottom topography	12
2	Cartesian coordinates located at the nominal lake surface.	15
3	Wind shear stress relation.	19
4a	Surface displacement as a function of time at Cleveland.	25
4b	Surface displacement as a function of time offshore of Cleveland half-way across the lake.	26
5	Vertically-averaged velocities, t = 87.5 sec.	28
6	Vertically-averaged velocities, t = 262.5 sec.	28
7	Vertically-averaged velocities, t = 937.5 sec.	29
8	Vertically-averaged velocities, t = 1575 sec.	29
9	0.805 kilometer (0.5 mile) grid for Island region	38
10	Shoreline of Lake Erie on 3.22 km (2 mile) grid.	39
11	Horizontal velocities at a constant 0.4 meters (1.5 ft) from surface. Wind direction, W 50 S; wind magnitude, 10.1 meters per second (22.7 mph); friction depth, 27.4 meters (90.0 ft); rivers: Detroit, Niagara.	42
12	Horizontal velocities at a constant 6.7 meters (22.0 ft) from surface. Wind direction, W 50 S; wind magnitude, 10.1 meters per second (22.7 mph); friction depth, 27.4 meters (90.0 ft); rivers; Detroit, Niagara.	43
13	Horizontal velocities at a constant 9.9 meters (32.8 ft) from surface. Wind direction, W 50 S; wind magnitude, 10.1 meters per second (22.7 mph); friction depth, 27.4 meters (90.0 ft); rivers: Detroit, Niagara.	44

No.		Page
14	Horizontal velocities at a constant 14.9 meters (49.2 ft) from surface. Wind direction, W 50 S; wind magnitude, 10.1 meters per second (22.7 mph); friction depth, 27.4 meters (90.0 ft); rivers: Detroit, Niagara.	45
15	Vertical velocities at mid-depth. Wind direction, W 50 S; wind magnitude, 10.1 meters per second (22.7 mph); friction depth, 27.4 meters (90.0 ft); rivers: Detroit, Niagara.	46
16	Horizontal velocities at a constant 3.6 meters (12.0 ft) from surface. Wind velocity: 5.2 meters per second (18 mph), N7.5W. Frictional depth: 18.2 meters (60.0 ft). Rivers: Detroit, Sandusky, Maumee, Niagara.	51
17	Horizontal velocities at a constant 6.7 meters (22.0 ft) from surface. Wind velocity: 5.2 meters per second (18 mph), N7.5W. Frictional Depth: 18.2 meters (60.0 ft). Rivers: Detroit, Sandusky, Maumee, Niagara.	52
18	Topography of jetport and grid structure in the shore region near Cleveland.	54
19	Horizontal velocities at the surface.	55
20	Horizontal velocities at a constant depth of 30 ft. from the surface	56
21	Horizontal velocities at the surface.	57
22	Steady-state near-shore currents in the presence of a jetport island with extension to the shore with $(\tau_x, \tau_y) = (1.55 \text{ dyne/cm}^2, 1.1 \text{ dyne/cm}^2)$. Horizontal velocities at the surface.	58
23	Horizontal velocities at a constant depth of 30 ft. from the surface.	59

No.		Page
24	Thermocline depth contours with wind stress curl of order one ($\delta = 1/24$).	64
25	Thermocline profile at $x = 48.3$ km with wind stress curl of order one.	65
26	Horizontal surface velocities ($\delta = 1/24$).	65
27	Horizontal velocities at 20 meter depth.	66
28	Horizontal velocities at 35 meter depth.	66
29	Horizontal grid pattern in part of Lake Erie.	72
30	Stress interpolation function of six data points around the lake.	76
31	Surface displacement as a function of time at Cleveland.	78
32	Surface displacement contours ($\tau_x = 1$ dyne/cm^2)	79
33	Horizontal velocity component at Cleveland.	80
34	Horizontal velocity component in central part of Eastern Basin.	81
35	Wind conditions during storm Agnes on June 22, 1972 at 2400 hours.	83
36	Wind conditions during storm Agnes on June 23, 1972 at 1200 hours.	84
37	Magnitude of wind stress as a function of time during storm Agnes.	86
38	Calculated and measured water level fluctuations at Cleveland during storm Agnes.	87
39	Calculated and measured water level fluctuations for Port Stanley during storm Agnes.	88
40	Contours of surface elevation for Storm Agnes at 0400 hours on June 23, 1972.	90
41	Grid pattern at boundary between Eastern and Central Basins.	93

No.		Page
42	Surface displacement as a function of time along a line across the lake at Cleveland.	95
43	Surface displacement at $x = 0$ as a function of time for an infinitely long lake with $L = 300$ km, $H = 10$ meters, $E_v = 1.0$, $\tau = 1$ dyne/cm^2.	98
44	Surface displacement at $x = 0$ as a function of time for an infinitely long lake with $E_v = .025$ and $\tau = 1$ dyne/cm^2 for different values of β.	99
45	Surface displacement at $x = .05$, $y = .05$ as a function of time for a square basin with $E_v = .025$, $\tau_x = 1$ dyne/cm^2, $\tau_y = 0$.	101
46	Bottom topography for the Point Beach power plant.	106
47	Surface velocities. No wind, no crossflow.	112
48	Velocities at a depth of 2.1 meter. No wind, no crossflow.	113
49	Surface temperature distribution. No wind, no cross-flow.	114
50	Surface velocities. With wind and cross-flow.	116
51	Surface temperatures. With wind and cross-flow.	117
52	Surface temperature decay along centerline. No wind, no cross-flow.	118
53	Surface isotherm areas. No wind, no cross-flow.	119
54	Surface temperature decay along centerline. With wind and cross-flow.	120
55	Surface isotherm areas. With wind and cross-flow.	121
56	Horizontal velocities at the surface. Wind direction, East. Wind magnitude, 5.2 m/sec. Friction depth, 18.2 m.	125
57	Velocities in vertical plane along major axis and through the center of the Central Basin.	126

No.		Page
58	Temperatures in vertical plane along minor axis and through the center of the Central Basin.	127
59	Temperatures in vertical plane along major axis and through the center of the Central Basin.	128
60	Temperatures in vertical plane along minor axis and through the center of the Central Basin. Constant eddy coefficients.	129
61	Temperatures in vertical plane along major axis and through the center of the Central Basin. Constant eddy coefficients.	130

ACKNOWLEDGMENTS

The writer wishes to acknowledge with appreciation the support of this project by the Environmental Protection Agency. Mr. William L. Richardson served as Grant Project Officer.

Specific applications of these models have been partially funded by the U.S. Army Corps of Engineers (Lake Erie Jetport study) and the Argonne National Laboratories (Point Beach power plant study).

The National Aeronautics and Space Administration through Dr. Richard Gedney has given us considerable computer time, for which we are grateful. T.H. Maruna of the Babcock and Wilcox Company, Alliance Research Center, has also assisted us with computer time.

Many researchers have contributed to the work summarized in this report. Their names appear as authors in the list of publications in the appendix and their assistance is acknowledged with sincere thanks.

SECTION I

CONCLUSIONS

The present project is mainly concerned with the understanding of fundamental aspects of the dispersion of contaminants in the near-shore regions of large lakes. As part of this effort, we have developed numerical models which are capable of realistically describing the currents throughout a lake and, in particular, in the near-shore regions of these lakes. The present report summarizes to date our work on the numerical modeling of currents.

In our work, the emphasis has been on the investigation of three-dimensional models, three of which were developed, applied to various situations, and compared with observational data. The first model developed was a steady-state, constant-density model. Applications of this model have been made for (a) the overall circulation in Lake Erie, (b) the circulation in Lake Erie when it is partially ice covered, and (c) a near-shore region including the effects on the circulation of a proposed jetport. The model was also extended to describe a two-layer, stratified lake. Although limited because of the assumptions of steady state and constant density, the model is realistic and can be solved relatively quickly on the computer. Solutions with high spatial resolution (a relatively fine numerical grid) were obtained. Comparisons with field observations were made and the agreement was good.

The second model developed was a time-dependent, constant-density model. This is a free-surface model and is therefore valid for describing storm surges and similar motions. The model has been applied (a) to storm surges in Lake Erie, and (b) to a near-shore region including the effects of a proposed jetport. Limited comparison with field data shows good agreement.

The third model developed was a time-dependent, variable-density, rigid-lid model. The main application of this model has been to river discharges and thermal plumes. Numerical results show good agreement with field observations. This model is presently being used to investigate both the overall and near-shore circulation in a stratified lake.

Also developed were vertically averaged models, models which are relatively simple but generally (except with additional work) do not give details in the vertical of the flow. In addition, the functional form of the bottom stress in the vertically-averaged model is incorrect and leads to errors for both small time and in variable-depth situations. However, because of their relatively short computation times, these models are useful for parametric studies. The models have been applied to lake circulation problems and to river discharges and thermal plumes.

SECTION II

RECOMMENDATIONS

Although the models to be presented are sufficiently general (by themselves or with slight extensions) for almost all lake circulation problems, a great deal of further numerical experimentation using these models needs to be done. The purposes of these computations should be to:

(1) Understand the general characteristics of flows in lakes, especially in the near-shore under stratified conditions, e.g., upwelling and mass flux through the thermocline;

(2) Calculate details of specific flows and verify these by means of field observations, again especially in the near-shore. A combination of field observations, numerical experiments, and laboratory work needs to be done to determine more accurately the magnitude and functional dependence of the vertical and horizontal eddy diffusion coefficients, the wind stress-wind velocity relation, and the wind factor ratio;

(3) Understand the numerical accuracy and characteristics of the various models. The models must be simplified in design as well as application. Numerical experiments must be performed comparing the various models and learning how to simplify them.

Hydrodynamic models are becoming quite detailed. Sufficient information on their use is becoming available so that confidence may be placed in their predictions. In particular, these models are sufficiently accurate so that they can be used as bases for models of sediment resuspension and transport, dredging problems, phytoplankton and zooplankton growth, community succession, etc. and should be so used.

The numerical models discussed in this report do not consider the effects of waves, effects which become increasingly important as the depth of water decreases. For an adequate understanding of the dispersion of contaminants in these shallow, near-shore regions, further work needs to be done on the effects of waves. The direct effect of waves in causing contaminant transport and sediment resuspension and transport as well as the indirect effects in causing long-shore currents need to be investigated, made quantitative, applied to specific cases, and verified by means of field observations.

SECTION III

INTRODUCTION

A contaminant (either a chemical or biological substance or heat) disperses through a lake by convection and turbulent diffusion. As the contaminant moves from its source to a sink, it may be degraded or converted to other forms by chemical, biological, and physical processes. An understanding of these dispersion and degradation processes is essential in understanding aquatic ecosystems.

In particular, a knowledge of these processes in near-shore regions is necessary since (a) the near-shore regions are where contaminants are generally introduced and therefore their concentrations and effects are different and generally greater than in off-shore areas, and (b) the near-shore areas are of more particular interest to all of us for such uses as recreation, water supplies, and fishing. However, at present, our knowledge of these dispersion and degradation processes is insufficient to either understand or predict the concentrations of contaminants in near-shore areas.

As part of a research effort sponsored by the U.S. Environmental Protection Agency to study these processes in the near-shore areas of large lakes, we have developed numerical models which are capable of realistically describing the currents, both steady and time-dependent, throughout large lakes and in particular in the near-shore regions of these lakes. The present report summarizes our work on these hydrodynamic models to date.

Since it is not feasible to discuss all the details on all of our numerical models and investigations in one report, the emphasis here is on a general description of the models, the assumptions involved in their formulation, and their uses. More details of the models, applications, results, and documented programs, are reported in the articles cited. A list of publications and reports by us on numerical modeling of currents is given in Section X. Further work, in particular, hydrodynamic applications of these models, numerical experiments to more fully understand these models, and applications of these models to the prediction of the dispersion of contaminants is continuing but is not reported here.

A brief outline of the present report is as follows. In the following section, Section IV, a general description of lake currents is first given followed by a presentation and general discussion of the three-dimensional, time-dependent equations and boundary conditions basic to all the models.

In Section V, vertically averaged models are discussed. These models result from an averaging of the three-dimensional equations over the depth. A bottom friction parameter, which is difficult to determine a priori, must also be introduced and related to the mean flow. The result of these manipulations is a reduced two-dimensional set of equations which is comparatively easy to analyze, requires relatively little computer time, but does not give details of the flow in the vertical. This vertical detail is necessary for the complete understanding of the flow characteristics and for an accurate description of problems such as the dispersion of a contaminant. However, for some problems, this detail is not necessary and the two-dimensional model is adequate. The two-dimensional model is also useful for preliminary qualitative investigations of flows, especially parametric studies. These flows can then be later investigated more thoroughly by use of the three-dimensional models. In Section V, typical results of calculations are shown for (a) the time-dependent flow in Lake Erie, and (b) the plume from a power plant situated on the shore of a lake.

In Section VI, the simplest three-dimensional model is discussed, a constant density, steady-state model. Although limited by the assumptions of constant density and steady state, the model has been shown (by comparison with field observations) to give good results for periods when the winds were relatively constant. In this model, a major assumption is that the vertical eddy diffusivity is constant. This assumption along with other more minor ones (discussed in Section VI) allows one to integrate the equations of motion in the vertical direction analytically (without introducing a new parameter such as the bottom stress relation used in the two-dimensional, vertically averaged models mentioned above and discussed in Section V). This procedure reduces the governing equation to two dimensions. Further manipulations lead to a comparatively simple set of equations which can be solved relatively quickly on the computer but which still give vertical details of the flow. Applications of these models are described and representative results of the calculations are shown for (a) the overall circulation in Lake Erie, (b) the overall circulation in Lake Erie with partial ice cover, (c) a near-shore analysis with applications to the proposed Lake Erie Jetport, and (d) an extension of the single layer model to a two-layer stratified model (for simple basins only).

In Section VII, a constant density, time-dependent, free-surface model is described. This involves similar assumptions to those used in the constant density, steady-state model. However, vertical analytic integration is no longer possible and a complete, three-dimensional numerical integration is necessary. Because of the free surface assumption, the model is valid for describing storm surges and similar motions. Applications are made to (a) a general Lake Erie model, and (b) a near-shore model including studies of the proposed Lake Erie Jetport. Some analytic work has also been done utilizing this model, particularly in regard to the significant time scales in a general time-dependent flow in a lake. This work is also described in Section VII.

In Section VIII, our time-dependent, variable-density models are discussed. These models employ the rigid-lid approximation and therefore filter out the free-surface gravity waves, thus allowing longer time steps in the numerical integration. The models are therefore obviously not valid to describe storm surges, where free surface oscillations are important, but are valid and have been used to describe flows with slowly time-varying temperature and velocity fields. Representative results are shown for (a) river discharges and thermal plumes, and (b) the overall circulation in a stratified lake.

SECTION IV

GENERAL CONSIDERATIONS IN MODELING OF CURRENTS

4.1 CHARACTERISTICS OF LAKE CURRENTS

The currents in the Great Lakes are primarily driven by the wind. Currents due to through flows from incoming rivers to a single outflowing river are comparatively small except locally near the mouths of the rivers. In addition to these two causes of currents which are present more or less continuously, temperature, and hence density, gradients cause currents and in addition modify existing currents. These density gradients may have a relatively large influence on currents and must be considered during the late spring, summer, and early fall when stratification occurs and these gradients are large. The Great Lakes are large enough (horizontal dimensions of 100 to 300 km) so that Coriolis forces are important.

In shallow water, usually near shore, the effects of waves become important. The direct effect of waves on the water is to cause an oscillatory motion of the water particles. Because the motion is oscillatory, it is generally unimportant in causing transport (except in a narrow layer near the bottom in relatively shallow water) although it may be significant in causing a bottom shear stress and hence resuspension of bottom sediments. The major effect of waves on transport is indirectly through long-shore currents caused by the breaking of waves and the resulting dissipation of energy and momentum. Wave effects are under investigation by us but are not discussed in this report.

The currents due to the combined actions of winds, temperature gradients, and through flows and as modified by the basin geometry are quite complex and involve many different length and time scales. A thorough description of the dynamics of a lake will not be given here but a brief discussion of some of the more significant motions and the associated length and time scales will be given because of the relevance of these matters to numerical modeling. An excellent and more thorough discussion on the significant physical processes occurring in lakes is given by Boyce (1974).

It is convenient to separate the currents into quasi-steady motions and time-dependent motions although in practice this is difficult to do. Steady-state currents will be discussed first. When the winds act on the surface of a deep, constant-density body of water, a circulation is set up which in the steady state consists approximately of (a) top and bottom boundary layers (Ekman layers) in which vertical turbulent mixing is important, (b) horizontal boundary layers near shore in which horizontal turbulent mixing is important, and (c) a geostrophic, inviscid core. In shallow lakes, or shallow, near-shore areas of deep lakes, this description is no longer valid. In these shallow regions, the Ekman layers are merged and vertical turbulent diffusion is important throughout the water column.

In the oceans, an Ekman layer is typically on the order of a hundred meters thick and hence is small by comparison with the depth of the ocean. In most of the Great Lakes, where the thickness of an Ekman layer d is on the order of 20 to 40 m, the depth of the lake h is generally several times as great as d. In Lake Erie, the average depth of the lake is only about 20m and is about the same as the thickness of an Ekman layer. The thickness of the boundary layers near shore in which horizontal mixing is important is generally on the order of a few kilometers or less, and is therefore quite small by comparison with the horizontal dimensions L of a lake.

Heating and the subsequent stratification introduce additional phenomena. During the summer, a thermocline or region of large vertical temperature gradients generally develops. The depth of this thermocline is generally 20 to 100 m while its thickness may be as little as a few meters. Again because of its shallow depth, Lake Erie is atypical in that the thermocline is quite often very near the bottom, sometimes only a few meters from the bottom.

Time-dependence introduces even more complexities. Consider first the constant density flow in a lake which is initially still but at time zero is acted on by a uniform and constant wind stress. The time t_s to reach a new steady state, which of course is determined by this wind stress, depends on the parameter $\beta = gh/L^2f^2$ (Haq and Lick, 1975), where $f = 10^{-4}$ sec $^{-1}$ and is the Coriolis parameter. For the Great Lakes, this parameter can be assumed to be large and as a first approximation the result for t_s is independent of β. For a shallow lake where $h/d<<1$ or $O(1)$, t_s is then of order h^2/A_v, where A_v is the vertical eddy viscosity. That is, t_s is a viscous diffusion time. For a deep lake where $h/d>>1$, the time t_s is of order $2\pi h/df$. In this case, t_s is the usual spin-up time for a rotating container with a rigid lid (Greenspan, 1968). For the Great Lakes, the time to reach steady state varies from one or two days (Lake Erie) to probably one or two two weeks for Lake Superior. This is to be compared with the average period of storm cycles in the Great Lakes region of two to seven days (Oort and Taylor, 1969). On a smaller time scale are the periodic surface oscillations, or seiches of lakes. For shallow wide lakes, these have a period of oscillation close to the inertial period $2\pi/f$, which is about 17.5 hours. For deep narrow lakes, they have a period close to the period of gravitational waves, i.e., $L/\sqrt{gh}$.

If the lake is stratifed, internal oscillations analogous to the free surface seiches may be present. The period of these waves is close to the inertial period. The time to reach a steady state in stratified conditions may be considerably longer than that in non-stratified conditions due to the effect of the stratification on turbulent mixing.

These are just a few of the many different physical phenomena that occur in lakes and the length and time scales that are associated with them. No model is capable of describing all of these phenomena. Therefore the modeler must decide which phenomena are important to his problem and then choose or develop his model accordingly.

Most of the applications of our models thus far have been to flows in Lake Erie. The topography of this lake is shown in Fig. 1. Some of its more important features are as follows. Lake Erie is approximately 386 km long and 80 km wide near the mid-point of its long axis.

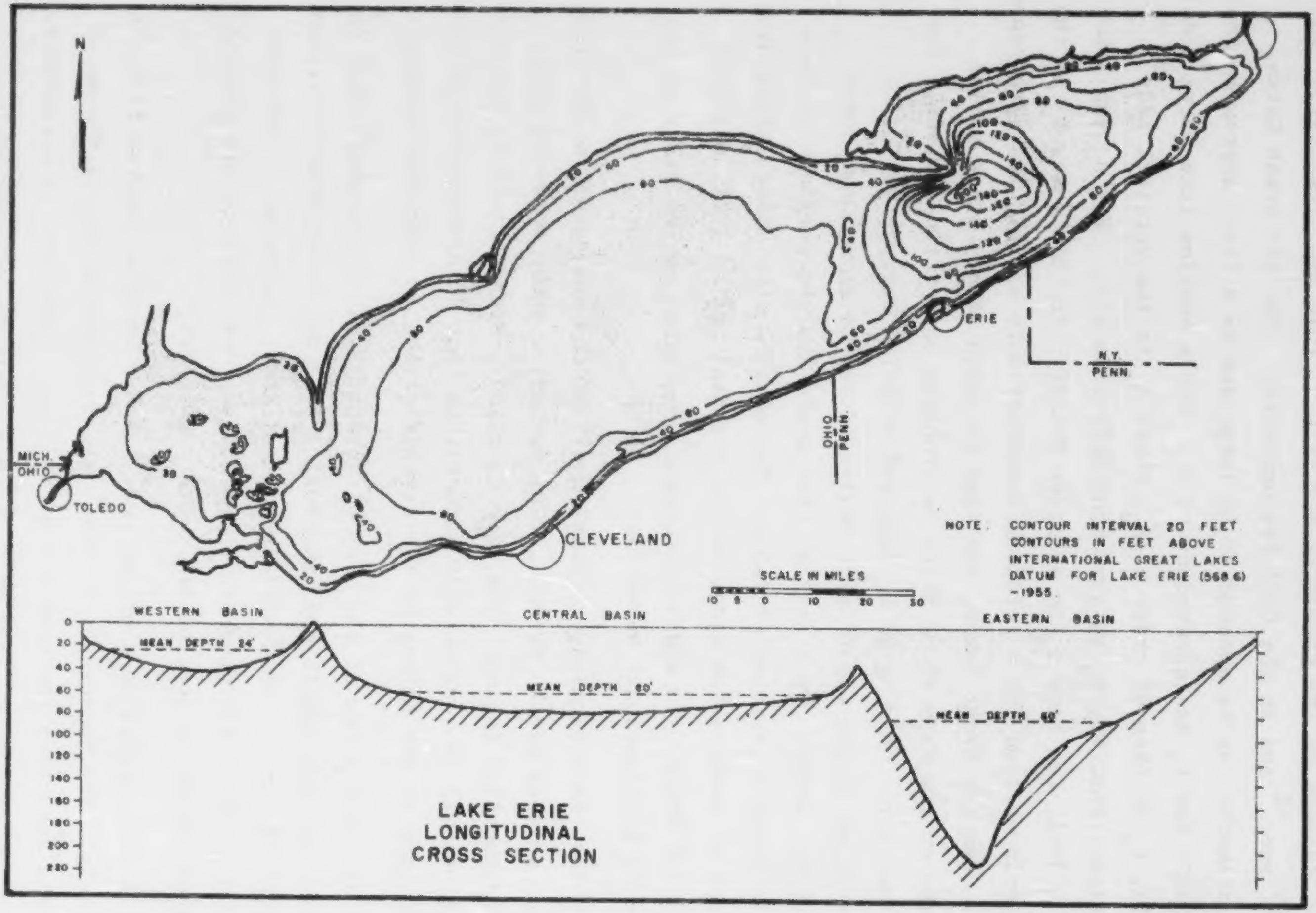
N
MICH.
OHIO
TOLEDO
CLEVELAND
ERIE
OHIO
PENN.
N.Y.
PENN.
NOTE: CONTOUR INTERVAL 20 FEET
CONTOURS IN FEET ABOVE
INTERNATIONAL GREAT LAKES
DATUM FOR LAKE ERIE (568.6)
-1955
SCALE IN MILES
10 5 0 10 20 30
WESTERN BASIN
CENTRAL BASIN
EASTERN BASIN
MEAN DEPTH 24'
MEAN DEPTH 60'
MEAN DEPTH 80'
0
20
40
60
80
100
120
140
160
180
200
220
LAKE ERIE
LONGITUDINAL
CROSS SECTION

Figure 1. Lake Erie bottom topography

Topographically, it can be separated into three basins: (1) a shallow Western basin with an average depth of 7 m; (2) a large, relatively flat Central basin with an average depth of 18 m; and (3) a deeper, cone-shaped Eastern basin with an average depth of 24 m. The Western and Central basins are separated by a rocky chain of islands. Of the water supply to Lake Erie, about 80% comes from Lake Huron via the Detroit River, 10% comes from other tributaries, and 9% is precipitation on the lake's surface. Of the loss of water from Lake Erie, 89% is out through the Niagara River and Welland Canal and 11% is evaporation.

4.2 BASIC EQUATIONS, BOUNDARY CONDITIONS, AND IMPORTANT PARAMETERS

Basic Equations and Boundary Conditions

The basic equations used in the modeling of lake currents are the usual hydrodynamic equations for conservation of mass, momentum, and energy plus an equation of state. In sufficiently general form for most lake modeling these equations are

$$\frac{\partial u}{\partial x} + \frac{\partial v}{\partial y} + \frac{\partial w}{\partial z} = 0 \tag{1}$$

$$\frac{\partial u}{\partial t} + \frac{\partial u^2}{\partial x} + \frac{\partial uv}{\partial y} + \frac{\partial uw}{\partial z} - fv = -\frac{1}{\rho_r}\frac{\partial p}{\partial x} + \frac{\partial}{\partial x}\left(A_H \frac{\partial u}{\partial x}\right) + \frac{\partial}{\partial y}\left(A_H \frac{\partial u}{\partial y}\right) + \frac{\partial}{\partial z}\left(A_v \frac{\partial u}{\partial z}\right) \tag{2}$$

$$\frac{\partial v}{\partial t} + \frac{\partial uv}{\partial x} + \frac{\partial v^2}{\partial y} + \frac{\partial vw}{\partial z} + fu = -\frac{1}{\rho_r}\frac{\partial p}{\partial y} + \frac{\partial}{\partial x}\left(A_H \frac{\partial v}{\partial x}\right) + \frac{\partial}{\partial y}\left(A_H \frac{\partial v}{\partial y}\right) + \frac{\partial}{\partial z}\left(A_v \frac{\partial v}{\partial z}\right) \tag{3}$$

$$\frac{\partial p}{\partial z} = -\rho g \tag{4}$$

$$\frac{\partial T}{\partial t} + \frac{\partial uT}{\partial x} + \frac{\partial vT}{\partial y} + \frac{\partial wT}{\partial z} = \frac{\partial}{\partial x}\left(K_H\frac{\partial T}{\partial x}\right) + \frac{\partial}{\partial y}\left(K_H\frac{\partial T}{\partial y}\right) + \frac{\partial}{\partial z}\left(K_v\frac{\partial T}{\partial z}\right) + S \qquad (5)$$

$$\rho = \rho(T) \qquad (6)$$

were u,v, and w are the fluid velocities in the x,y, and z directions respectively (see figure 2), t is the Coriolis parameter which is assumed constant, p is the pressure, ρ is the density, ρ_r is the ambient or reference density, A_H is the horizontal eddy viscosity while A_v is the vertical eddy viscosity, K_H is the horizontal eddy conductivity while K_v is the vertical eddy conductivity, g is the acceleration due to gravity, T is the temperature, and S is a heat source term.

Several approximations are implicit in these equations. These are (a) the pressure is assumed to vary hydrostatically, (b) the Boussinesq approximation, which assumes that density variations are small and can be neglected compared to other terms except in the hydrostatic equation, is valid, and (c) eddy coefficients are used to account for turbulent diffusion effects in both the momentum and energy equations.

The appropriate boundary conditions are dependent on the particular problem to be solved. At the free surface, $z = \zeta$, usual conditions are: (a) the specification of a stress due to the wind,

$$\rho A_v \frac{\partial u}{\partial z} = \tau_x \quad , \quad \rho A_v \frac{\partial v}{\partial z} = \tau_y \qquad (7)$$

where τ_x, τ_y are the specified wind stresses in the x and y directions respectively; (b) a kinematic condition on the free surface,

$$\frac{\partial \zeta}{\partial t} + u\frac{\partial \zeta}{\partial x} + v\frac{\partial \zeta}{\partial y} - w = 0; \qquad (8)$$

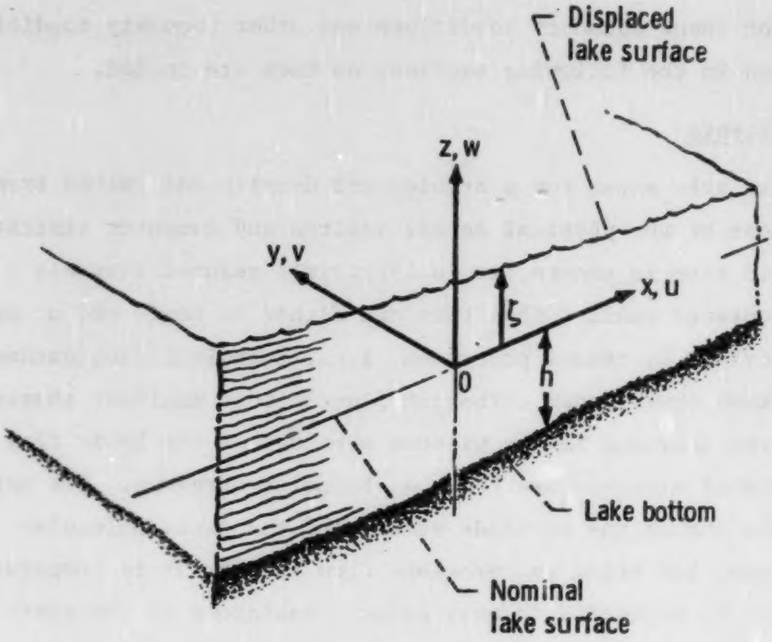

Figure 2. Cartesian coordinates located at the nominal lake surface.

(c) the pressure is continuous across the water-air interface and therefore the fluid pressure at the surface equals atmospheric pressure p_a,

$$p(x,y,\zeta,t) = p_a; \tag{9}$$

and (d) a specification of the heat flux at the surface,

$$q = -\rho K_v \frac{\partial T}{\partial z} = H(T - T_a) \tag{10}$$

where q is the energy flux, H is the surface heat transfer coefficient, and T_a is the air temperature.

At the bottom, the conditions are (a) those of no fluid motion or a specification of stress in terms of either integrated mass flux or bottom velocity, and (b) either a specification of temperature or a specification of heat flux.

Variations on these boundary conditions and other boundary conditions are discussed in the following sections as they are needed.

Eddy Coefficients

The numerical grid sizes for a problem are usually determined from considerations of the physical detail desired and computer limitations. Once the grid size is chosen, it is implicitly assumed that all physical processes smaller than this can either be neglected or approximately described by random processes, i.e., turbulent fluctuations. It can be shown that random turbulent fluctuations manifest themselves in an apparent increase in the viscous stresses of the basic flow. These additional stresses are known as Reynolds stresses. The total stress is the sum of the Reynolds stress and the usual molecular viscous stress, but since in turbulent flow the latter is comparatively small, it may be neglected in many cases. Analagous to the coefficients of molecular viscosity, an eddy viscosity coefficient can be introduced (as has been done in the equations above) so that the shear stress is proportional to a velocity gradient. Similarly an eddy conductivity coefficient can be introduced so that the heat flux is proportional to a temperature gradient. In turbulent flow, these coefficients are not properties of the fluid as in laminar flow but depend on the flow itself, i.e., on the processes generating the turbulence. The determination of these turbulent eddy coefficients in terms of mean flow variables is a major problem in hydrodynamic modeling.

Although considerable work has been done on the theory of turbulence, in practice one must resort to experiments and semi-empirical theories for realistic values of the eddy coefficients. Since the scale and intensity of the vertical and horizontal components of turbulence are generally quite different, it is convenient to consider these effects separately as has been done in the equations presented above. The vertical eddy viscosity A_v in general should vary throughout the lake. Some of the more important generating processes of this vertical turbulence and causes for its variation are (a) the direct action of the wind stress on the lake surface, (b) the presence of vertical shear , in currents due to horizontal pressure gradients, (c) the presence of internal waves, and (d) the effect of bottom irregularities and friction on currents.

In addition, if the density of the water changes with depth, stability effects will change the intensity of the turbulence. The stability effect is dependent on the Richardson number, defined by

$$Ri = - \frac{g\frac{\partial\rho}{\partial z}}{\rho\left(\frac{\partial\bar{u}}{\partial z}\right)^2} \tag{11}$$

where $\bar{u}$ is the mean horizontal velocity. Various empirical values have been developed relating the variation of the eddy viscosity coefficient with the Richardson number (see, e.g., Koh and Chang (1973) or Sundarem and Rehm (1970) for summaries). A typical relation is that developed by Munk and Anderson (1948)

$$A_v = A_{vo} (1 + 10Ri)^{-1/2} \tag{12}$$

Where A_{vo} is the value of A_v in a non-stratified flow. Typical values for A_{vo} in the Great Lakes are on the order of 1 to 50 cm^2/sec.

Horizontal viscosity coefficients are generally much greater than the vertical coefficients. It is found from experiments that the values of the horizontal viscosity coefficient increase with the scale ℓ of the turbulent eddies, i.e.,

$$A_H = a\,\varepsilon^{1/3}\,\ell^{4/3} \tag{13}$$

where a is a proportionality constant and ε is the rate of energy dissipation (Stommel 1949, also see Orlob 1959, Okubo 1971, Csanady 1973). Observations indicate values of 10^4 to 10^5 for A_H for the overall circulation in the Great Lakes (Hamblin, 1971) with smaller values indicated in the near-shore regions.

In a non-stratified flow, it is believed that the eddy conductivity is approximately equal to the eddy viscosity. However, for a stratified flow, the mechanisms of turbulent transfer of momentum and heat are somewhat different and this leads to different dependences of these coefficients on the Richardson number. For example, a semi-empirical relation (Munk and Anderson, 1948) similar to Eq. 12 suggests that

$$K_v = K_{vo} (1 + 3.33 \text{ Ri})^{-3/2} \tag{14}$$

where K_{vo} is the value of the vertical eddy conductivity in a non-stratified flow.

Wind Stress

In the modeling of the wind-driven circulation in a lake, it is necessary to know the horizontal shear stress imposed as a boundary condition at the surface of the lake. This stress is due to the interaction of the turbulent air and water. The relation of this stress to the wind speed is very difficult to determine from theoretical considerations and its value is usually based on semi-empirical formulas and on observations. A common relation assumed between these quantities is

$$\underline{\tau} = \rho_a C_d W_a^{n-1} \underline{W}_a \tag{15}$$

where C_d is a drag coefficeint, ρ_a is the density of the air, W_a is the wind velocity at 10m above the water surface, n is an empirically determined exponent not necessarily integer, and the bar under a function denotes a vector.

Wilson (1960) has analyzed data from many different sources and has given a best fit to the data (see figure 3). For W_a in units of cm/sec, ρ_a in units of gm/cm^3, and τ in units of dynes/cm^2, Wilson suggests a value of $n = 2$ and $C_d = 0.00237$ for strong winds and 0.00166 for light winds. Simons (1974), from a comparison of field data and results of numerical models, suggests values of $n = 2$ and $C_d = 0.003$.

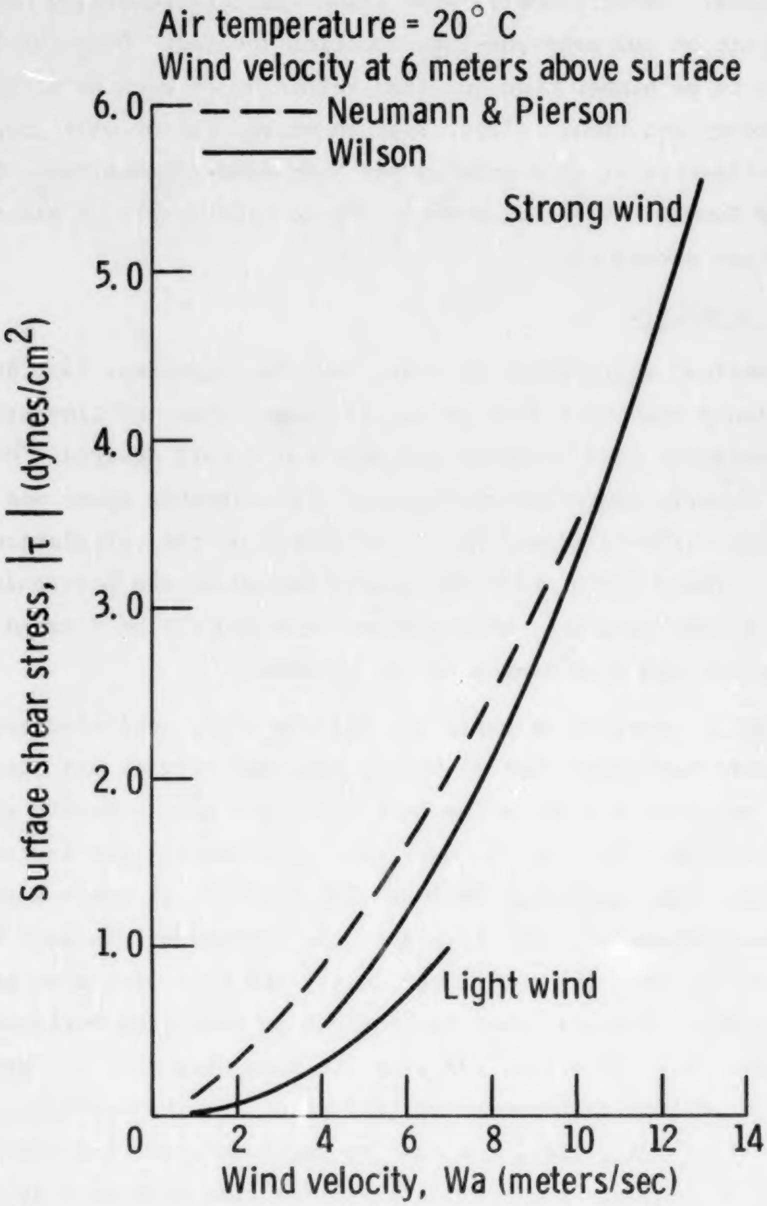

Figure 3. Wind shear stress relation

An additional problem in determining the wind stress is that W_a in the above formula is the wind velocity at the specified location over the lake. Unfortunately, wind velocities are generally measured on shore and not at the over-the-lake location desired. Over-the-lake winds tend to be higher than the land values by as much as a factor of 1.5 (Gedney and Lick, 1972). This phenomena is not well understood. Some investigation of this problem has been done (Simons 1974, Donelin, Elder, and Hamblin 1974) but more is needed before this effect can be determined accurately.

Numerical Stability

In the numerical calculation of space and time dependent lake problems, for efficiency one would like to use as large space and time steps as are consistent with accuracy and physical detail desired. However, there are usually other restrictions on the allowable space and time steps, restrictions dictated by the stability of the calculation procedure. These restrictions of course depend on the particular numerical scheme used but, when present, can usually be related to the physical space and time scales of the problem.

As an example, consider an explicit, forward-time, central-space scheme. Simple theory indicates that limits on the time step Δt and space steps Δz in the vertical and Δx in the horizontal are approximately given by the following: (a) $\Delta t < \Delta x/\sqrt{gh}$. This restriction indicates that the numerical time step must be less than the time it takes a surface gravity wave (speed of $\sqrt{gh}$) to travel the horizontal distance between two grid points Δx. (b) $\Delta t < \Delta x/u$, i.e., the time step must be less than the time it takes a fluid particle to be convected horizontally a distance Δx. (c) $\Delta t < (\Delta z)^2/2A_V$, or the time step must be less than the time for diffusion between two grid points in the vertical. (d) $\Delta t < (\Delta x)^2/2A_H$, i.e., the same argument as above but for horizontal diffusion. (e) $\Delta t < 2\pi/f$, or the time step must be less than the inertial period. (f) $\Delta t < \Delta x/u_i$, where u_i is the speed of an internal wave, a similar argument to (a) above but for internal waves. All of these restrictions may be eliminated by various numerical procedures. However, each numerical method has its own difficulties and which procedure is most advantageous depends on the particular problem being studied.

SECTION V

VERTICALLY-AVERAGED MODELS

Vertically-averaged models have proved to be quite useful, especially in the prediction of lake levels during storms and of long-time contaminant transport. The model is relatively simple conceptually and requires little computer time compared to three-dimensional models. The model does not predict the vertical variation of the flow field but can give vertically averaged velocities and surface elevations fairly accurately in many cases. An important limitation of the model is that it does not consider the effects of density variations.

The basic equations for this model are obtained by integrating the equations of motion, Eqs. 1 to 5, from the bottom $z = -h(x,y)$ to the surface $z = \zeta(x,y)$. The linear terms can then be expressed in terms of the integrated velocities, U and V, and the surface displacement ζ, where $U \equiv \int_{-h}^{\zeta} u\,dz \doteq \int_{-h}^{0} u\,dz$ and $V \equiv \int_{-h}^{\zeta} v\,dz \doteq \int_{-h}^{0} v\,dz$. However, nonlinear terms of the form $\int_{-h}^{\zeta} (\partial u^2/\partial x)dz$ are also obtained and can not be expressed in terms of U and V or their derivatives without a further assumption. A convenient assumption is that the velocity profiles are similar, i.e., $u(x,y,z) = UF(\sigma)/h$ and $v(x,y,z) = VF(\sigma)/h$ where $\sigma = z/h$ and $F(\sigma)$ is a shape factor normalized such that $\int_{-1}^{0} F(\sigma)d\sigma = 1$.

The resulting equations can be written as (Welander 1961, Paul 1975)

$$\frac{\partial \zeta}{\partial t} + \frac{\partial U}{\partial x} + \frac{\partial V}{\partial y} = 0 \qquad (16)$$

$$\frac{\partial U}{\partial t} + \beta\left[\frac{\partial (U^2/h)}{\partial x} + \frac{\partial (UV/h)}{\partial y}\right] - fV$$

$$= -\frac{h}{\rho}\frac{\partial p_a}{\partial x} - \frac{gh\partial \zeta}{\partial x} + A_H\left(\frac{\partial^2 U}{\partial x^2} + \frac{\partial^2 U}{\partial y^2}\right) + \frac{1}{\rho}\left(\tau_x - \tau_x^{B}\right) \qquad (17)$$

$$\frac{\partial V}{\partial t} + \beta\left[\frac{\partial(UV/h)}{\partial x} + \frac{\partial(V^2/h)}{\partial y}\right] + fU$$

$$= -\frac{h}{\rho}\frac{\partial p_a}{\partial y} \; \frac{-gh\partial\zeta}{\partial y} + A_H\left(\frac{\partial^2 V}{\partial x^2} + \frac{\partial^2 V}{\partial y^2}\right) + \frac{1}{\rho}\left(\tau_y - \tau_y^B\right) \qquad (18)$$

where τ_x, τ_y are the surface shear stresses due to the wind in the x,y directions, τ_x^B, τ_y^B are the bottom shear stresses in the x,y directions, and $\beta = \int_{-1}^{0} F^2(\sigma)d\sigma$. A reasonable guess must be made for the functional relation $F(\sigma)$ in order to evaluate β. A constant or quadratic $F(\sigma)$ is generally assumed.

The wind shear stresses are related to the wind over the lake and are specified parameters. However, the bottom shear stresses are dependent on the flow and in vertically-averaged models must be related somehow to U and V. It is usually assumed that $\tau_x^B = \rho\ \alpha\ U^n/h^m$ and $\tau_y^B = \rho\ \alpha\ V^n/h^m$, where α is a coefficient of proportionality and n and m are constants, usually integers. If sufficient field data is available, these parameters can be determined from the best fit between the calculated results and observational data.

Alternatively, theoretical arguments can be presented which relate τ to U and V at least for limiting cases. If one considers flow in a shallow basin and assumes similar velocity profiles as above, then one can show that $\tau_x^B = \rho\ \alpha\ U/h^2$ and $\tau_y^B = \rho\ \alpha\ V/h^2$, where $\alpha = A_v\ dF/d\sigma$. If one considers flow in a deep lake with an interior geostrophic flow of magnitude U and assumes the presence of a bottom Ekman layer, then one can show that $\tau_x^B \sim U/h$ and $\tau_y^B \sim U/h$. In addition, if one postulates that the eddy viscosity is proportional to the wind stress and hence the integrated velocities, then it follows that the bottom shear stress is proportional to the square of the integrated velocities, a common assumption.

The form of the above equations is such that the most obvious method of numerical integration is some sort of explicit method, of which a variety exist (Roache, 1972). Numerous applications of the vertically-averaged equations exist in which an explicit procedure has been used.

For example, the flow in Lake Ontario has been studied by Rao and Murthy (1970), Simons (1971), and Paskausky (1971) while Lake Erie has been studied by Haq, Lick, and Sheng (1975) and Simons (1976).

Results of a representative calculation by us are given in Fig. 4, which shows the time-dependent surface displacement at two locations in Lake Erie for a spatially uniform wind impulsively started from rest. It is assumed that the wind blows along the long axis of the lake imparting a stress to the water surface of 1 dyne/cm^2. Fig. 4a shows the surface displacement near Cleveland while Fig. 4b shows the surface displacement off-shore of Cleveland approximately half-way across the lake. The bottom stress is assumed to be given by $\tau_x = \rho \alpha U/h^2$ and $\tau_y = \rho \alpha V/h^2$, where $\alpha = 50$.

Also shown in these figures are the results from the three-dimensional calculations (see Section VII). Although qualitatively similar, the results of the two calculations differ by as much as 35%. This is due to the fact that the vertically-averaged model does not reproduce the bottom stress correctly, or at least the bottom stress is not the same as that in the three-dimensional model. The functional form of the bottom stress in the vertically-averaged model is incorrect. It is incorrect for small time when the effects of the wind stress have not reached the bottom but the vertically-averaged model predicts a bottom stress. It is incorrect even in the steady state since the bottom stress is generally not proportional to the averaged velocity divided by some power of the depth. In particular, from the calculations it can be shown that off-shore the vertically-averaged model indicates a bottom stress much less than that predicted by the three-dimensional model while near-shore the opposite is true. From this it follows that off-shore the slope of the surface elevation (which is proportional to the sum of the surface wind stress and the bottom stress) and therefore the surface elevation itself as predicted by the vertically-averaged model should be less than that predicted by the three-dimensional model. This is shown from the calculations in Fig. 4b and is typical of off-shore positions. Near shore (Fig. 4a), the surface elevation is approximately the same for both models.

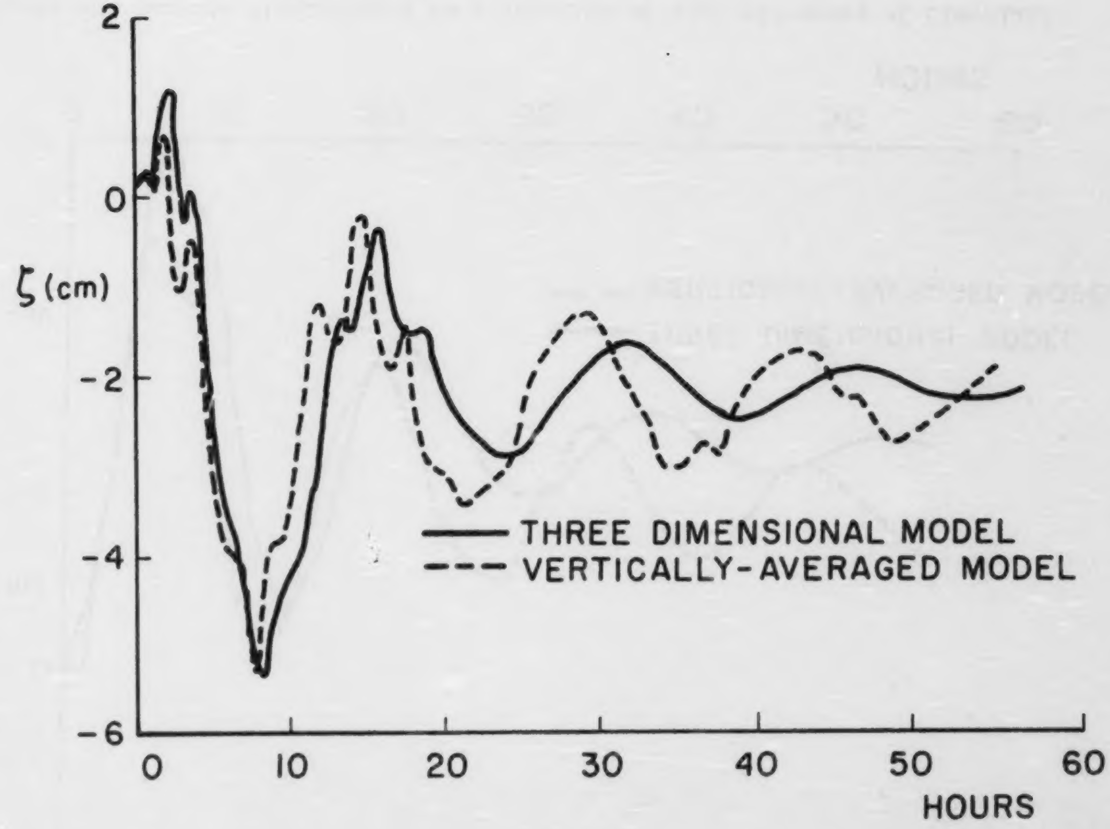

Figure 4a. Surface displacement as a function of time at Cleveland.

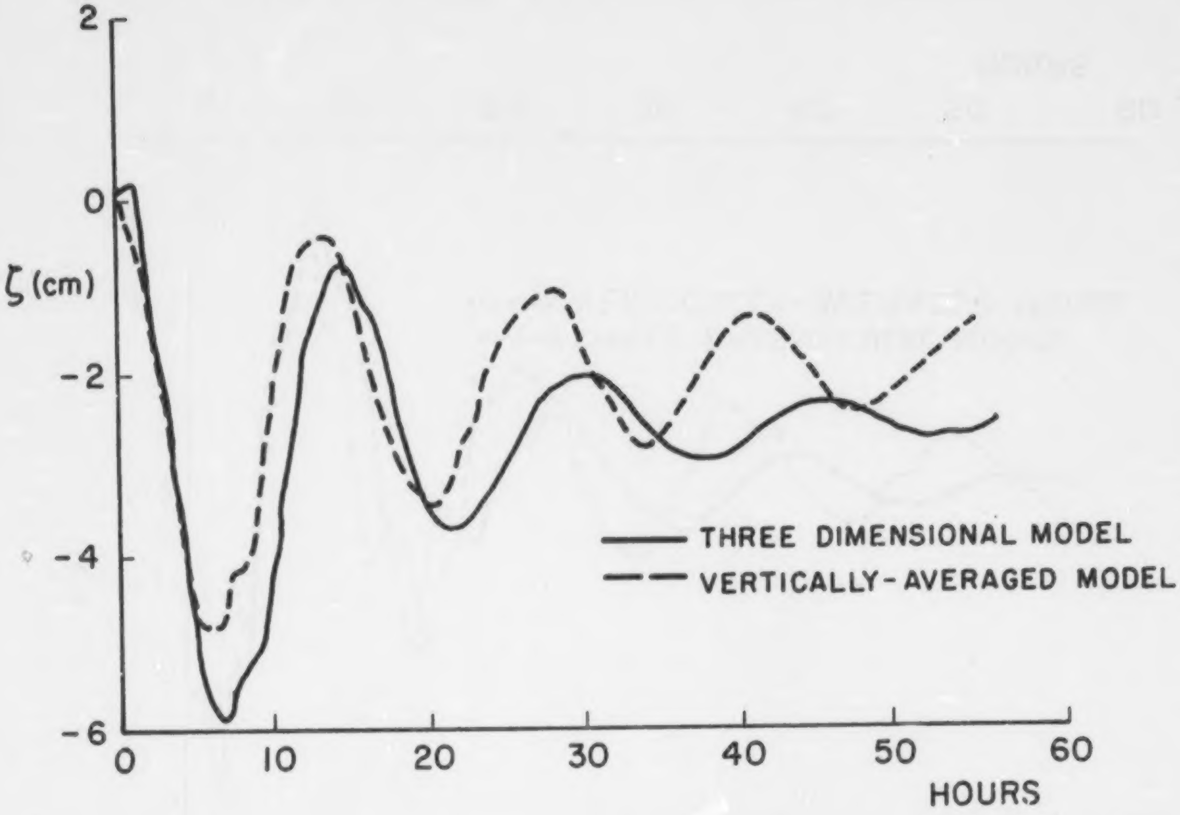

Figure 4b. Surface displacement as a function of time off-shore of Cleveland half-way across the lake.

The differences in the results of the two models are probably more obvious in Lake Erie since Lake Erie is relatively shallow and the bottom stress is comparable in magnitude to the wind stress. Limited numerical experiments with other bottom friction laws and parameters showed similar results to those above.

An alternative numerical procedure is the use of the rigid-lid assumption (Berdahl 1968, Bryan 1969), i.e., $w(z = 0) = 0$. This approximation is used to eliminate surface gravity waves and the small time scales associated with them, greatly increasing the maximum time step possible in the numerical computations. In this approximation, the high frequency surface variations associated with gravity waves are neglected while the steady-state results are calculated correctly and are the same as for the free-surface case.

Some interesting calculations using the vertically-averaged equations and the rigid-lid assumption have been made of the thermal discharge from the Point Beach power plant into Lake Michigan (discussed more extensively in Section 8.1 on the basis of a three-dimensional model). For simplicity, an idealized case of a discharge into a constant depth basin is discussed here. Relevant parameters are based on field measurements taken at the outfall site (Policastro and Tokar, 1972) and are as follows: flow rate, 24.7 m^3/sec; outfall width, 10.8 m; outfall depth, 4.2 m; maximum discharge velocity, 0.9 m/sec. No winds or cross-currents are present.

The steady state or quasi-steady state is of major interest. However, the result is obtained by solving a time-dependent problem. The steady-state solution is obtained as the limit of the time-dependent problem as time increases. The flow is initiated by assuming an impulsive start to the discharge and a steady discharge thereafter. Figs. 5 to 8 show the integrated velocities at various times (t = 87.5 secs, 262.5 secs, 937.5 secs, and 1575.0 secs) as the flow develops to a steady state. The vortices formed initially and then swept out with the flow are quite apparent. Similar features are evident in the three-dimensional case.

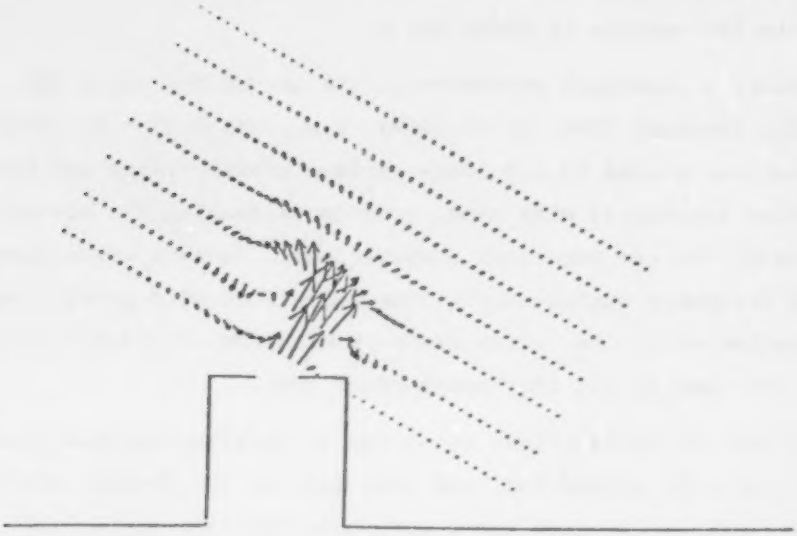

Figure 5. Vertically-averaged velocities, t = 87.5 sec.

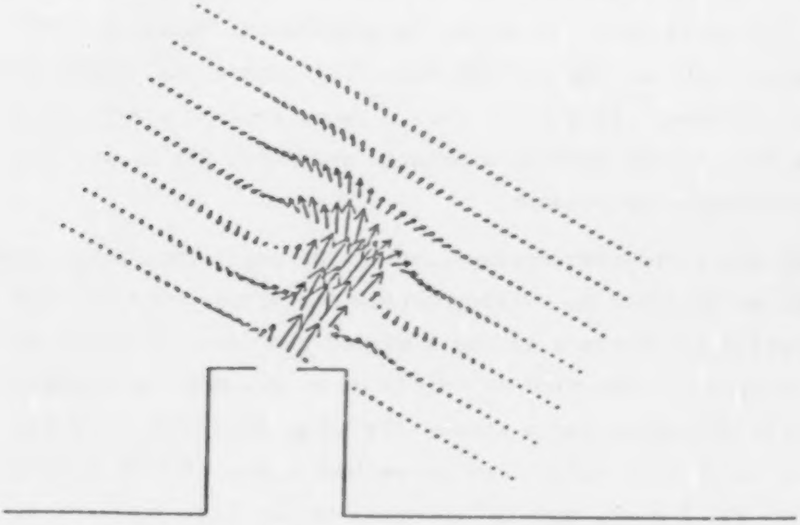

Figure 6. Vertically-averaged velocities, t = 262.5 sec.

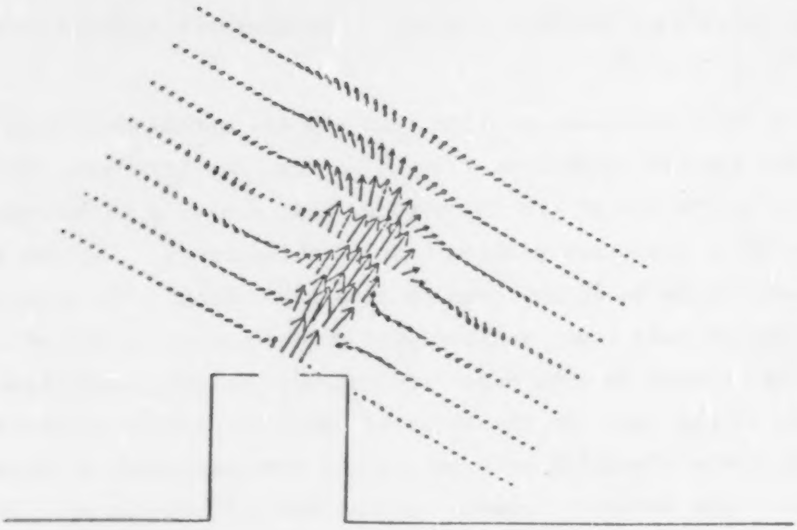

Figure 7. Vertically-averaged velocities, t = 937.5 sec.

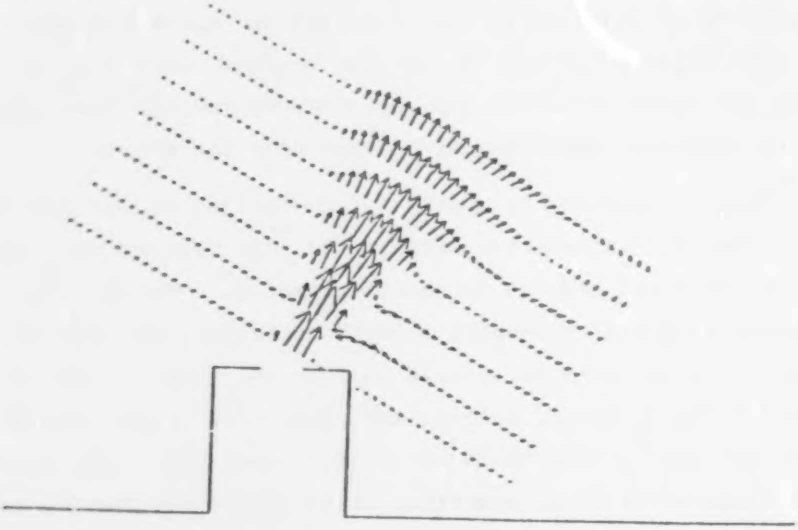

Figure 8. Vertically-averaged velocities, t = 1575 sec.

Another promising numerical method is the alternating-direction-implicit (ADI) method (Peaceman and Rachford 1955, Douglas 1955). The method is usually stable for much larger numerical time steps than is allowed by explicit methods. Considerable savings in computer time may be possible.

The vertically-averaged equations and the ADI method have been used to solve for the time-dependent flow in Saginaw Bay (Allender, 1975). In addition to the use of the ADI method, this analysis is interesting because of an important problem that it illustrates. Saginaw Bay is a large bay (30 km by 70 km) opening into Lake Huron. The average depth of the bay is only 9 m. Surface wind stresses and forcing of the bay waters by seiches in Lake Huron are the main driving mechanisms of the currents in the bay. In the Allender analysis, seiche activity in Lake Huron was simulated by specifying a time-dependent surface elevation along the open boundary between Saginaw Bay and Lake Huron. It is known (Reid and Bodine 1968, Wurtelle, Paegle, and Sielecki 1971) that specifying the flow or surface elevation at an open boundary will partially block the flow at the boundary and reflected waves will result. Less restrictive conditions at an open boundary have been investigated by Chen and Miyakoda (1974) and satisfactory results have been obtained by using numerical smoothing techniques near the boundary.

An alternative approach to specifying conditions at the open boundary is to allow full interaction between the solutions in the region being investigated and the surrounding region. Using a fine grid size in the surrounding region usually requires considerable computer capacity so that a coarser grid is usually used there. However, it is known (Matsuno 1966, Browning, Kreiss, and Oliger 1973) that wave motions in two unequal grids have different phase speeds due to the truncation error. Because of this, numerical difficulties may develop in this method also.

As indicated previously, a vertically-averaged model does not give details of the vertical variation of the flow. In particular, it should be noted that the maximum horizontal velocity can be many times as great as the averaged horizontal velocity. Indeed, for a constant depth basin with a constant wind, the vertically-averaged steady-state velocity is zero everywhere while in general the actual steady-state velocity at any depth is non-zero and proportional to the wind velocity. Because of this, contaminants may be transported to much greater distances and in different directions than is indicated by the mean flow (Sheng and Lick, 1975). To approximately include the effect of vertical velocity gradients in the vertically-averaged models, one must use an effective eddy coefficient which is greater than the eddy coefficient used in a three-dimensional model. This procedure is valid when the sub-grid scale convection can be approximately treated as random, as implied by the use of an eddy coefficient (Csanady 1973, Galloway and Vakil 1975).

SECTION VI

STEADY-STATE MODELS

In this section, models describing the steady-state, wind-driven circulation in shallow lakes will be discussed. The basic model (discussed in Section 6.1) is an extension of an analysis due to Welander (1957). In the present analysis, the assumptions are made that (1) the flow is steady, (2) the density is constant, (3) the nonlinear convection terms can be neglected, (4) the horizontal diffusion terms can be neglected, (5) the vertical eddy diffusivity is constant, and (6) the pressure is hydrostatic. In these models, currents due to through flows have been included.

Time-dependent effects can be very important and are treated in the following sections. However, there are periods when currents in lakes are essentially steady, or can be treated in a quasi-steady manner, and this makes a steady-state analysis applicable. The Great Lakes are stratified during the summer months but, during the rest of the year, the density is fairly constant throughout the lake, making the constant density assumption valid. For the overall lake circulation, it can be shown (Janowitz 1970, 1972, Gedney and Lick 1972, Sheng and Lick 1975) that approximations (3) and (4) are valid except in narrow regions or boundary layers near shore, regions smaller than the usual grid size used in calculations of lake circulation. Very little is known quantitatively of the spatial variation of eddy viscosity and therefore the assumption of constant eddy viscosity is a necessary evil.

In Section 6.2, the effects of partial ice cover are discussed using the same basic model as in 6.1 except that the inclusion of ice cover requires that the boundary condition at the ice-water interface be that of no slip. In Section 6.3, a discussion is given of how the model is extended to more accurately take into account near-shore topography and geometry. For maximum accuracy, the near-shore model must be coupled to the overall lake circulation model and this coupling process is also described. In Section 6.4, a further extension of the basic model to a two-layer stratified model is described. This gives an idealized description of the flow in a stratified lake. Only flows in simple basins have been calculated using this model.

6.1 THE WIND-DRIVEN CIRCULATION IN LAKE ERIE

By means of a model utilizing the assumptions discussed above, the wind-driven circulation in Lake Erie has been investigated. Details of the investigation can be found in several reports by Gedney and Lick (1970, 1971, 1972) and the computer program has been documented and is available. A brief summary of this work is presented here.

In discussing the equations, it is convenient to introduce the following dimensionless variables:

$$x^* = \frac{x}{L} \;, \quad y^* = \frac{y}{L} \;, \quad z^* = \frac{z}{\varepsilon L}$$

$$u^* = \frac{u}{u_r} \;, \quad v^* = \frac{v}{u_r} \;, \quad w^* = \frac{w}{\varepsilon u_r}$$

$$p^* = \frac{p}{\rho g h_r} \;, \quad \varepsilon = \frac{h_r}{L} \;, \quad \zeta = \frac{\zeta}{\zeta_r}$$

$$Eu = \frac{g h_r}{L\, u_r f} \;, \quad E = \frac{A_v}{f\, h_r^2} \;, \quad \zeta_r = \frac{\tau_r L}{\rho g h_r}$$

where L is a characteristic horizontal dimension of the lake, u_r is a characteristic horizontal velocity, ζ is the displacement of the water surface from nominal, τ_r is a characteristic wind stress, ζ_r is a characteristic surface displacement, h_r is a characteristic depth, Eu is the Euler number, and E is the Ekman number. It is also convenient to define the quantities

$$\tau = \tau_x + i\,\tau_y \quad , \quad q = u^* + i\,v^*$$

$$d = \pi \left(\frac{2\,A_v}{f} \right)^{1/2} \quad , \quad \lambda = \frac{2\,\pi\,h_r}{d}$$

$$\tau^* = \frac{\tau}{\tau_r}$$

where $i = \sqrt{-1}$, τ is the wind shear stress with components τ_x and τ_y, q is the velocity, and d is the friction depth.

In the rest of this section, the above non-dimensional variables will be used. However, for simplicity of notation, the asterisks will be dropped. The resulting system of equations and boundary conditions is

$$\frac{\partial u}{\partial x} + \frac{\partial v}{\partial y} + \frac{\partial w}{\partial z} = 0 \tag{19}$$

$$-v = -Eu\frac{\partial p}{\partial x} + E\,\frac{\partial^2 u}{\partial z^2} \tag{20}$$

$$+u = -Eu\frac{\partial p}{\partial y} + E\,\frac{\partial^2 v}{\partial z^2} \tag{21}$$

$$\frac{\partial p}{\partial z} = -1 \tag{22}$$

$$z = 0: \quad \tau = \frac{2}{\lambda^2}\,\frac{\partial q}{\partial z} \quad , \quad p = p_a \quad , \quad w = 0 \tag{23}$$

$$z = -h: \quad q = 0, \quad w = 0 \tag{24}$$

Governing Equation for the Stream Function

Eq. (22) for the vertical pressure gradient can be integrated to give

$$\frac{\partial p}{\partial n} = \alpha\,\frac{\partial \zeta}{\partial n} \tag{25}$$

where $\partial/\partial n = \partial/\partial x + i\,\partial/\partial y$, and $\alpha = \rho_r/h_r$. The horizontal derivatives of the atmospheric pressure are $O(10^{-1})$ smaller than $\alpha\,\partial\zeta/\partial n$ and therefore have been neglected.

The pressure can be eliminated from Eq. (20) and Eq. (21) by the use of Eq. (25). Eqs. (20) and (21) can then be solved to give the horizontal velocities as functions of the local slope and wind stress. The resulting solution is

$$q = i\frac{\partial\zeta}{\partial n}\left(\frac{\cosh\lambda' z}{\cosh\lambda' h} - 1\right) + \frac{\tau\lambda}{(1+i)}\,\frac{\sinh[\lambda'(h+z)]}{\cosh\lambda' h} \tag{26}$$

where $\lambda' = (1 + i)\lambda/2$. The w velocity can be readily determined from Eq. (19) using Eq. (26).

The above equation and the continuity equation can be integrated vertically to give

$$U + iV = a\tau + b\frac{\partial\zeta}{\partial n} \tag{27}$$

$$\frac{\partial U}{\partial x} + \frac{\partial V}{\partial y} = 0 \tag{28}$$

where a and b are functions of the local depth, $U = \int_h^0 u\,dz$ and $V = \int_h^0 v\,dz$.

A volume transport stream function can be defined so as to satisfy Eq. (28) identically, i.e., $U = \partial\psi/\partial y$ and $V = -\partial\psi/\partial x$. By substituting these relations into the set of equations given by the real and imaginary parts of Eq. (27), and by eliminating $\partial\zeta/\partial x$ and $\partial\zeta/\partial y$, one obtains a single equation for the stream function, which is

$$\nabla^2\psi + \gamma_1\frac{\partial\psi}{\partial x} + \gamma_2\frac{\partial\psi}{\partial y} = \gamma_3 \tag{29}$$

where γ_1, γ_2, and γ_3 are functions of the local depth and bottom slopes, and γ_3 is also a function of the applied wind stress. The expressions for γ_1, γ_2, and γ_3 are fairly lengthy and are omitted here. See Gedney and Lick (1971) for these expressions and all details associated with the formulation of the problem.

Method of Solution

The region of Lake Erie for which the above stream function equation must be solved is multiply connected because of the islands in the western basin. The value of the stream function on the main land shore can be specified within a single arbitrary constant as determined by the river inflows and outflows. The value of the stream function for the island boundaries is not known a priori. This value is determined by requiring the surface elevation to be continuous around each island, i.e.,

$$\oint \frac{\partial \zeta}{\partial s} ds = 0 \tag{30}$$

where the integration path is around an island.

In the present calculations for Lake Erie, three islands were incorporated. The value for the stream function on each island boundary was uniquely determined by summing four solutions, i.e.,

$$\psi = \psi^0 + d_1\psi^1 + d_2\psi^2 + d_3\psi^3$$

The boundary and wind conditions for these four solutions are shown in Table 1. In Table 1, $\psi_r(s)$ is the value of the stream function on the external shore boundary and is specified by the river inflows and outflows. The d_1, d_2, d_3 constants were then determined so that the above line integral around each island was satisfied. In the present problem, three equations are given for these three unknowns. The summed solution determines the proper stream-function value on each island boundary.

Table 1. STREAM FUNCTION BOUNDARY CONDITIONS

ψ^i Solution	External Shore	Island 1	Island 2	Island 3	Wind Condition
ψ^0	$\psi_r(s)$	1	1	1	τ_x, τ_y
ψ^1	0	1	0	0	0
ψ^2	0	0	1	0	0
ψ^3	0	0	0	1	0

Eq. (29) was solved by finite difference methods. At all grid points, a five point central difference equation was used. Lake Erie was divided into two regions. One was an island region as shown in Fig. 9 in which a 0.805 km (0.5 mile) square grid was used. The boundaries in this region were approximated by taking the closest 0.805 km grid point as the boundary. The second region was composed of the remainder of Lake Erie and in this region a 3.22 km (2 mile) square grid was used except for the points adjacent to the boundary. For these points, nonsymmetrical difference equations were written that used the actual distance from the grid point to the boundary. Fig. 10 shows the shoreline of Lake Erie using the 2 mile grid as well as the island region in relation to the entire lake. The island region contained some 2800 grid points and the rest of the lake contained some 2250 grid points. The Lake Erie bottom depth at the regular grid points was determined by curve-fitting irregularly spaced data taken from the U.S. Lake Survey charts.

A combination of successive over-relaxation by points and lines was used to solve the system of finite-difference equations. A complete iteration was performed in one region. Then from these new values, interim interface values between the two regions were formed for the second region. A complete iteration was then performed in the second region. For these new values in the second region, interface values were in turn formed for the first region. The process was repeated

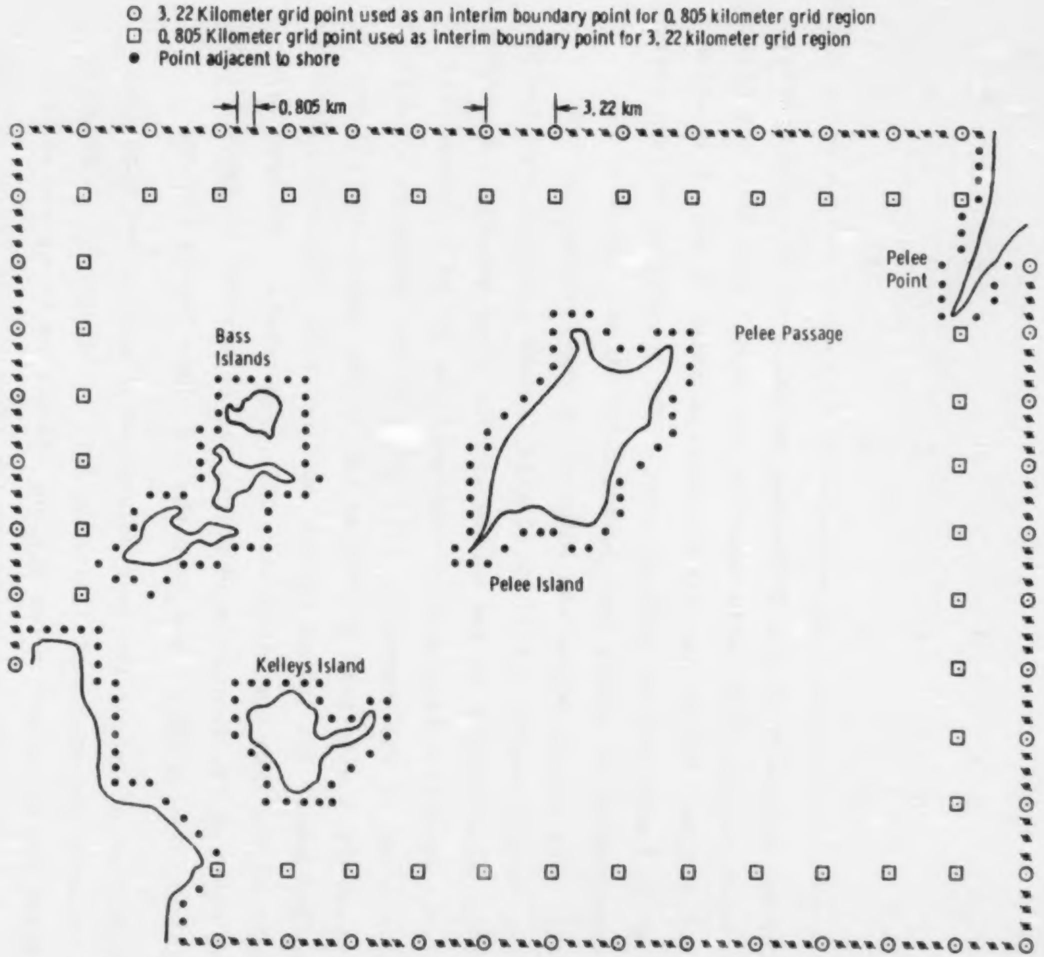
3.22 Kilometer grid point used as an interim boundary point for 0.805 kilometer grid region
0.805 Kilometer grid point used as interim boundary point for 3.22 kilometer grid region
Point adjacent to shore
0.805 km
3.22 km
Pelee Point
Pelee Passage
Bass Islands
Pelee Island
Kelleys Island

Figure 9. 0.805 kilometer (0.5 mile) grid for Island region

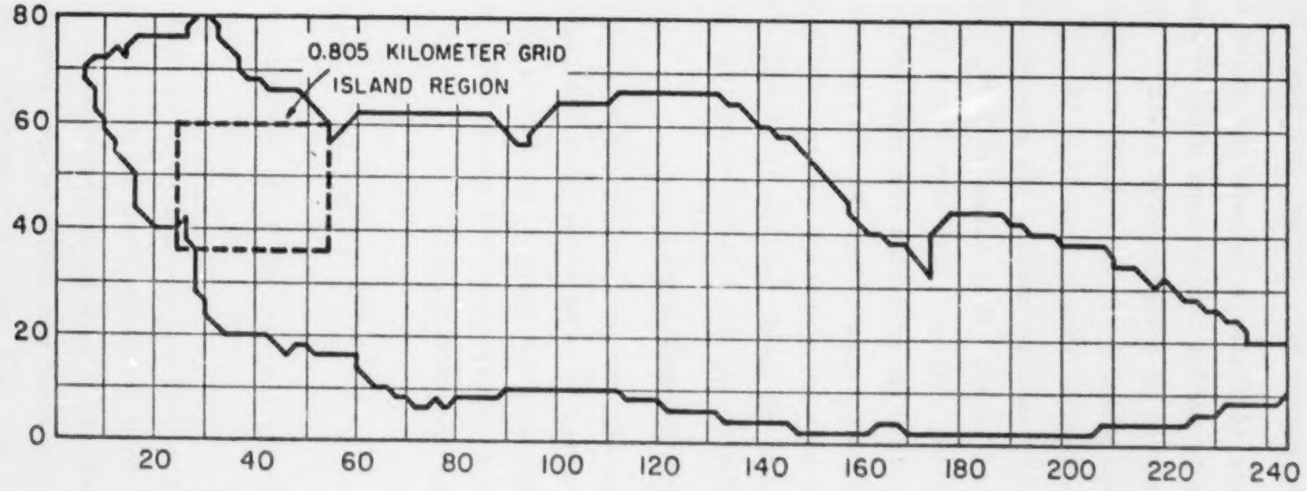
0.805 KILOMETER GRID
ISLAND REGION
80
60
40
20
0
20
40
60
80
100
120
140
160
180
200
220
240

Figure 10. Shoreline of Lake Erie on 3.22 km (2 mile) grid.

until the maximum relative error between successive iterations at any grid point was less than 10^{-5}. The grid points, where the interface values between the two regions were formed, are shown in Fig. 9.

The discretization error (difference between the exact and numerical solutions) was checked by making comparisons with an analytical solution for the deep-water equation in a rectangular basin. For a square mesh with nondimensional spacing of $\Delta = 1/50$, the numerical and analytical solutions agreed to within less than 1%. By changing grid sizes for simple geometry shallow basins, the discretization error was found to be proportional to Δ^2. Grid sizes of 3.22, 1.6., and 0.805 km ($\Delta = 1/40$, 1/80, 1/160, respectively) were tried in the island region. It was found that the 0.805 km grid size was necessary to obtain consistent and accurate line integrals (Eq. 30) around each island. The 0.805-km grid size is also necessary to accurately represent the island boundaries. Based on these results it is felt that the grid sizes used are not inducing any significant numerical errors.

Results of the Numerical Calculations

Numerical solutions for the stream function and velocities in Lake Erie were obtained for a variety of wind directions and magnitudes. Shown and discussed here are the results for a wind of 10.1 m/sec. This speed was measured at 10 meters above the water. The shear stress used in the calculations was determined from

$$\tau = 0.00237\rho_a W_a^2$$

where ρ_a is the density of the air and W_a is the wind speed (see Section 4.2).

In the calculations, the wind was assumed to be uniform over the entire lake surface. This condition does not occur all the time on Lake Erie but it was found to be a good approximation for the periods for which the calculations and measurements were compared. A friction depth d of 27.4 meters was used because it provided the best agreement between the numerical results and current-meter measurements. This value corresponds to an eddy diffusivity A_v of 38.0 cm^2/sec.

All the results shown herein include a Detroit River inflow of 5380 m^3/sec and an equal outflow via the Niagara River. Other calculations have shown that the remaining rivers only modify the flow locally near the mouth of the rivers for moderate winds such as used here.

Lake velocity plots for the W 50°S wind are shown in Figs. 11 to 15. In these figures, the beginning of the arrow represents the actual location of the current represented by the arrow. The magnitude of the velocity can be determined from the velocity scale indicated on the figure. Note that the velocity scale is different from plot to plot. In Fig. 15, arrows pointing toward the top of the plot represent the vertical velocities toward the lake surface.

The solution given by Eq. (26) represents the sum of the Ekman drift currents and gradient current. Figs. 11 and 12 show that a top-surface mass flux is being transported toward the eastern and southern boundaries. A subsurface current driven by the surface gradients returns the surface mass flux in the opposite direction as shown in Figs. 13 and 14. In the central and eastern basins, surface currents at 0.4 meters are, in general, smaller in the center of the lake than near the shore. This effect is essentially due to the relatively large subsurface return current down the center of the lake, which is opposite in direction to the surface current and subtracts from it. Fig. 15 shows the vertical velocities at mid-depth. Strong vertical currents near shore are evident.

Comparison of the Numerical Results with Current Measurements in Lake Erie

The U.S. Federal Water Pollution Control Administration (now part of the Environmental Protection Agency (EPA)) established a system of automatic current-metering stations in Lake Erie in May, 1964. The EPA data consisted of velocity readings taken every 20 min. The data was never published but fortunately the EPA lent it to the authors.

To compare the water-current measurements with our calculations, the 20-min readings were vectorially summed over a 24-hour period to form

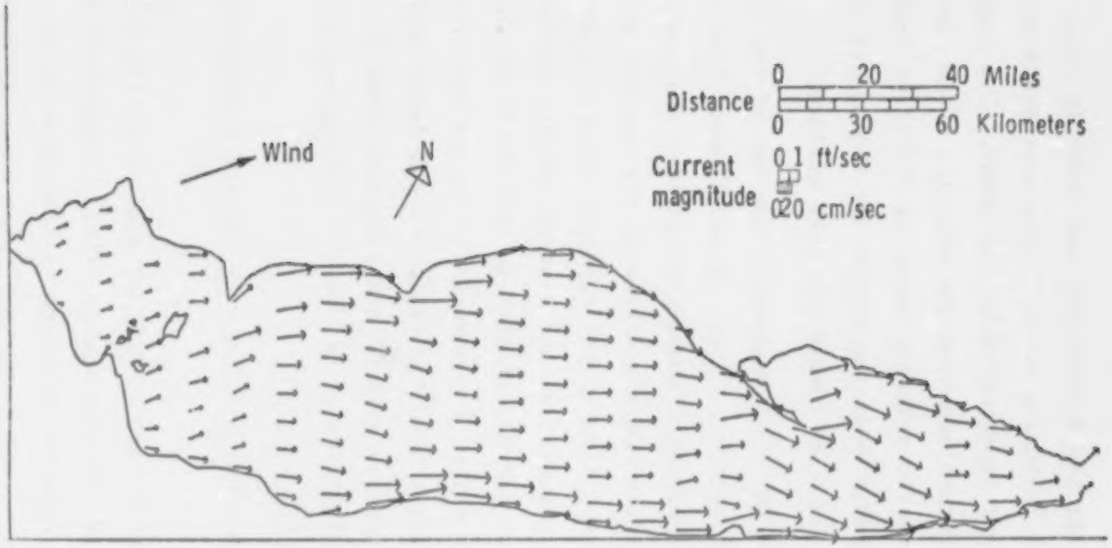
Distance
0
20
40 Miles
0
30
60 Kilometers
Current magnitude
0.1 ft/sec
0 20 cm/sec
Wind
N

Figure 11. Horizontal velocities at a constant 0.4 meters (1.5 ft) from surface. Wind direction, W 50 S; wind magnitude, 10.1 meters per second (22.7 mph); friction depth, 27.4 meters (90.0 ft); rivers: Detroit, Niagara.

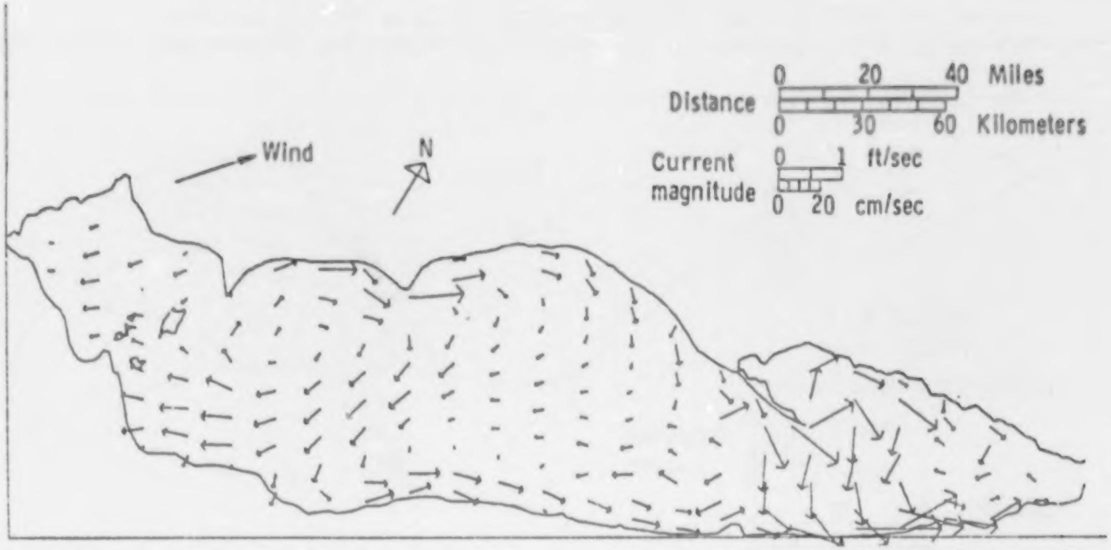
Wind
N
Distance
0 20 40 Miles
0 30 60 Kilometers
Current magnitude
0 1 ft/sec
0 20 cm/sec

Figure 12. Horizontal velocities at a constant 6.7 meters (22.0 ft) from surface. Wind direction, W 50 S; wind magnitude, 10.1 meters per second (22.7 mph); friction depth, 27.4 meters (90.0); rivers: Detroit, Niagara.

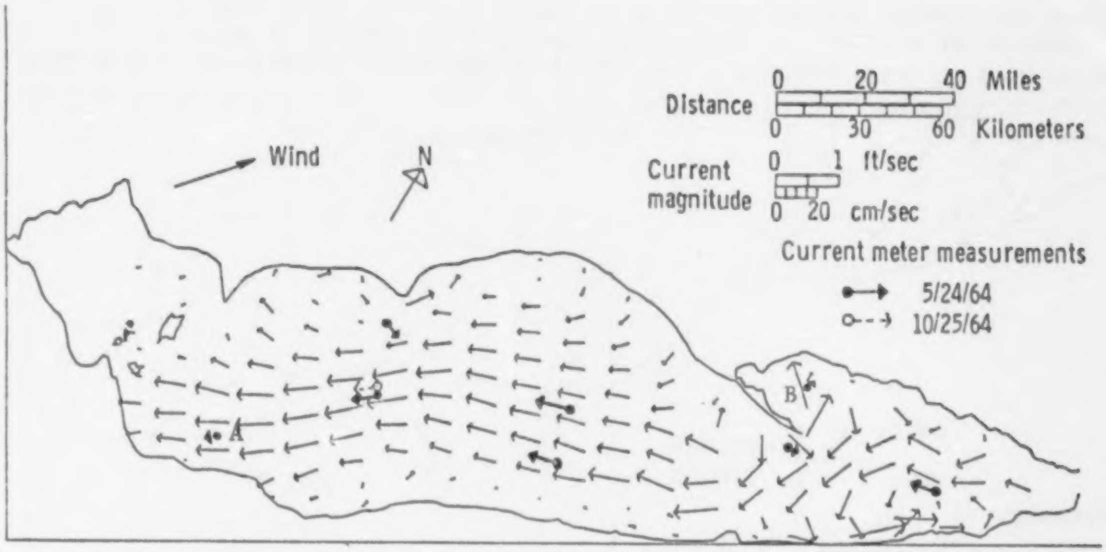

Wind
N
Distance
0 20 40 Miles
0 30 60 Kilometers
Current magnitude
0 1 ft/sec
0 20 cm/sec
Current meter measurements
5/24/64
10/25/64
A
B

Figure 13. Horizontal velocities at a constant 9.9 meters (32.8 ft) from surface. Wind direction, W 50 S; wind magnitude, 10.1 meters per second (22.7 mph); friction depth, 27.4 meters (90.0 ft); rivers: Detroit, Niagara.

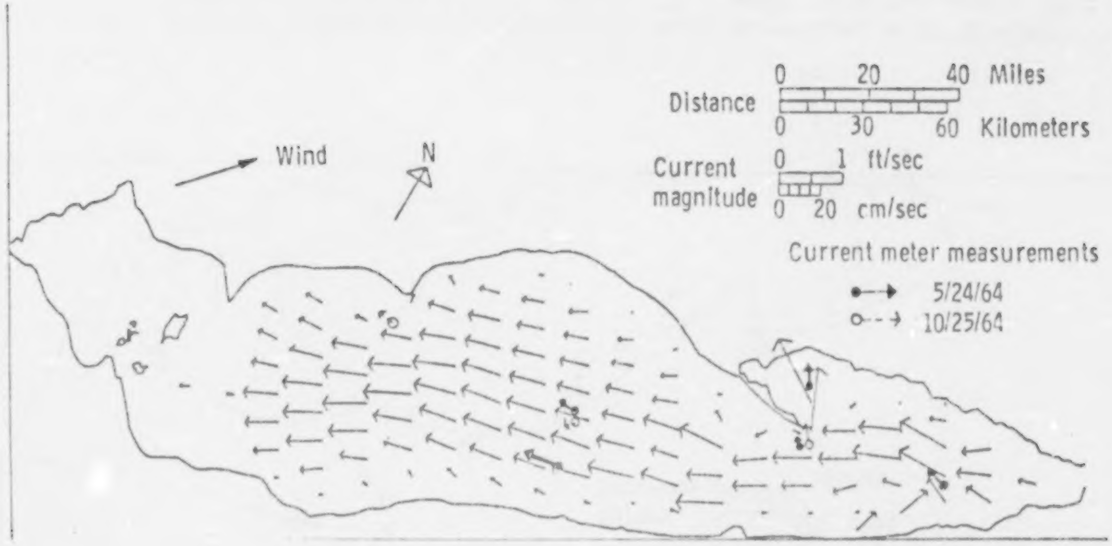
Wind
N
Distance
0
20
40
Miles
0
30
60
Kilometers
Current magnitude
0
1
ft/sec
0
20
cm/sec
Current meter measurements
5/24/64
10/25/64

Figure 14. Horizontal velocities at a constant 14.9 meters (49.2 ft) form surface. Wind direction, W 50 S; wind magnitude, 10.1 meters per second (22.7 mph); friction depth, 27.4 meters (90.0 ft) rivers: Detroit, Niagara.

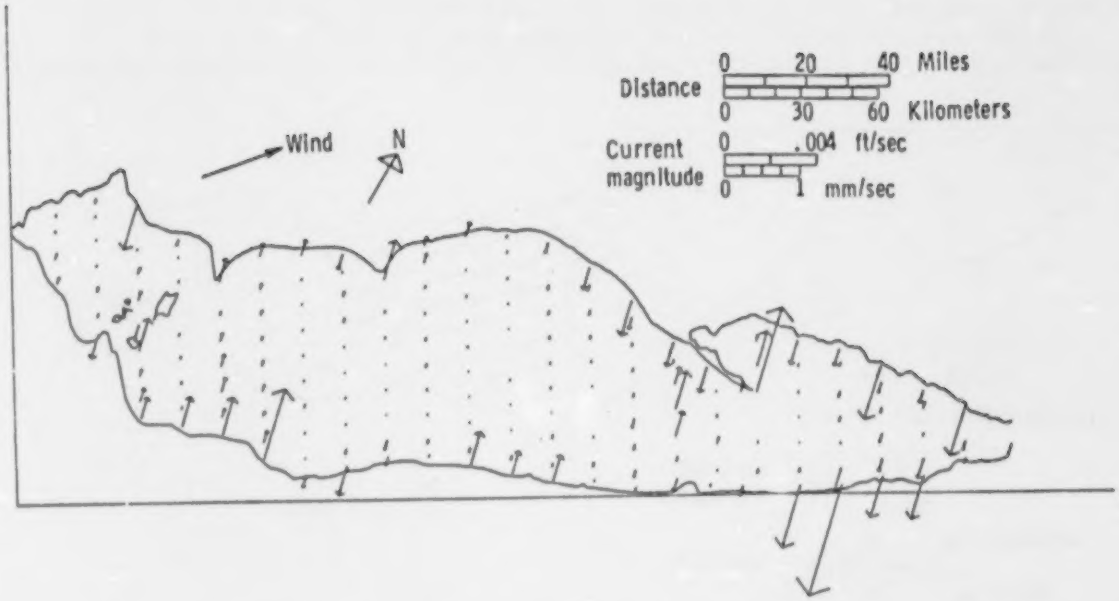
Wind
N
Distance
0 20 40 Miles
0 30 60 Kilometers
Current magnitude
0 .004 ft/sec
0 1 mm/sec

Figure 15. Vertical velocities at mid-depth. Wind direction, W 50 S; wind magnitude, 10.1 meters per second (22.7 mph); friction depth, 27.4 meters (90.0 ft); rivers: Detroit, Niagara.

a resultant current. The resultant magnitude is equal to the vector sum magnitude divided by the number of readings. The time periods used for comparison purposes were those for which the wind was fairly steady for 2 or more days so that any seiche currents were small. The vector summing of the data over a 24-hour period should remove part, if not all, of any small seiche current since the largest seiche period is 14 hours.

The procedure incorporated for determining what wind to use in the numerical calculations for a particular day was to take the average of both the direction and magnitude of the 24-hour resultant wind at each of the U.S. Weather Bureau shore stations. This average wind with its magnitude increased by 1.48 was then used to determine the shear stress at the water surface. The 1.48 factor was determined by comparing shore data with 'over-the-lake' wind data taken by the EPA. On May 24, 1964, the resultant 'over-the-lake' wind was determined to be 10.1 m/sec with direction W 50°S. The resultant winds for the prior two days had been within 20° of this direction and at somewhat less magnitude. However, on May 21, 1964, the resultant winds were approximately E 50°S at roughly 1 m/sec, which is significantly different from the wind on May 24.

The current-meter data for May 24, 1964, as measured at 10 and 15 meters below the surface, is shown in Figs. 13 and 14. Note that the positions of the measurements are different from those of the calculated current vectors. The agreement is markedly good in both magnitude and direction. The discrepancy between the magnitude of the measurements and calculations at point A in Fig. 13 is believed tobe a measurement error since this meter became erratic at a later date. The magnitude of the measurements in the region of point B at first appears to be considerably different from the calculated values. However, the agreement between measurements and calculations is believed to be satisfactory when one considers that the currents are changing rapidly with distance in the point B area. Also, in Figures 13 and 14, the meter measurements are plotted for a W 43°S wind at a velocity of 8.6 m/sec.

These measurements were taken on October 25, 1964. The agreement is again quite good.

The average value of the eddy diffusivity (38 cm^2/sec) used in the calculation of a 10.1-m/sec wind is of the same order of magnitude as that found by Nobel et al. (1968) in Lake Michigan. In addition, the value of the surface velocities in the western basin was found to agree in magnitude with those of Olsen (1950). Unfortunately, additional quantitative current data are not available to further check the numerical results.

The present model has also been applied to Lake Ontario (Bonham-Carter, Thomas, and Lockner 1973, Bonham-Carter and Thomas 1973). Lake Ontario (maximum depth of 220 m) is much deeper than Lake Erie (maximum depth of 70 m) and its depth is generally much greater than the thickness of an Ekman layer. However, there are extensive near-shore regions, such as the Rochester Embayment, which are shallow and therefore shallow-lake theory is essential.

In addition, in order to predict the hydrodynamics and especially the dispersion of contaminants in the near-shore with adequate accuracy, a much smaller grid is needed in the near-shore than that usually used in overall lake circulation models. Because of this, calculations were made using a large grid (2.5 km) for most of the lake and a finer grid (0.625 km) for the Rochester Embayment where more detail was needed. Coupling between the two regions was allowed as in the Lake Erie calculation above.

General comparison of the calculated results with field observations (Casey, 1965) was made for both Lake Ontario and the Rochester Embayment. General agreement was obtained. The calculated results were also compared with the results from a discrete four-layer model (Simons, 1972). There was excellent agreement between the two.

6.2 EFFECTS OF PARTIAL ICE COVER

The Great Lakes are all or partially ice-covered during the winter. However, relatively little work on currents in a partially ice-covered lake has been done. A brief summary of our work (Sheng and Lick, 1973) on the steady-state, wind-driven currents in a partially ice-covered lake follows.

Lake Erie, with average depths of 7.3, 18.3, and 24.4 m for its Western, Central, and Eastern Basins, respectively, is the shallowest of the five Great Lakes. Because of this, it cools comparatively rapidly and ice forms at a relatively early date. Extensive ice cover is first formed in the Western Basin in December and gradually extends to the Central and Eastern Basins. In the thawing period, about March or April, the ice generally drifts eastward and the western part of the lake is free of ice. Different forms of ice may exist on the lake surface, but their thickness is always small compared to the mean depth of the lake.

In our calculations, the basic model used was the same as in the previous section. In the region where the lake was ice covered, the upper boundary condition at $z=0$ was modified so as not to allow horizontal motions, i.e., $u = 0$, $v = 0$. The ice cover was assumed to have negligible thickness and rigidity. Across the interface of the ice-free and ice-covered portions of the lake, it was assumed that the surface displacement and the integrated stream function are continuous.

The method of solution is similar to that described in the previous section. Results were obtained for a rectangular, constant-depth basin, and for Lake Erie with (a) an ice-covered Western Basin, to approximate the freeze-up period, and (b) an ice-covered Eastern Basin, to approximate the thawing period. The values of wind velocities, wind stresses, and vertical turbulent eddy viscosities used in this analysis are the same as those used in the ice-free analysis so that the results could be compared easily. The magnitude of the vertical eddy viscosity is assumed to be the same in the ice-covered and ice-free portions of the lake.

Representative results for the case of Lake Erie with an ice-covered Western Basin are shown in Figs. 16 and 17. These results are for a N7.5 W wind with a velocity of 5.2 m/sec.

Flows at all depths in the region to the north of the Western Basin islands are primarily due to the Detroit River inflow only and therefore small in magnitude. However, horizontal velocities in other parts of the ice-covered portion of the lake are comparable in magnitude to currents in the ice-free portion. This is due to the pressure gradient caused by the wind stress and the subsequent tilting of the surface.

By comparing the present results with the ice-free case, it is found that in the vicinity of the interface the current magnitudes for the present case have generally increased. However, the large currents found in the southern part of the Western Basin in the ice-free case are not present here. At horizontal distances larger than about 45 km from the interface between the ice-covered and ice-free regions, the currents are approximately the same as in the ice-free calculation.

6.3 A NEAR-SHORE MODEL

In order to predict with adequate accuracy the dispersion of contaminants in the near-shore regions of lakes, a much smaller grid is needed than those used in overall lake circulation models. These small-grid, near-shore models must then be coupled with the large-grid, overall lake circulation models for a complete solution. These near-shore models and the coupling process have been investigated by us and a brief summary of a steady-state, near-shore model (Sheng and Lick 1975) is given here. Other near-shore models are discussed in Sections 7.2 and 8.1.

For the present steady-state model, the basic equations, assumptions, and solution procedure are the same as those described in Section 6.1. In most of the following work, grid sizes varying from 1/4 mile to 2 miles have been used. The model has been applied to an analysis of the currents in the off-shore Cleveland area in the absence of, and including, a proposed Lake Erie Jetport. Advocates of this airport have proposed that it be situated on a large man-made island in the lake.

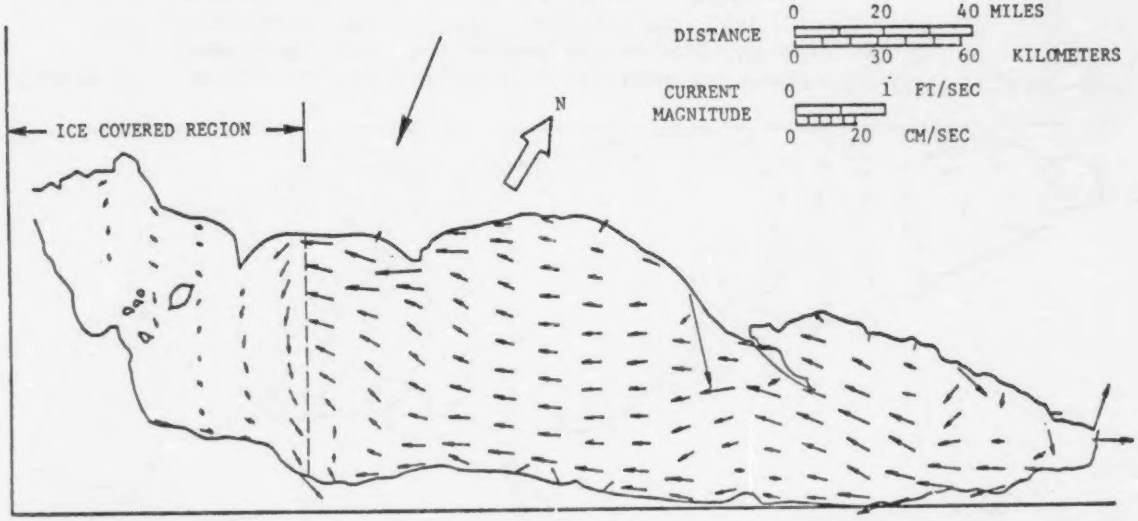
ICE COVERED REGION
N
DISTANCE
0 20 40 MILES
0 30 60 KILOMETERS
CURRENT MAGNITUDE
0 1 FT/SEC
0 20 CM/SEC

Figure 16. Horizontal velocities at a constant 3.6 meters (12.0 ft) from surface.
Wind Velocity: 5.2 meters per second (18 mph), N7.5W.
Frictional depth: 18.2 meters (60.0 ft).
Rivers: Detroit, Sandusky, Maumee, Niagara.

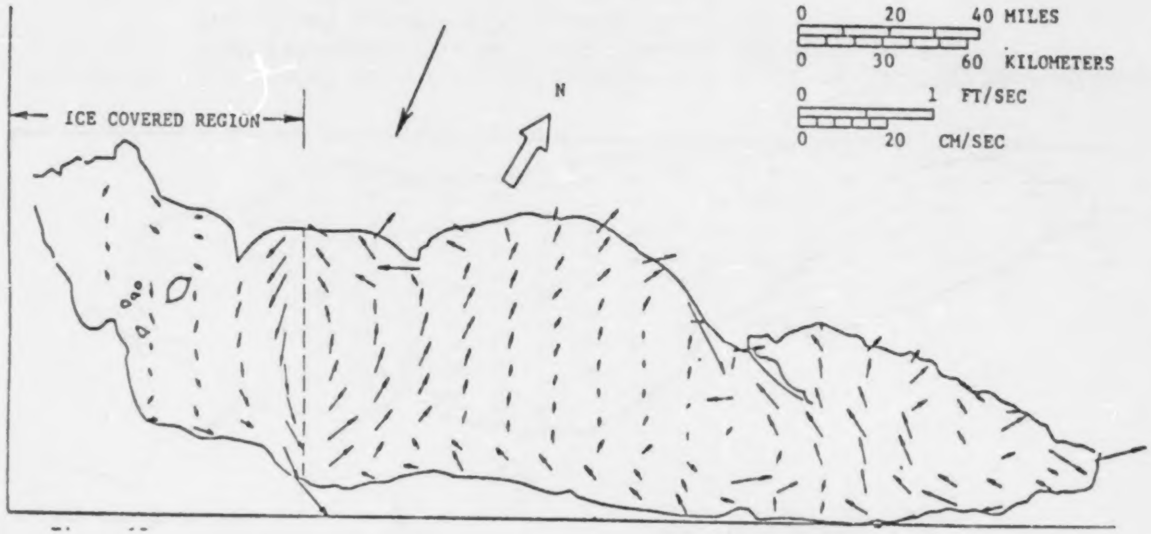
ICE COVERED REGION
N
0
20
40 MILES
0
30
60 KILOMETERS
0
1 FT/SEC
0
20 CM/SEC

Figure 17. Horizontal velocities at a constant 6.7 meters (22.0 ft) from surface.
Wind velocity: 5.2 meters per second (18 mph), N7.5W.
Frictional Depth: 18.2 meters (60.0 ft).
Rivers: Detroit, Sandusky, Maumee, Niagara.

This off-shore area on which a 1/4 mile grid is superposed is shown in Fig. 18.

The steady-state currents have been calculated for various Jetport configurations and for different conditions with wind speed and direction as variables. Representative results of our calculations are shown in Figs. 19 to 23. These results are all for a south-west wind with a velocity of 5.2 m/sec. In the calculations, a 1/4 mile grid was used. The Jetport is located in waters with depths averaging about 15m and gradually decreasing towards shore.

Fig. 19 shows the horizontal surface velocities under the conditions described above and in the absence of the Jetport. For this same case, fig. 20 shows the horizontal velocities at a depth of 30 ft. The return flow is evident. Near-shore currents parallel to the shore are apparent in both figures.

Fig. 21 shows the horizontal surface velocities under the same conditions for an island jetport with dimensions of 2 miles by 3 miles. The interesting result here, and it can be seen at all depths, is that the island configuration does not modify the flow field appreciably. The reason for this can be understood as follows. From the hydrodynamic calculations, it can be shown that in the absence of the Jetport, although there are strong currents near the surface at any horizontal location, there are generally also strong opposing currents near the bottom with the result that the vertically integrated mass flux in most locations near the island and off shore is approximately zero. This is not true near shore, where the vertically integrated mass flux is moderately large and directed towards the East. Because of this, the island does not appreciably block the flow. However, a Jetport which extends to shore would block the flow and extensively modify the near-shore flow field.

This blockage can be seen in Figs. 22 and 23 which show the flow field for a more advanced concept of the Jetport, i.e., an island with extension to shore. Major changes in the flow field are evident due to the blocking of the currents near shore by the Jetport extension.

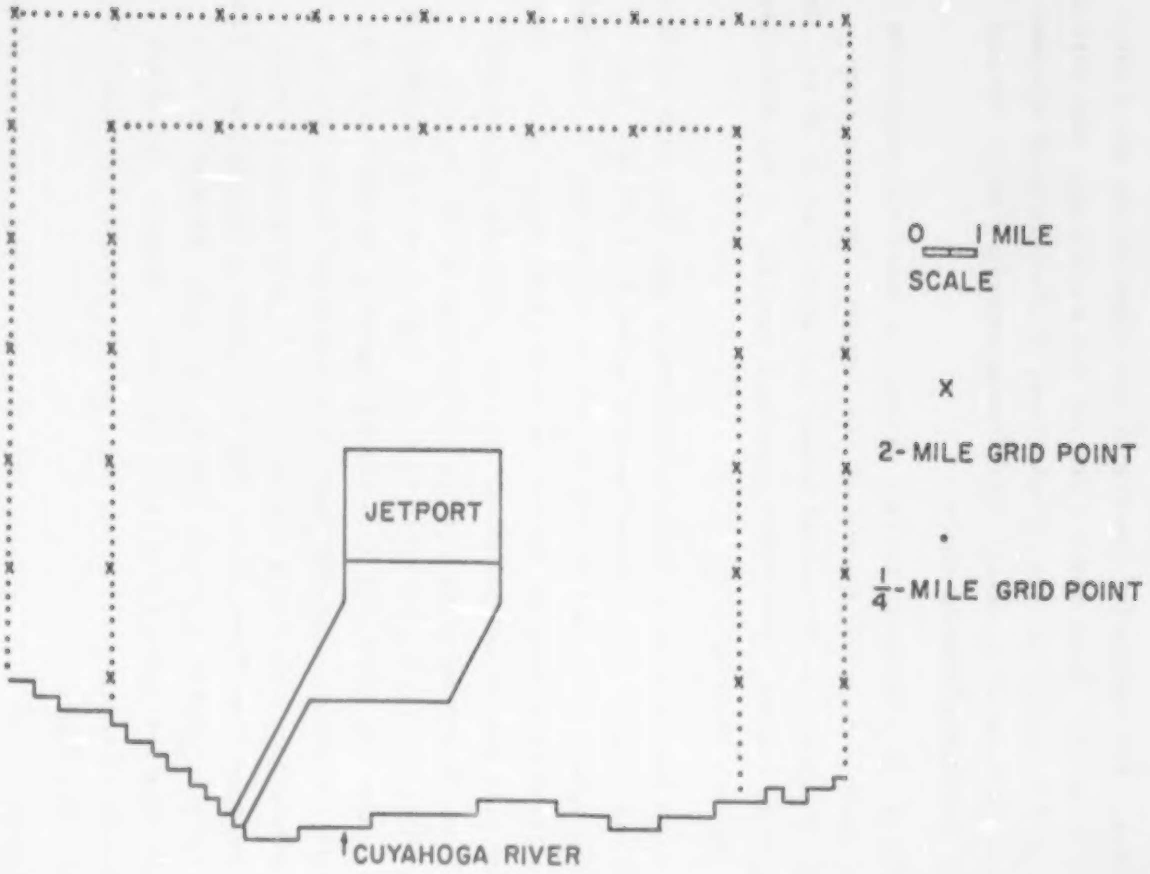
O I MILE
SCALE
X
2-MILE GRID POINT
•
$\frac{1}{4}$-MILE GRID POINT
JETPORT
CUYAHOGA RIVER

Figure 18. Topography of jetport and grid structure in the shore region near Cleveland.

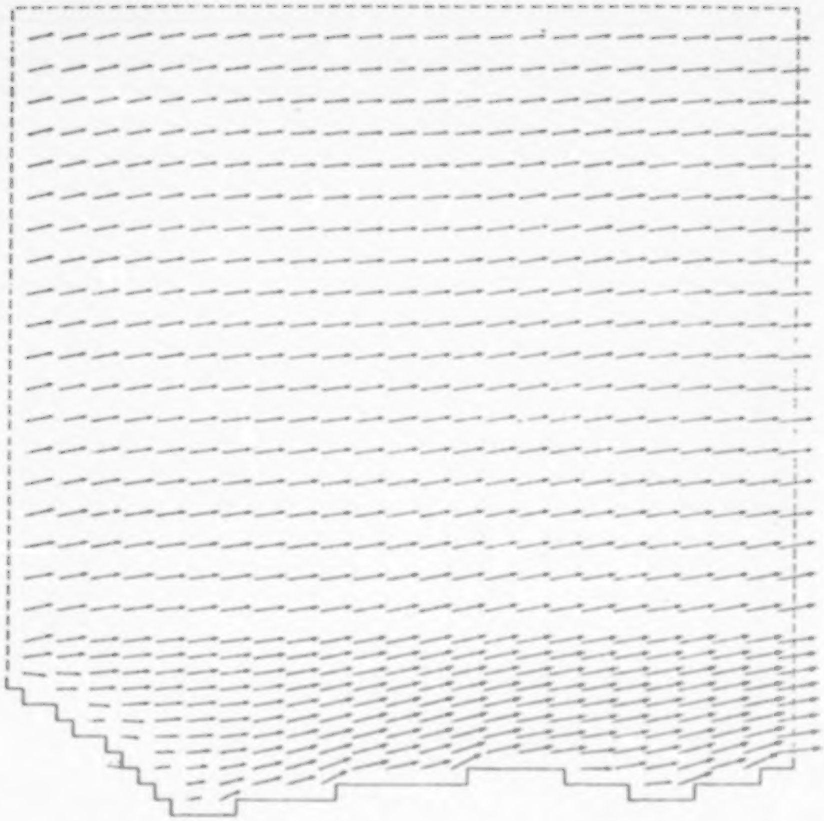

Figure 19. Horizontal velocities at the surface.

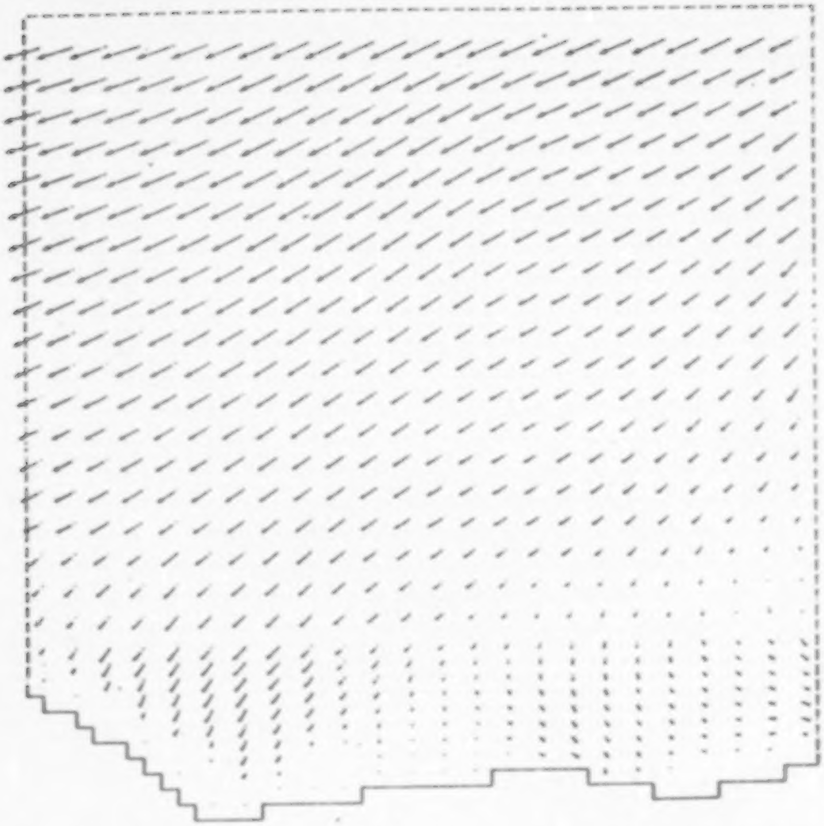

Figure 20. Horizontal velocities at a constant depth of 30 ft. from the surface.

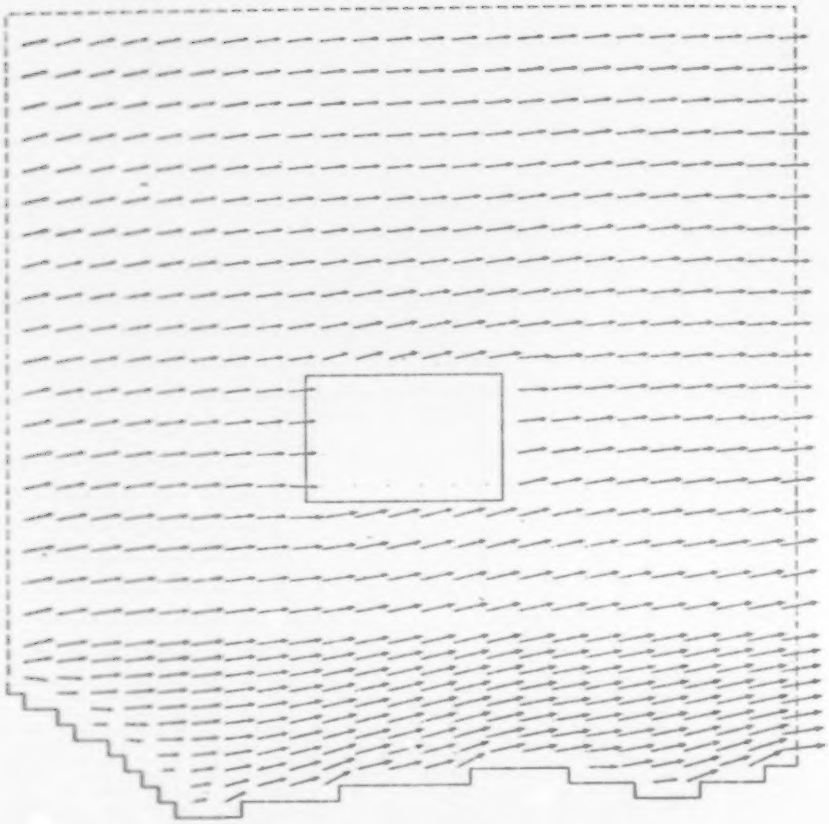

Figure 21. Horizontal velocities at the surface.

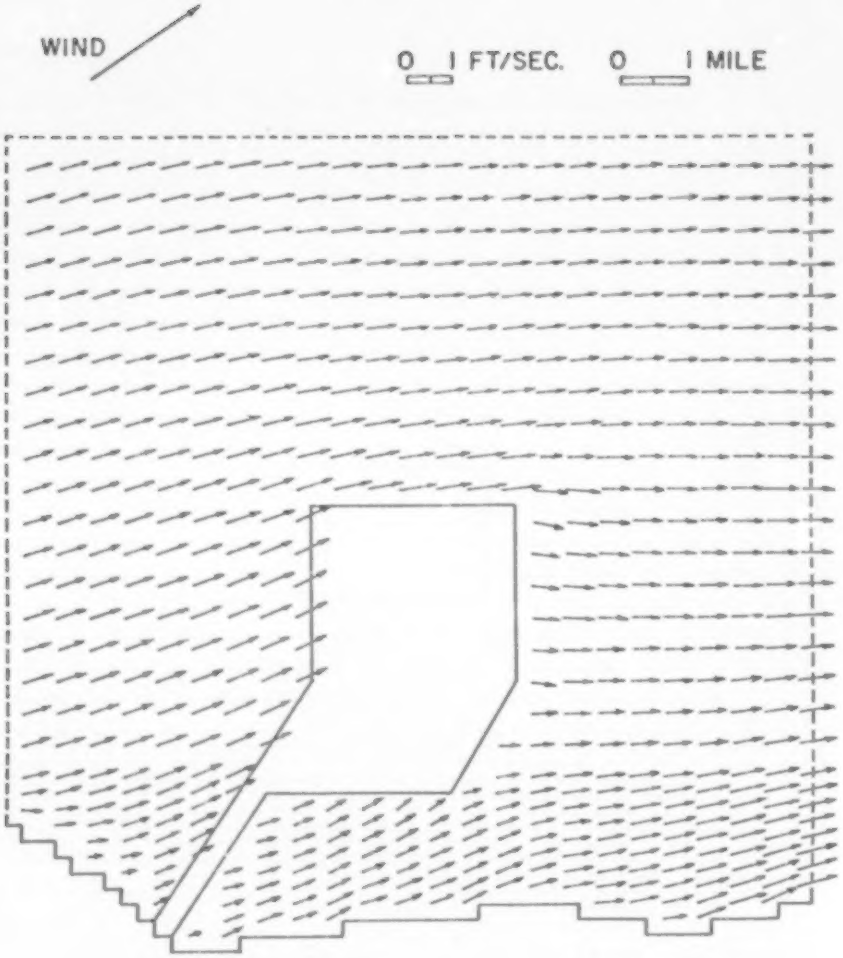

Figure 22. Steady-state near-shore currents in the presence of a jetport island with extension to the shore with $(\tau_x, \tau_y) = (1.55\ \mathrm{dyne/cm^2}, 1.1\ \mathrm{dyne/cm^2})$. Horizontal velocities at the surface.

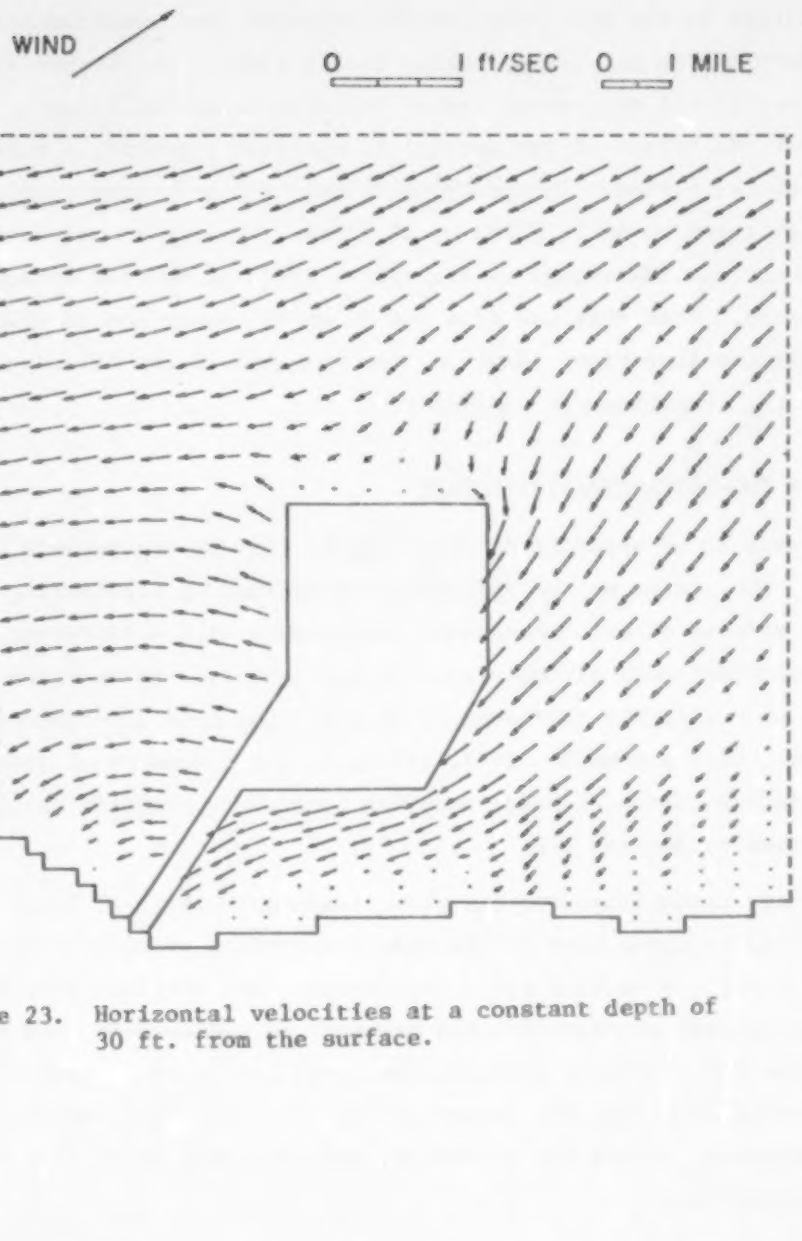

Figure 23. Horizontal velocities at a constant depth of 30 ft. from the surface.

In general, the coupling between the near-shore region and the overall lake is treated by an iteration process as described briefly in Section 6.1. A simpler procedure, although approximate, is to (a) calculate the overall circulation in the lake, and then (b) calculate the flow quantities in the near-shore region assuming that conditions at the boundary of the near-shore region remain fixed. No further iteration is required if the near-shore region is taken to be sufficiently large so that the effect of the Jetport is not felt appreciably outside of the near-shore region. In our calculations, the near-shore region was usually taken to be 12 miles by 12 miles. This region was sufficiently large so that the island configuration could be modeled without iteration. That this was true was shown by comparison of solutions with and without iteration. However, for the case of the island with extension to shore, iteration was necessary.

6.4 A TWO-LAYER, STRATIFIED LAKE

Observations of stratified lakes suggest that during periods of steady winds, the system may be approximately modeled by considering the lake to be made up of two homogeneous layers each with a different density and different eddy diffusivity with the interface between the two layers being of negligible thickness. This model has been investigated by us (Gedney, Lick and Molls, 1972, 1973 a,b) and a summary of these results is presented here. A model assuming continuous property variations is discussed in Section 8.2.

The basic assumptions for the flow within each layer of fluid are identical to those used in the models described previously in this section, i.e., the water density is constant, the vertical eddy diffusivity is independent of position, the pressure is hydrostatic, and the lateral friction and nonlinear acceleration terms can be neglected. The conditions connecting the two layers are (1) the horizontal shear stress is continuous across the interface, and (2) there is no flow normal to the thermocline.

With these assumptions, the basic equations and boundary conditions have been solved numerically (Gedney, Lick, and Molls 1972) and by an asymptotic procedure (Gedney, Lick and Molls 1973 a,b), asymptotic in the sense that the solution is valid as the ratio of hypolimnion to epilimnion eddy diffusivity becomes small. The assumption that this ratio is small is generally valid in moderately to strongly stratified lakes.

From the asymptotic analysis, it is shown that to the lowest approximation and for a constant wind stress the horizontal pressure gradient in the hypolimnion is zero. This does not mean that the velocities in the entire hypolimnion are zero. There is a transfer of shear stress across the thermocline which imparts motion to the hypolimnion water in a thin layer adjacent to the thermocline. Below this boundary layer, the zeroth order velocities in the hypolimnion are zero. When a spatially varying wind stress is present, the horizontal pressure gradient in the hypolimnion is not zero. In this case, velocities are significant throughout the hypolimnion. In previous analyses (Welander 1968, Hamblin 1969), researchers uncoupled the solution in the hypolimnion from that in the epilimnion by assuming that the motion in the hypolimnion can be neglected (quasi-compensation assumption) at least to lowest order. From our results, this assumption does not appear to be valid especially when a spatially variable wind stress is present or for a shallow lake.

Representative results of the asymptotic calculations are shown in Figs. 24 to 28. In general, the governing equations were solved for the position of the thermocline ξ, the position of the lake surface ζ, and the hypolimnion and epilimnion horizontal velocities u and v. All results are presented for a square basin with the following parameter values:

Basin length, L (km)	96.6
Epilimnion temperature (°C)	22
Hypolimnion temperature (°C)	4
Density difference, $\Delta\rho/\rho$	0.002203

Density ratio	0.9977969
Epilimnion eddy viscosity, A_e (cm^2/sec)	17
Nominal wind velocity, U_a (m/sec)	5

The A_e value corresponds to that generated by a wind velocity of 5 m/sec. Small variations in wind velocity about the nominal value are allowed. The wind shear stress is determined by:

$$\tau_x = -0.00237\ \rho_a U_a^2$$

$$\tau_y = 0$$

where ρ_a is the density of the air and the wind drag coefficient is that proposed by Wilson (1960).

The wind drag coefficient and the A_e values used here are the same as the ones used by Gedney and Lick (1972) for current calculations in Lake Erie during the uniform water temperature period (winter). The epilimnion in the two-layer model is considered to be of uniform temperature and for the cases calculated here will have an average thickness of approximately 20 m. Since 20 m is also near the average depth of Lake Erie, the A_e value should be very similar to that used in the Lake Erie calculations.

In obtaining all the thermocline solutions, the boundary conditions were adjusted to give the desired mean thermocline depth.

Case 1: Wind Stress Gradient of Order 1 With Variable Depth

The governing equations were solved for a variable wind stress of the form:

$$\left.\begin{array}{ll} \tau_x = -0.914 - 2.0(x - x^2)(y - y^2) & \begin{array}{l} 0 \le x \le 1 \\ 0 \le y \le 1 \end{array} \\ \tau_y = 0 & \end{array}\right\}$$

acting on the surface of a variable depth basin of the form:

$$\left.\begin{aligned} \frac{\partial h}{\partial x} &= 2.0(1 - 2x)(y - y^2) \\ \frac{\partial h}{\partial y} &- 2.0(1 - 2y)(x - x^2) \end{aligned}\right\} \quad \begin{aligned} 0 \leq x \leq 1 \\ 0 \leq y \leq 1 \end{aligned}$$

The wind stress creates a maximum wind stress curl ($\partial\tau_x/\partial y$) of -0.5 at x = 0.5 and y = 0.0 and 1.0.

The thermocline depth, ξ, contours for these conditions are shown in Fig. 24 for $\delta = 1/24$ where $\delta = (A_h/A_e)^{1/2}$ and A_h is the vertical eddy diffusivity in the hypolimnion. The ξ solution contains boundary layers along y = 0, y = 1.0 and x = 0 boundaries. These boundary layer regions are more clearly shown in Fig. 25 which is a plot of the thermocline depth along the x = 48.3 km (x = 0.5 in non-dimensional form) station. Figure 25 shows the thermocline to have a large shape variation in the cross wind direction.

The horizontal velocities at the surface and at 20 and 35 meter depths are shown in Figs. 26, 27, and 28. The figures show the effect of the shape of the thermocline on the velocities. The thermocline shape produces the clockwise gyre shown in Fig. 27. Below the thermocline at a depth of 35 m, geostrophic velocities of order 1.0-5.0 cm/sec occur. The high geostrophic velocities near the boundaries are created by the η boundary layers, where $\eta \equiv \xi + \zeta$.

The unit order wind stress gradient solution is very dependent on the value of the hypolimnion eddy diffusivity. Figure 25 shows the shape of the thermocline at x = 48.3 km for the same applied wind stress for the cases where $\delta = 1/24$, $1/12$ and ∞. The $\delta = \infty$ case corresponds to the solution where the velocities in the entire hypolimnion are zero, which is the quasi-compensation assumption referred to above.

Case 2: Uniform Wind with Variable Depth

To demonstrate the importance of wind stress curl, the thermocline

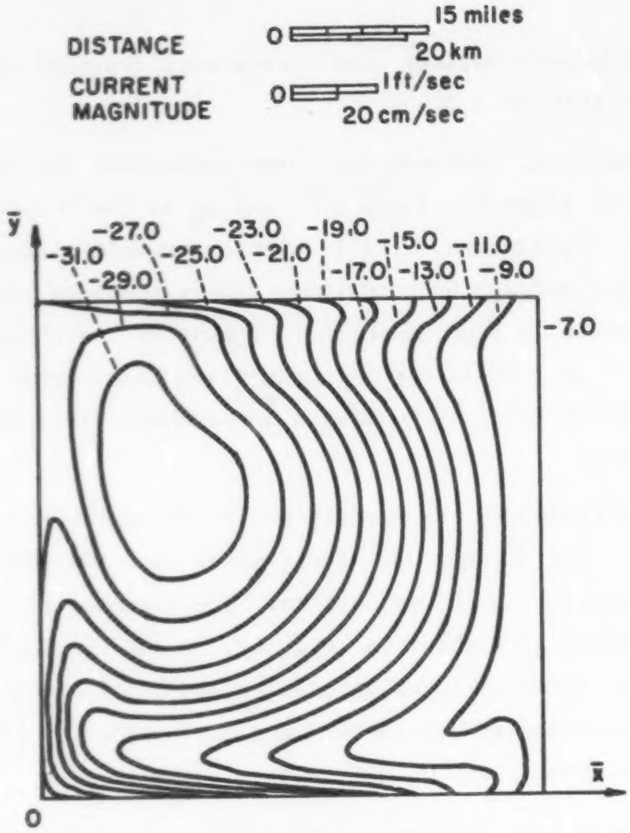

Figure 24. Thermocline depth contours with wind stress curl of order one ($\delta = 1/24$).

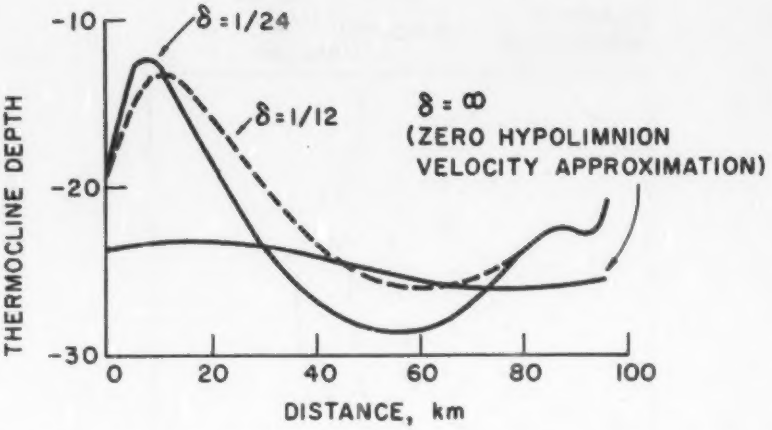

Figure 25. Thermocline profile at x = 48.3 km with wind stress curl of order one.

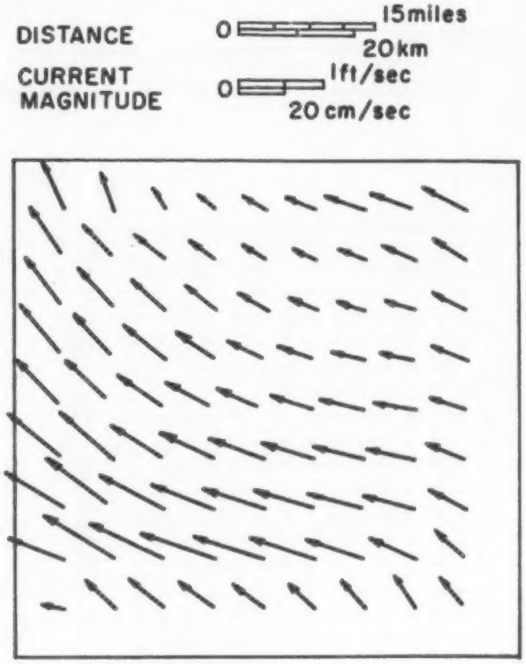

Figure 26. Horizontal surface velocities (δ = 1/24)

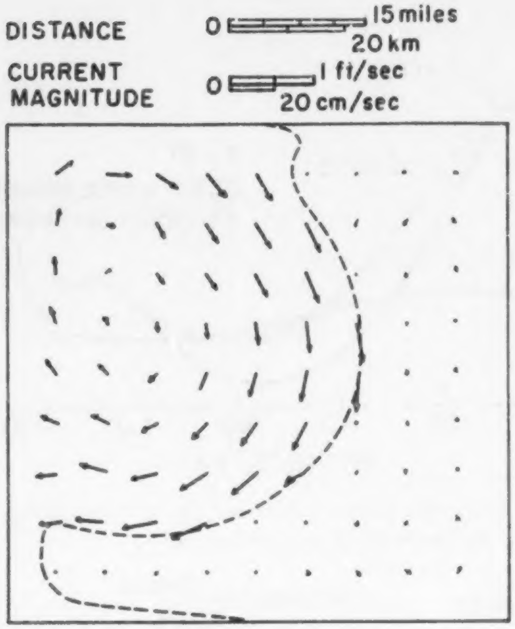

Figure 27. Horizontal velocities at 20 m depth.

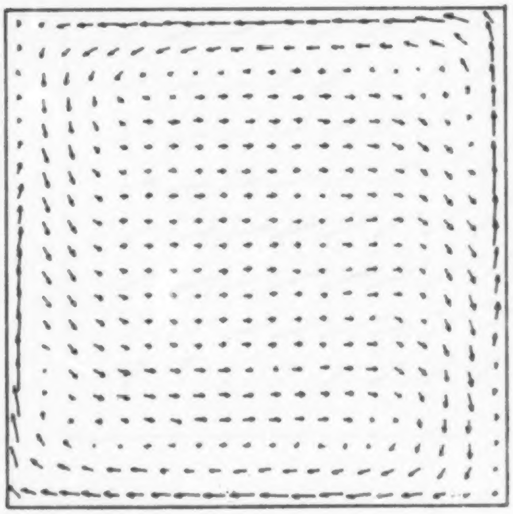

Figure 28. Horizontal velocities at 35 m depth.

contours for the same conditions as Case 1, except with a uniform wind, were calculated. It can be shown that, without the wind stress curl, there is very little cross-wind variation in the thermocline depth. The zeroth order solution for the uniform wind case also yields a zero hypolimnion pressure gradient. Therefore the uniform wind does not create any zeroth order geostrophic inviscid currents in the hypolimnion as in Case 1.

SECTION VII

TIME-DEPENDENT, CONSTANT DENSITY MODELS

Except that the flow is now varying with time, the models discussed in this section incorporate the same assumptions as those made in the previous section, i.e., the water density is constant, the pressure is hydrostatic, nonlinear acceleration and horizontal diffusion terms can be neglected, the vertical eddy diffusivity is constant, and surface displacements are small by comparison with the depth.

The basic model is presented and discussed in Section 7.1. Representative results are shown for (1) a spatially uniform wind varying as a step-function with time, and (2) a spatially and time-varying wind with the wind velocity determined from observations made during Storm Agnes in June, 1972. Results from the latter case are compared with observed surface displacements. In Section 7.2, the extension of this model to take into account a finer grid near shore and coupling with the coarser off-shore grid is discussed and results of the calculations are given. With this basic model, some analytic investigations of the important time scales governing the flow were made. In addition, the rigid-lid and free surface models were investigated and compared. These latter investigations are presented in Section 7.3.

7.1 AN OVERALL LAKE ERIE CIRCULATION MODEL

With the approximations discussed above, the equations of motion reduce to

$$\frac{\partial u}{\partial x} + \frac{\partial v}{\partial y} + \frac{\partial w}{\partial z} = 0 \qquad (31)$$

$$\frac{\partial u}{\partial t} - fv = -\frac{1}{\rho}\frac{\partial p}{\partial x} + A_v \frac{\partial^2 u}{\partial z^2} \qquad (32)$$

$$\frac{\partial v}{\partial t} + fu = -\frac{1}{\rho}\frac{\partial p}{\partial y} + A_v\frac{\partial^2 v}{\partial z^2} \tag{33}$$

$$\frac{\partial p}{\partial z} = -\rho g \tag{34}$$

The boundary conditions are

$$z = 0: \quad \rho A_v\frac{\partial u}{\partial z} = \tau_x \ , \quad \rho A_v\frac{\partial v}{\partial z} = \tau_y \tag{35}$$

$$w = \frac{\partial \zeta}{\partial t} \tag{36}$$

$$z = -h(x,y): \quad u = 0,\ v = 0,\ w = 0 \tag{37}$$

For simplicity, it is also generally assumed in our calculations (although not necessary for the calculations) that the water is initially at rest and therefore

$$t = 0: \quad u = 0,\ v = 0,\ w = 0,\ \zeta = 0 \tag{38}$$

The hydrostatic equation, Eq. (34), can be integrated to give

$$p = p_a + \rho g(\zeta - z) \tag{39}$$

where p_a is the atmospheric pressure and may be a function of x, y, and t. From this and neglecting the variations in the atmospheric pressure, it follows that

$$\frac{\partial p}{\partial x} = \rho g\frac{\partial \zeta}{\partial x} \ , \quad \frac{\partial p}{\partial y} = \rho g\frac{\partial \zeta}{\partial y} \tag{40}$$

and therefore p can be eliminated from Eqs. (32) and (33). It is convenient to integrate the continuity equation over the depth. The result is

$$\frac{\partial\zeta}{\partial t} + \frac{\partial U}{\partial x} + \frac{\partial V}{\partial y} = 0 \qquad (41)$$

In many studies of lake and ocean hydrodynamics, the rigid-lid approximation is invoked. This assumption implies that no vertical motions are allowed at the surface z = 0. The upper boundary condition, Eq. (36), then reduces to

$$z = 0: \quad w = 0 \qquad (42)$$

and the integrated continuity equation, Eq. (41), reduces to

$$\frac{\partial U}{\partial x} + \frac{\partial V}{\partial y} = 0 \qquad (43)$$

Stretched Coordinate System

It is convenient to transform the equations from an x,y,z system to an x,y,σ system where $0 \leq \sigma \leq 1$ and $\sigma = 0$ corresponds to the bottom of the lake while $\sigma = 1$ corresponds to the surface of the lake (Freeman, Hale, and Danard, 1972). With this transformation and a uniform σ grid spacing, the spacing in the x,y,z system is smaller in shallow regions of the lake and increases in proportion to the depth. This ensures that in the shallow areas there is no loss of accuracy in the computations due to lack of vertical resolution. The transformation also makes it easier to incorporate the bottom topography into the numerical program and to apply the boundary conditions.

The σ coordinate is defined by

$$\sigma = 1 + \frac{z}{h} \qquad (44)$$

where $h = h(x,y)$ is the depth at the location (x,y). With this transformation and the modifications discussed above, the governing equations reduce to

$$\frac{\partial u}{\partial t} - fv = -\rho g\frac{\partial \zeta}{\partial x} + \frac{A_v}{h^2}\frac{\partial^2 u}{\partial \sigma^2} \tag{45}$$

$$\frac{\partial v}{\partial t} + fu = -\rho g\frac{\partial \zeta}{\partial y} + \frac{A_v}{h^2}\frac{\partial^2 v}{\partial \sigma^2} \tag{46}$$

$$\frac{\partial \zeta}{\partial t} + \frac{\partial U}{\partial x} + \frac{\partial V}{\partial y} = 0 \tag{47}$$

where $U = \int_{-h}^{0} u dz = h \int_{0}^{1} u d\sigma$ and $V = \int_{-h}^{0} v dz = h \int_{0}^{1} v d\sigma$. The boundary conditions are

$$\sigma = 1: \quad \rho A_v \frac{\partial u}{\partial \sigma} = h\tau_x \, , \quad \rho A_v \frac{\partial v}{\partial \sigma} = h\tau_y \tag{48}$$

$$\sigma = 0: \quad u = 0, \; v = 0 \tag{49}$$

At the coast, it is assumed that there is no net normal mass flux.

Spatial Grid and Time Differencing

To set up the finite difference scheme, the spatial grid shown in Fig. 29 is used. The indices i,j,k refer to grid points in the x, y, σ directions respectively. Constant grid spacings Δx, Δy, $\Delta\sigma$ are used in the x,y,σ directions and, generally, $\Delta x = \Delta y$. The variables are defined in such a way that the only variable occurring on boundary segments parallel to the y-axis is U and the variable occurring on boundary segments parallel to the x-axis is V. Such an arrangement is convenient since the boundary condition of no normal flow through the coast involves U or V on appropriate boundary segments.

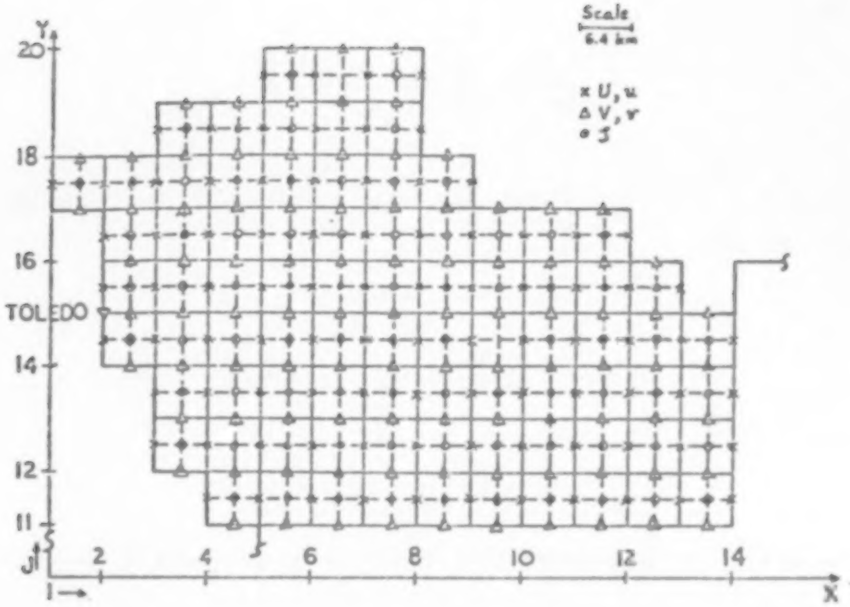
Scale
6.4 km
× U, u
Δ V, v
○ ζ
Y
20
18
16
TOLEDO
14
12
11
J
I
2
4
6
8
10
12
14
X

Figure 29. Horizontal grid pattern in part of Lake Erie.

The staggering of the variables in the horizontal plane makes it possible to use centered differences in space to evaluate derivatives with respect to x and y. Values for variables are sometimes needed at points at which they are not defined. These values are obtained by linearly interpolating from the values immediately adjacent to the point under consideration. Forward differences in time are used in the numerical calculations. The vertical diffusion terms in Eqs. (45) and (46) are evaluated by the Du-Fort Frenkel scheme [Smith, 1965] to ensure numerical stability.

The numerical procedure can be summarized as follows:
(1) Assume that the values at time t_n are known (initially at t_1, $u = v = \zeta = 0$).
(2) Use Eq. (45) to calculate u^{n+1}.
(3) Use Eq. (46) to calculate v^{n+1}.
(4) Evaluate U^{n+1} and V^{n+1} by numerically integrating u and v over the depth.
(5) Set U and V equal to zero on appropriate boundary segments.
(6) Evaluate ζ^{n+1} from Eq. (47).
This completes the calculation at time t_{n+1} and the computation for the next time step can now be started with step 1.

Numerical Stability Considerations

The numerical model consists of a system of 3 differential equations together with 2 numerical integrations. The determination of a stability criterion for the complete system is quite difficult and, in general, simple closed form results cannot be obtained for the allowable time step. However, by examining the various physical processes individually, some estimates of the stability limits can be obtained. This procedure has been found to provide reasonable guidelines for the choice of the allowable time step Δt [Crowley, 1968].

The physical processes that place the most stringent limitations on Δt are vertical diffusion (particularly in shallow regions of the lake) and surface gravity waves. The use of a Du-Fort Frenkel scheme makes it possible to overcome the limitations due to viscous diffusion [Roache, 1972]. The scheme used in the present model is a modified form of the Du-Fort Frenkel scheme in which forward time differencing is used instead of a leap-frog scheme. However, even this modified scheme is found to be stable in practice. The time step is therefore limited only by surface gravity waves.

The stability criterion introduced due to the surface waves is that the time step be less than the time it takes for the waves to move across one grid spacing, the Courant-Friedrichs-Lewy condition [Richtmyer and Morton, 1967]. A simple stability analysis for these waves shows that for stability $\Delta t < \Delta x / \sqrt{gh}$, where Δt, Δx and h are dimensional quantities [Richtmyer and Morton, 1967]. In practice, for the full set of equations used in the present model, it is found that the numerical procedure is stable as long as

$$\Delta t \leq \frac{\Delta x}{5\sqrt{gh}} \quad , \tag{50}$$

where h is the maximum depth in the lake.

Determination of the Wind Stress

The relationship between the wind stress and the wind velocity is taken to be that discussed in Section 4.2, i.e.,

$$\underline{\tau} = \rho_a C_d W_a \underline{W}_a \tag{51}$$

In general, the winds are not uniform over the lake. Furthermore, the wind velocities are only measured at a few points on the shores of the lake. Therefore the wind stress over the remainder of the lake has to be determined by interpolating from the known values at a few points. The method of interpolation used in this study is similar to that used by Platzman (1963). The stress at any point (x,y) in the lake is assumed to be given by

$$\tau(x,y,t) = \sum_m \lambda_m(x,y,)\tau_m(t) \tag{52}$$

where m is an index identifying a particular station, $\tau_m(t)$ is the wind stress at station m at the time t and $\lambda_m(x,y)$ is a dimensionless interpolating function. τ_m can be determined from Eq. (51) from the known wind velocity at station m.

To specify the interpolating function $\lambda_m(P)$, where P denotes an arbitrary point (x,y), define

$$a_m(P) = (x-x_m)^2 + (y-y_m)^2 \tag{53}$$

the square of the distance between P and P_m. Further, let

$$f_m(P) = \prod_{n \neq m} a_n(P) \tag{54}$$

then

$$\lambda_m(P) = \frac{f_m(P)}{\sum_m f_m(P)} \tag{55}$$

Instead of defining $a_m(P)$ as in Eq. (53), any monotone function of the distance between P and P_m could be used.

For each data point P_m, contours of the interpolating function $\lambda_m(P)$ can be determined. Results for the interpolating function obtained from six data points around the lake are shown in Fig. 30. It can be seen that the influence of any data point diminishes as the distance from it increases. In particular, the influence of point 5 on the stresses in the lake is small, since point 5 is at a larger distance from the lake compared to the other points. From Eq. (55), it is evident that the sum of the influences of all the data points at P is unity, i.e.,

$$\sum_m \lambda_m(P) = 1. \tag{56}$$

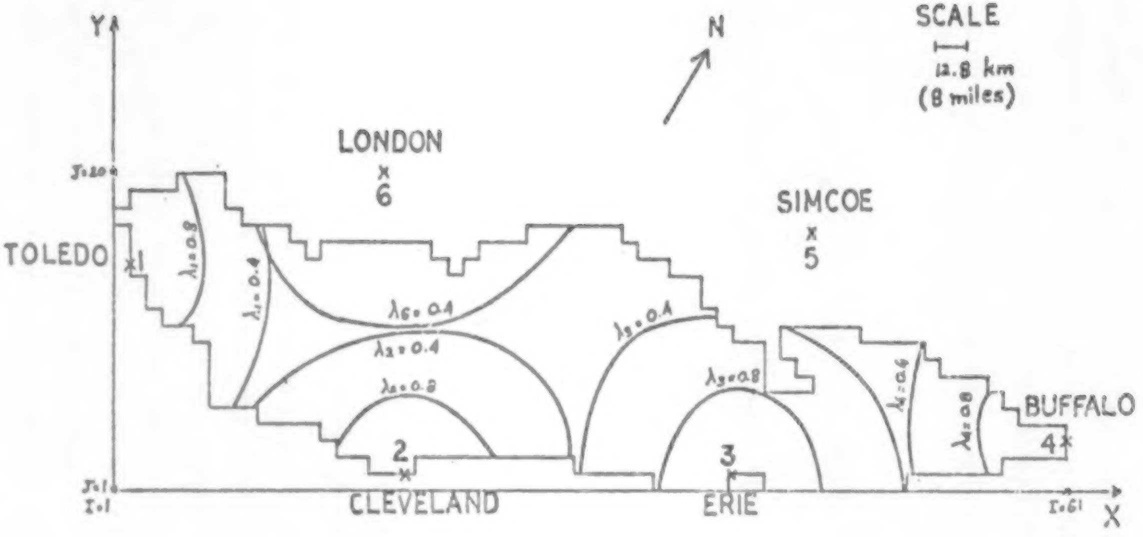

Y
J=20
J=1
I=1
TOLEDO
1
LONDON
6
N
SCALE
12.8 km
(8 miles)
SIMCOE
5
$\lambda_1=0.8$
$\lambda_1=0.4$
$\lambda_6=0.4$
$\lambda_2=0.4$
$\lambda_2=0.8$
$\lambda_3=0.4$
$\lambda_3=0.8$
$\lambda_4=0.6$
$\lambda_4=0.8$
2
3
4
BUFFALO
CLEVELAND
ERIE
I=61
X

Figure 30. Stress interpolation function for six data points around the lake.

Numerical Grid Pattern and Choice of Time-Step

To set up the numerical grid in the lake, the boundaries of the lake are first approximated by straight line segments parallel to the x and y axis (see Fig. 30). A uniform horizontal grid with $\Delta x = \Delta y = 6.4$ km (4 miles) was used. In the vertical direction, the region from the bottom to the top ($\sigma=0$ to $\sigma=1$) is divided into five intervals of length $\Delta\sigma=0.2$.

To determine the allowable time step for the calculations in Lake Erie, the maximum depth of 67 meters is used. Then, with $\Delta x=6.4$ km, Eq. (50) requires that Δt be less than or equal to about 50 seconds. With this time step, the calculations showed no evidence of instability.

Results for a Uniform Wind

As the first example of the time dependent flow in Lake Erie, consider a uniform wind blowing along the long axis of the lake with $\tau_x = 1$ dyne/cm^2 and $\tau_y = 0$. According to Wilson's formula for the determination of the wind stress from the wind speed, this corresponds to a wind speed of 5.5 meters per sec. The wind direction is W32°S. Calculations were made for eddy diffusivities of 25 cm^2/sec and 40 cm^2/sec. These values are approximately the same as the values used by Gedney and Lick (1972) for comparable winds (but steady state) and for which the numerical results compared well with measured data. For $A_v=25$ cm^2/sec, the calculations were carried out to about 57 hours, while for $A_v=40$ cm^2/sec the calculations were terminated at about 21 hours.

A representative sample of the numerical results for $A_v=25$ cm^2/sec is shown in Figs. 31 to 34. From Fig. 31, it can be seen that there is a dominant period of about 14 hours. Henry [1902] has examined a series of limnograms at the western and eastern ends of Lake Erie. He found that the uninodal oscillation of the lake was most conspicuous for several days and it had a period of 14 hours. Evidently the period observed in the numerical results corresponds to these uninodal oscillations along the long axis, since the wind is in the direction of this axis. The transverse oscillations and the effects of the

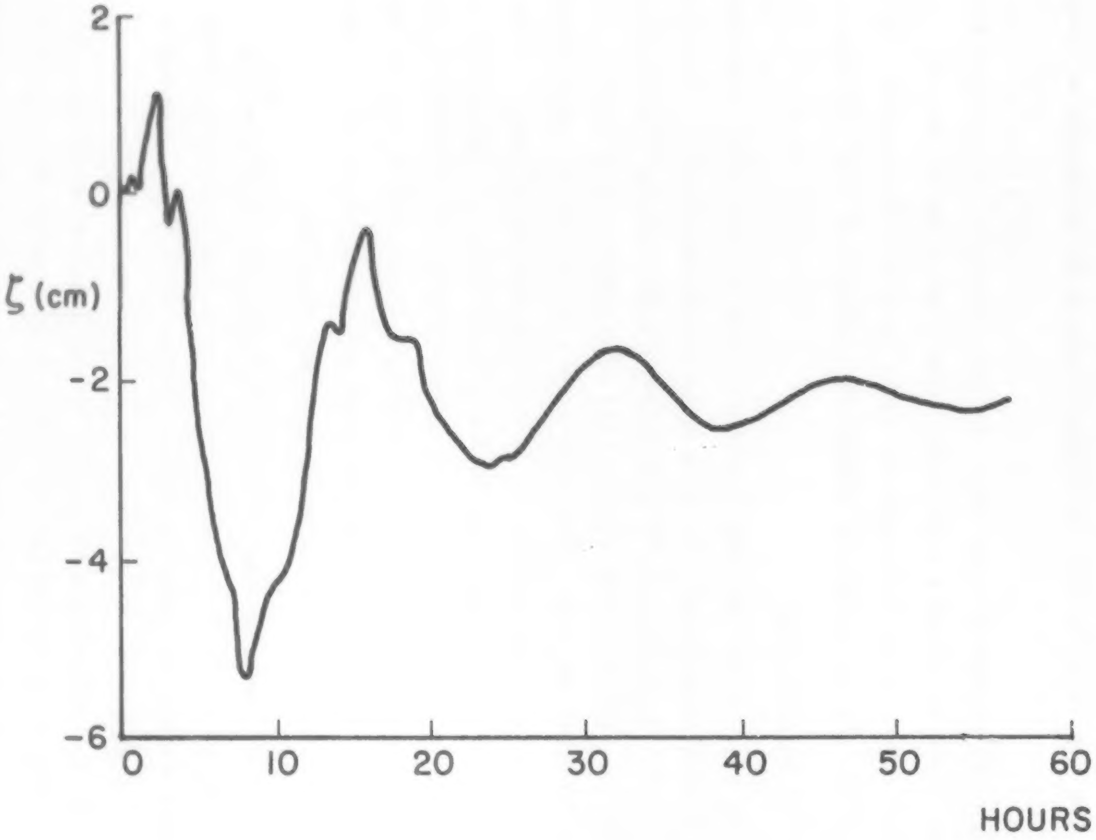

Figure 31. Surface displacement as a function of time at Cleveland.

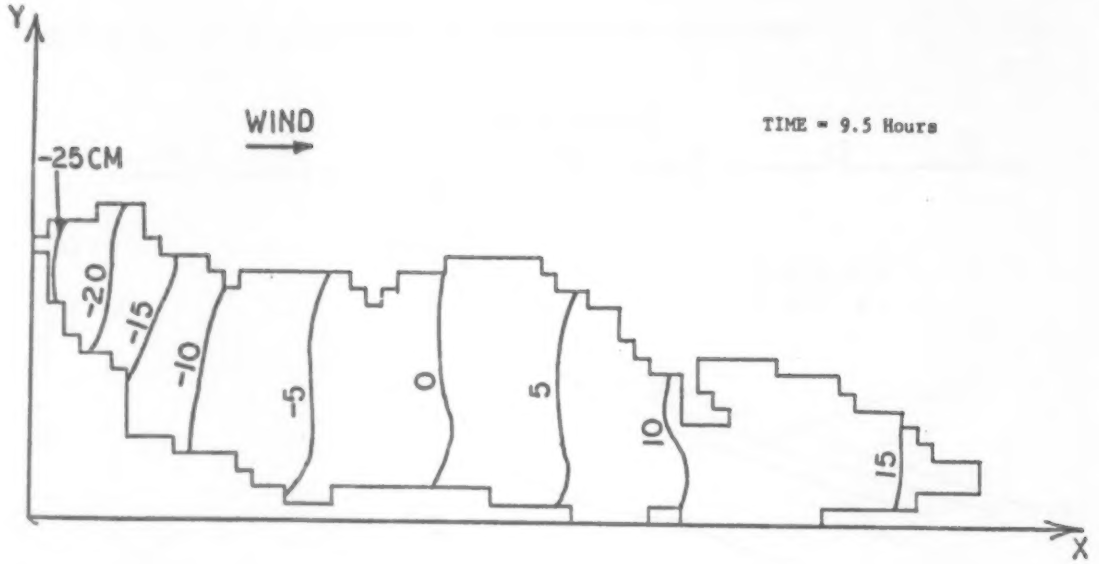

Figure 32. Surface displacement contours (τ_x 1 dyne/cm^2).

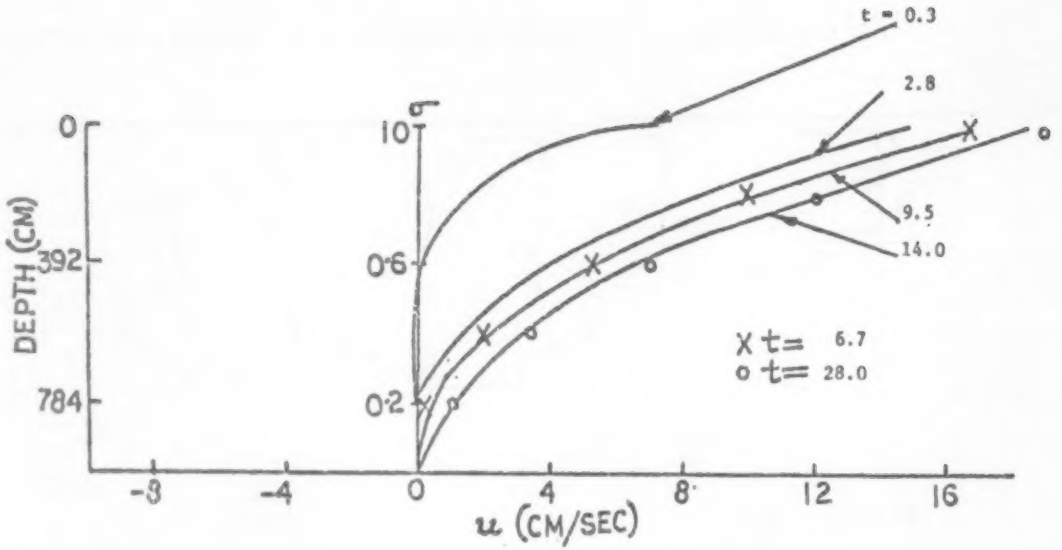

Figure 33. Horizontal velocity component at Cleveland.

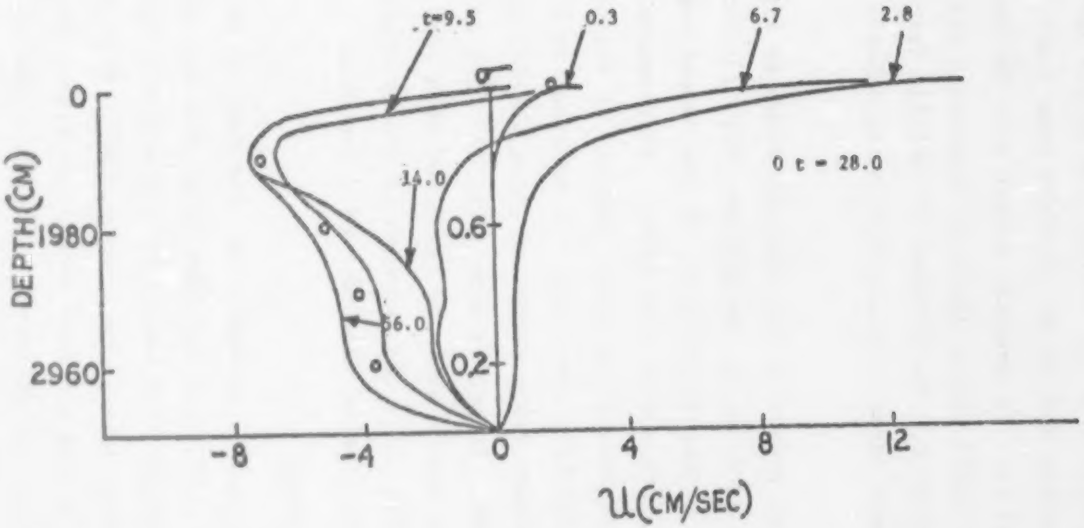

Figure 34. Horizontal velocity component in central part of Eastern Basin.

irregular boundaries can be seen in some of the smaller oscillations that are superimposed on the main oscillation.

Contours of the surface displacement at $t = 9.5$ hours are shown in Fig. 32. The lowest point is at the western end of the lake and the highest point is near Buffalo at the eastern end of the lake. The peak set-up between Buffalo and Toledo (Buffalo lake level-Toledo lake level) is about 40 cm. In general, except near the northern and southern coasts and at small times, lines of constant ζ are almost normal to the wind direction. The effects of Coriolis forces and the bottom topography prevent these contours from being exactly normal to the wind.

Velocity profiles at two points in the lake are shown in Figs. 33 and 34. The difference in profiles in the shallow (Fig. 33) and deep (Fig. 34) regions of the lake is evident. In the deeper region, the top and bottom Ekman layers can be identified. Furthermore, in the deeper regions, Coriolis forces are large compared to viscous forces, and therefore the v velocities are large. In contrast to this, v is much smaller in the Western Basin where the water is shallow and Coriolis forces are not important. It can be seen (Fig. 33) that in the shallow region, the approach to steady state is rapid and much less than a day. In the deeper region (Fig. 34), the approach to steady state is much slower with a relaxation time on the order of a few days.

Results for an Actual Storm

To verify the numerical model, consider next the case of an actual storm on Lake Erie for which wind and lake level data are available. Tropical storm Agnes stalled near Lake Erie and produced northerly winds over the lake during June 21 to June 25, 1972. Wind data during the storm is available at six stations around the lake. The wind magnitude and direction at two different times are shown in Figs. 35 and 36. All of the observed data for the storm has been taken from Paskausky (1973).

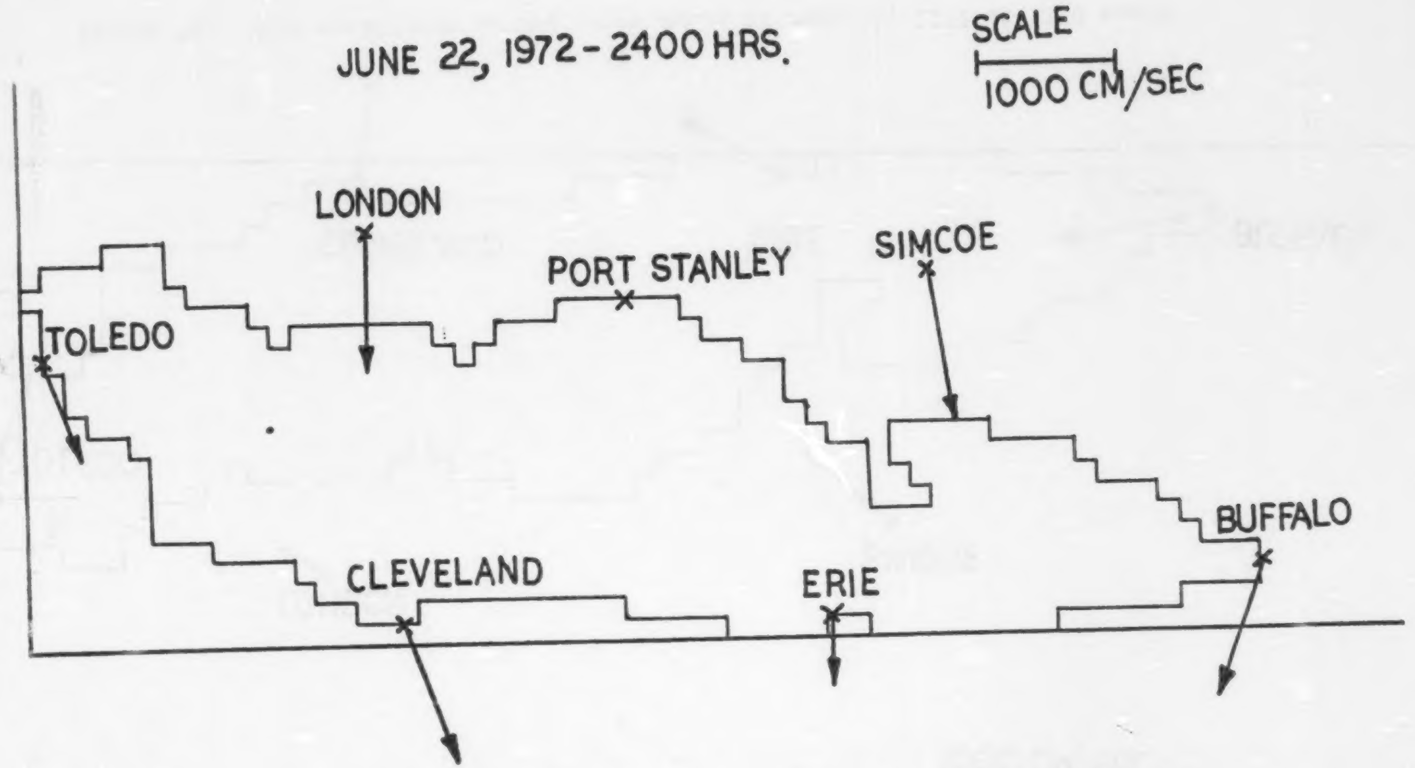
JUNE 22, 1972 - 2400 HRS.
SCALE
1000 CM/SEC
LONDON
PORT STANLEY
SIMCOE
TOLEDO
CLEVELAND
ERIE
BUFFALO

Figure 35. Wind conditions during storm Agnes on June 22, 1972 at 2400 hours.

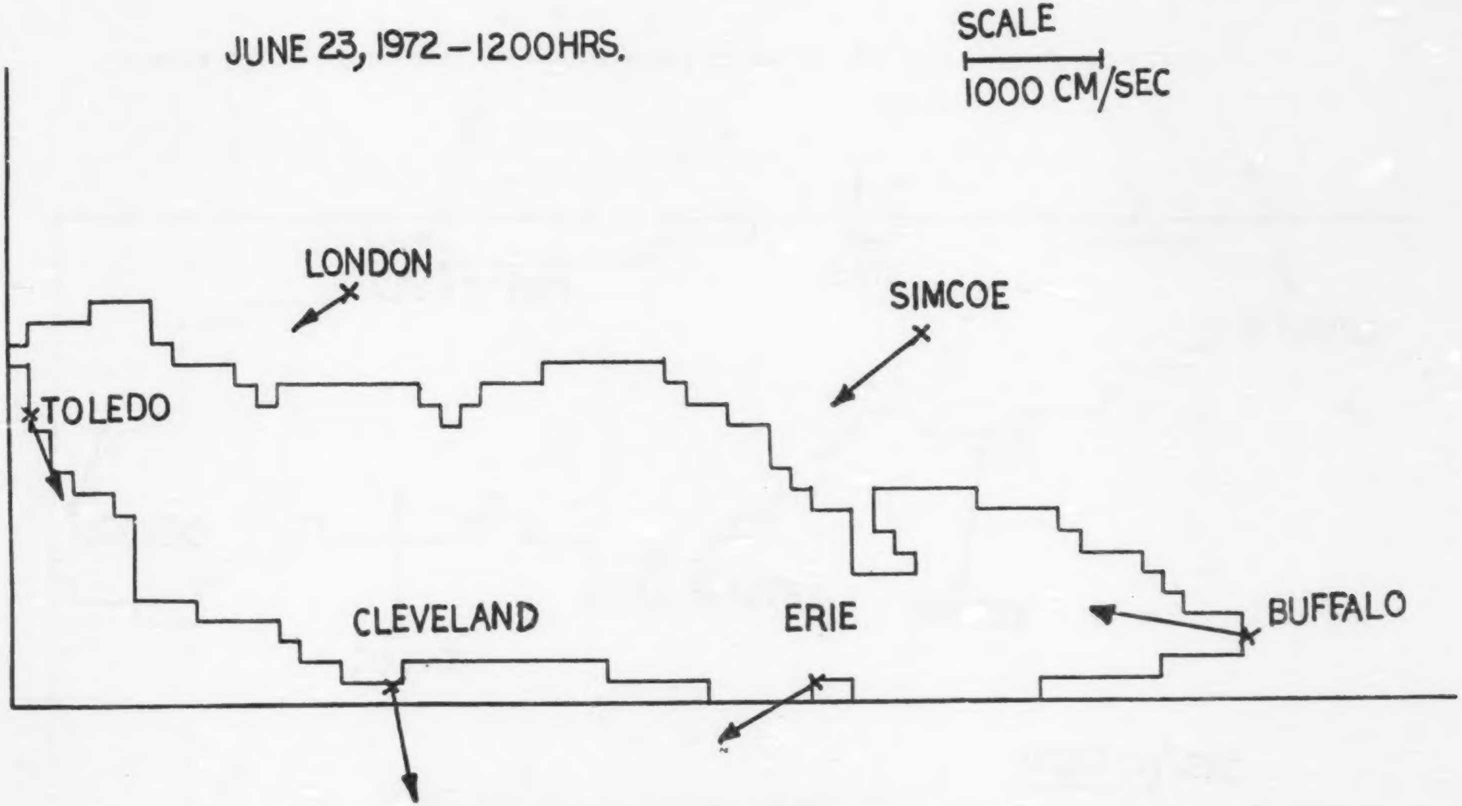
JUNE 23, 1972 – 1200HRS.
SCALE
1000 CM/SEC
LONDON
SIMCOE
TOLEDO
CLEVELAND
ERIE
BUFFALO

Figure 36. Wind conditions during storm Agnes on June 23, 1972 at 1200 hours.

From the wind velocities, the wind stress at the six locations can be determined. However, the velocities over water are generally greater than those over land. A factor of 1.0 to 1.5 is usually taken (Reid and Bodine 1968, Gedney and Lick 1972). In the present case, a factor of 1.25 gave reasonable agreement with observational results, as will be seen below. Once the wind stress at the six locations is known, the stress over the remainder of the lake can be determined by the interpolation procedure discussed above.

Wind data for the storm is given at hourly intervals starting at 1000 hours on 6/22/72. Examination of the measured surface displacement curves shows that by this time the lake level had been sufficiently disturbed and the initial condition of zero surface displacement everywhere in the lake would be inappropriate if calculations were started at this time. However, about 10 hours earlier, i.e., at 2400 hours on 6/21/72, the lake level appeared to be relatively undisturbed and this time was chosen to be the starting point for the numerical computations. The wind velocities during the period from 2400 hours on 6/21/72 to 1000 hours on 6/22/72 were determined by linearly interpolating from zero to the observed value at 1000 hours on 6/22/72. Furthermore, since only hourly values of the wind stress can be determined from the observed wind data, any intermediate stress values were obtained by linear interpolation between two hourly values. The wind stress as a function of time at Cleveland and Toledo is shown in Fig. 37. The rapid changes in the magnitude of the wind stress are evident.

The numerical calculations were carried out with a time step of 50 sec and for eddy diffusivities of 25 cm^2/sec and 40 cm^2/sec. For A_v=25 cm^2/sec, numerical results for the surface displacement as a function of time at Cleveland and at Port Stanley are shown in Figs. 38 and 39. The results compare favorably with the measured values of the surface displacement. In particular, the numerical and observed data have a similar variation.

Calculations were also made for an eddy diffusivity of 40 cm^2/sec. The results for the surface displacement were practically indisting-

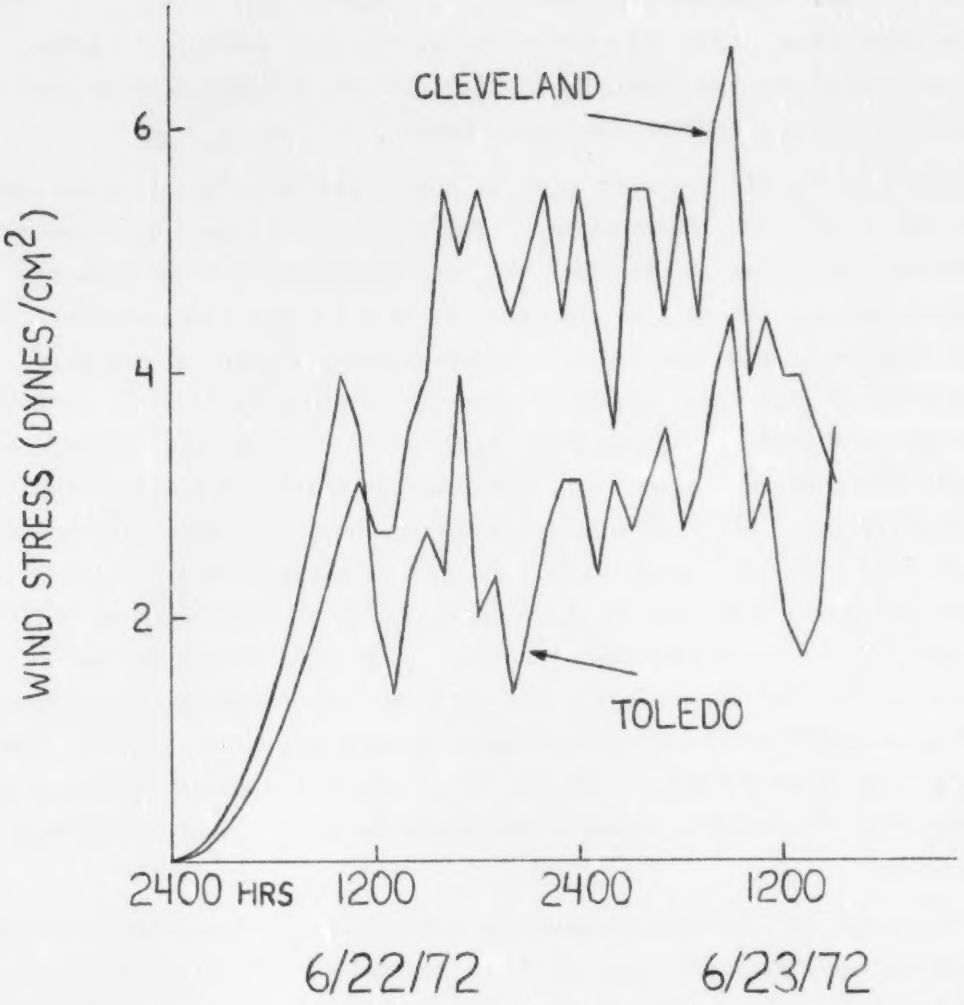

Figure 37. Magnitude of wind stress as a function of time during storm Agnes.

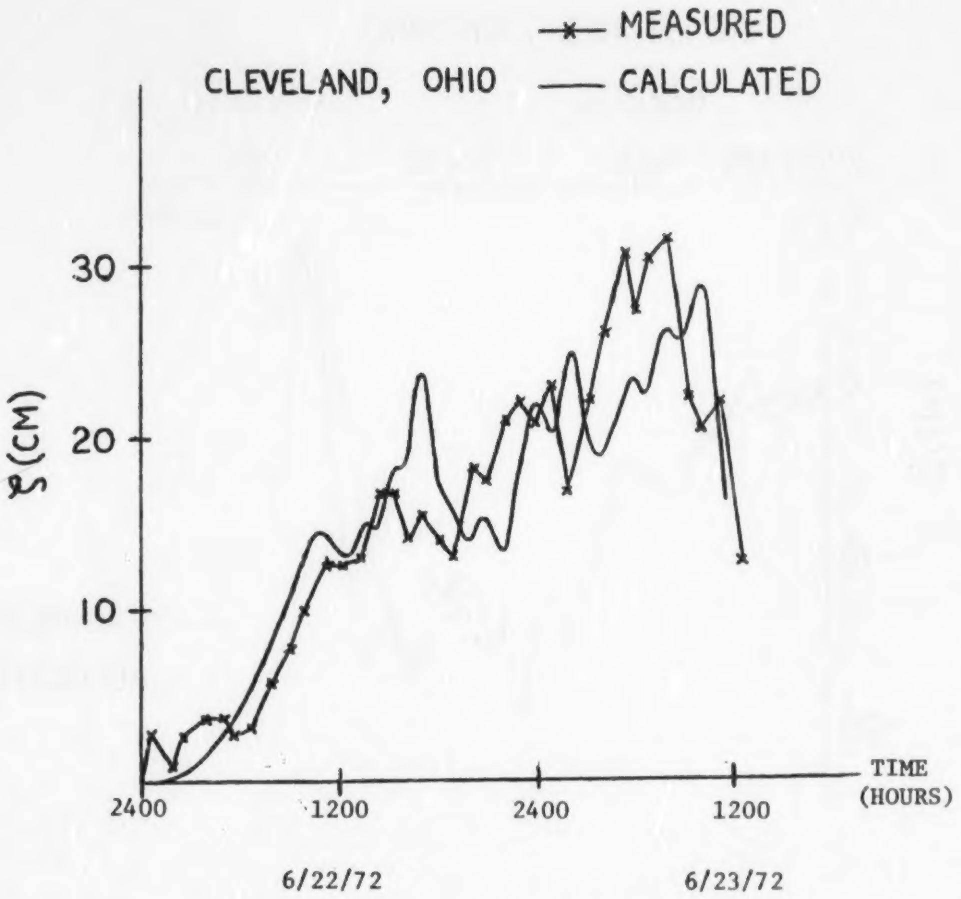

Figure 38. Calculated and measured water level fluctuations at Cleveland during storm Agnes.

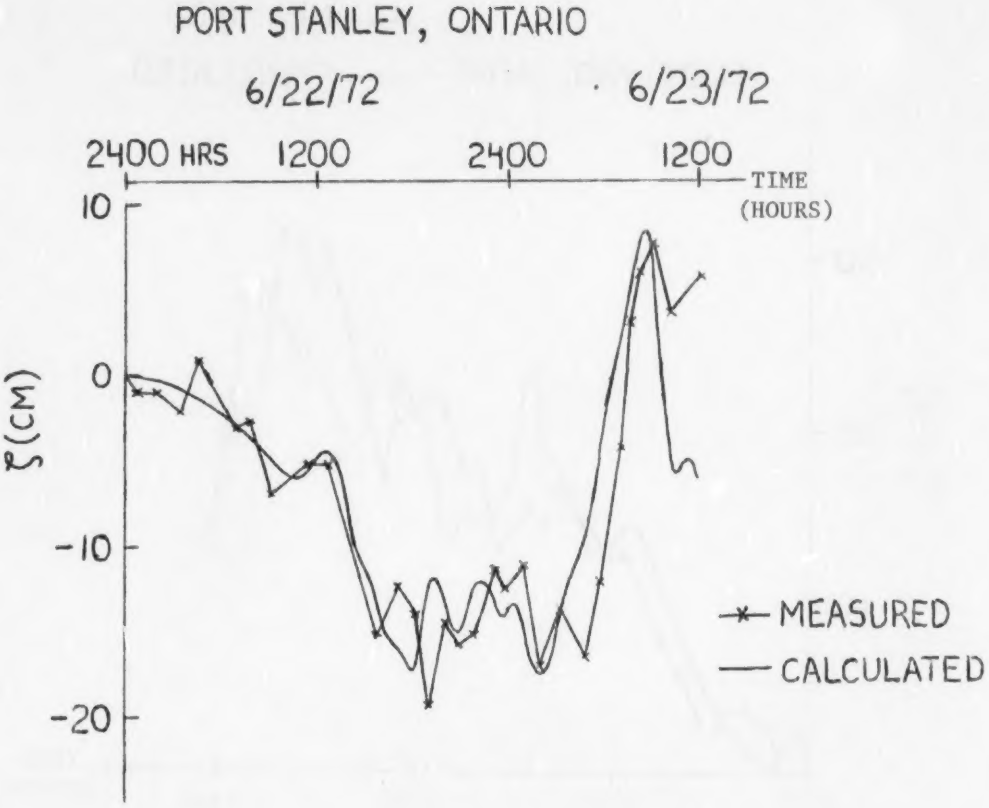

Figure 39. Calculated and measured water level fluctuations for Port Stanley during storm Agnes.

uishable from those for A_v=25 cm^2/sec. This shows that the magnitude and direction of the wind velocity dominate the flow. Of course, after the storm, as the surface oscillates and decays to an equilibrium position, the differences between the results for A_v=25 cm^2/sec and A_v=40 cm^2/sec would be more significant, as indicated by the constant wind case.

It was mentioned previously that a linear interpolation for the wind velocity was used for the first ten hours. Varying the magnitude of this initial wind set-up of course changed the surface displacement during the first ten hours. However, after this time, the results were practially independent of what wind velocity was assumed for the first ten hours.

Further verification of the numerical model was obtained by comparing the numerical results with the observed water level at four points around the lake at the time of approximately peak set-up at Cleveland. This is shown in Fig. 40 where the surface displacement contours are shown at 0400 hours on June 23. It can be seen that the northern end of the lake is at a much lower level than the southern end. The measured values of ζ at Port Stanley, Marblehead, Cleveland and Barcelona are also shown in the figure. The calculated values at these four points are -12, 5, 22 and 9 cm respectively and these are in reasonable agreement with the measured values of -15, 6.4, 26, and 12 cm. Thus the spatial variation of ζ obtained from the numerical model is also in accord with observed data.

Although the above numerical procedure is correct, it is not very efficient. Two alternate and useful procedures have been developed for modeling of three-dimensional, time-dependent lake currents. Both are more efficient than the method indicated above and both have been used previously in atmospheric and oceanic modeling. One method is that developed for lakes by Simons (1971, 1972, 1974, 1975). In this method, the external (vertically-averaged) and internal modes of the flow field are treated separately. The time step used in the calculation of the external mode is limited by the stability requirements indicated

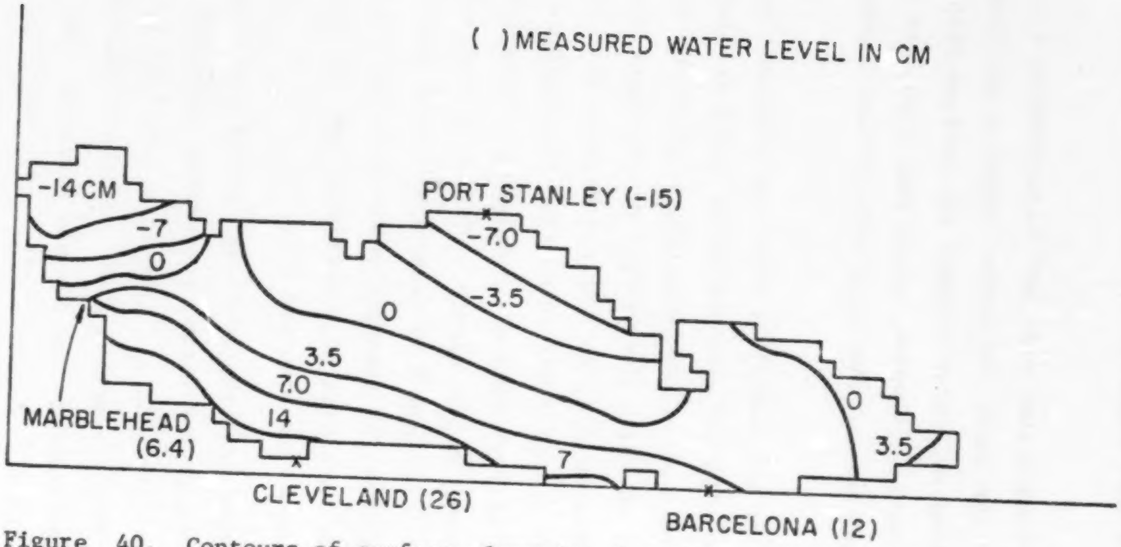
( ) MEASURED WATER LEVEL IN CM
-14 CM
-7
0
PORT STANLEY (-15)
-7.0
-3.5
0
3.5
7.0
14
MARBLEHEAD
(6.4)
7
0
3.5
CLEVELAND (26)
BARCELONA (12)

Figure 40. Contours of surface elevation for Storm Agnes at 0400 hours on June 23, 1972.

above. However, the calculation of the internal structure of the flow is not limited by these requirements and a much larger time step can be taken for these calculations. This procedure has been incorporated into the above model and further computations are presently being made. The second method (Paul and Lick 1973, 1974) also involves separating the calculations into external and internal modes. However, the external mode is treated by using a rigid-lid assumption, an assumption which effectively eliminates free surface gravity waves. More details on this method are given in Section VIII.

7.2 THE NEAR SHORE

The time-dependent model described in the previous section has been modified so as to describe in more detail the flow in a near-shore area near Cleveland (Sheng and Lick, 1975). This area is the same as that described in Section 6.3, where the flow was calculated by means of a steady-state model. In this near-shore region, a one mile or 1/2 mile grid is necessary for adequate detail. This reduction in grid size not only increases the number of grid points and therefore the number of calculations per time step but also decreases the maximum allowable size of the time step, Δt_{max}, and therefore increases the number of time steps necessary for calculations over a specified time interval.

It is unrealistic to describe the entire lake by means of a one mile, or finer, grid. By comparison with the four mile grid used in the overall lake calculation, a one mile grid would increase the number of grid points by a factor of 16 and, in addition, reduce Δt_{max} by a factor of 4.

In order to conserve computer time while still retaining the necessary grid size in the near shore, the lake has been divided into regions, each with its own grid size and, correspondingly, its own maximum allowable size of time step. These regions are: (1) The near shore. The grid size is one mile. The maximum depth is 22 m. This yields a Δt_{max} of 22 sec. (2) The Eastern Basin. In this basin, an eight

mile grid is used. The maximum depth is 65m and $\Delta t_{max} = 100$ sec. Although the grid is fairly crude, this will have comparatively little influence on the motion in the near-shore region near Cleveland.
(3) The Central and Western Basins. A four mile grid is used in the rest of the lake. The maximum depth is 26 m which gives a Δt_{max} of 82 sec.

It was decided to use a time step of 20 sec. in the near shore and 80 sec. in the rest of the lake. This satisfies the above requirements and, in addition, four time steps in the near shore are then exactly equivalent to one time step in the rest of the lake, a computational convenience.

The coupling between regions with different grid sizes and different time steps can of course create problems. See a discussion of these problems in Section V. To investigate these problems, the coupling process was first studied for one and two dimensional systems. From this experience, the present computational procedure evolved. In this procedure, it can be shown that: (1) Mass is conserved exactly as fluid moves from one region to another. (2) Pressure forces (due to surface displacements) are transmitted smoothly across the interface between two regions. (3) The results agree with the results obtained with a single grid size and a single time step throughout the entire domain, and therefore the results vary smoothly throughout the domain.

The coupling process can be illustrated by a discussion of the coupling between the Eastern and Central Basins. The grid pattern near the boundary between the two regions is shown in Fig. 41. The two grids overlap over a region of four miles. Let all variables in the Eastern Basin be denoted by the subscript e and all variables in the Central Basin by the subscript c. The solution procedure is: (1) Along the vertical line $I_{ue} = 1$ and $I_{uc} = 40$, calculate the u_e's from the finite difference equations. The u_c's along this same line are then interpolated from the u_e's. (2) Along $I_{ve} = 1$ and $I_{vc} = 40$, calculate the v_c's and the ζ_c's from the finite difference equations. The v_e's and the ζ_e's along this line are then interpolated from the v_c's and the ζ_c's.

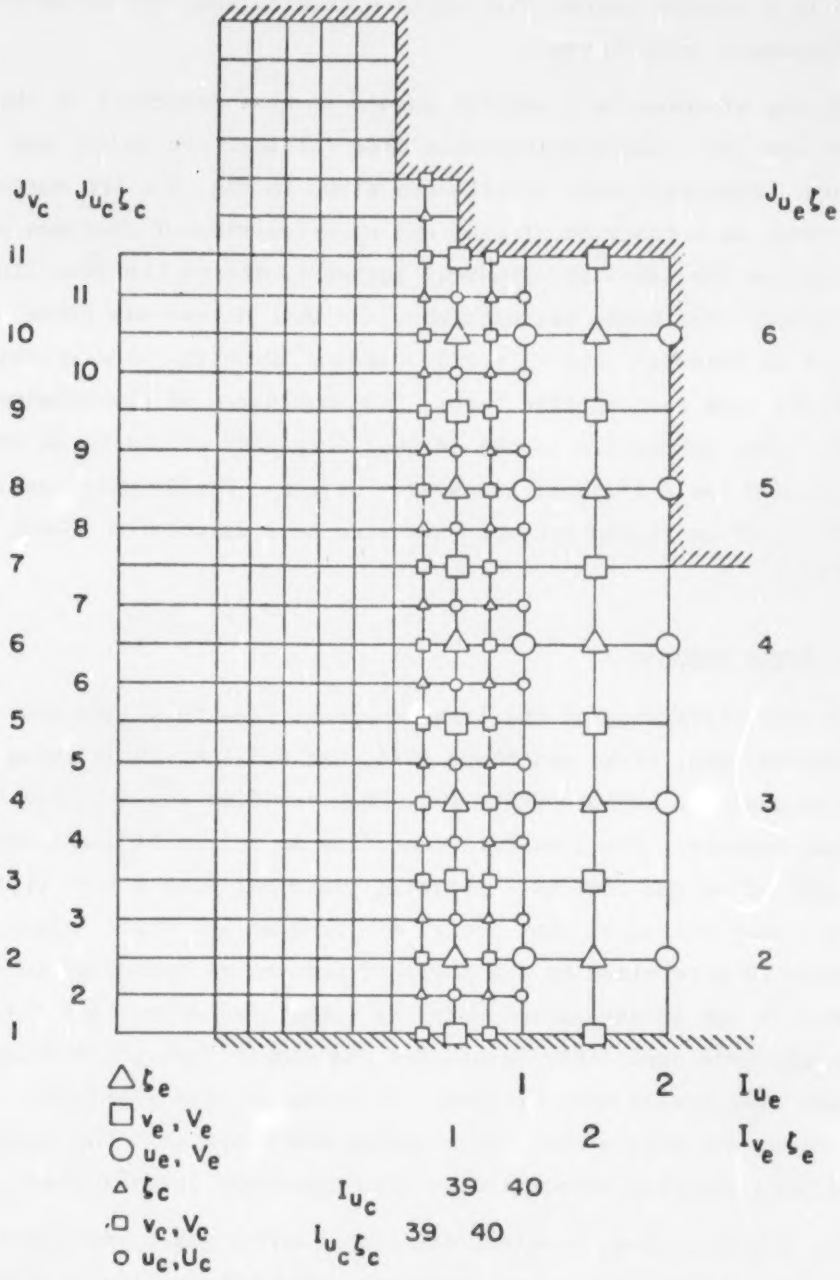
J_{v_c}
$J_{u_c}\zeta_c$
$J_{u_e}\zeta_e$
J_{v_e}
11
11
10
10
9
9
8
8
7
7
6
6
5
5
4
4
3
3
2
2
1
6
6
5
5
4
4
3
3
2
2
1
1
2
I_{u_e}
1
2
$I_{v_e}\zeta_e$
I_{u_c}
39
40
$I_{u_c}\zeta_c$
39
40
△ ζ_e
□ v_e, V_e
○ u_e, V_e
△ ζ_c
□ v_c, V_c
○ u_c, U_c

Figure 41. Grid pattern at boundary between Eastern and Central Basins.

The coupling between the near-shore region and the Central Basin is treated in a similar manner with obvious changes when the orientation of the boundary is different.

Calculations are made in a similar manner to that described in the previous section. Calculations were made initially to verify the procedure. Representative results are shown in Fig. 42, the surface displacement as a function of time and as a function of distance along a line across the lake approximately perpendicular to the shoreline at Cleveland. For these calculations, the wind stress was taken to be $\tau_x = 1.55$ dynes/cm^2 and $\tau_y = 1.1$ dynes/cm^2 with the wind starting impulsively from rest at time zero. The smoothness of the results is evident. Also noticeable is the 14 hour longitudinal seiche on which is superposed the 2 1/2 hour transverse seiche. Preliminary results on the effects of an island jetport have also been calculated (Sheng and Lick, 1975)

7.3 ANALYTIC RESULTS

General characteristics of the time-dependent flow in a lake were investigated (Haq, Lick, and Sheng 1974, Haq and Lick 1975) using primarily analytic methods which were then verified and extended by numerical methods. The time-dependent flow in a lake or ocean can be thought of as the flow in a rotating container with a free upper surface. Many different time scales are present and their relative importance is determined by the physical parameters appearing in the problem. In the investigation which is summarized here, time scales of interest were explicitly identified and simple analytic formulas for these time scales were derived. In addition, the rigid-lid and free-surface models were investigated and compared. The analytic results were verified by comparison with numerical calculations.

For this investigation, a relatively simple model was investigated, i.e., a constant density, time-dependent, wind-driven flow in a basin of constant depth. The emphasis is on values of parameters (especially Ekman number) corresponding closely to those in the Great Lakes and in particular to those in Lake Erie, the shallowest of the Great Lakes.

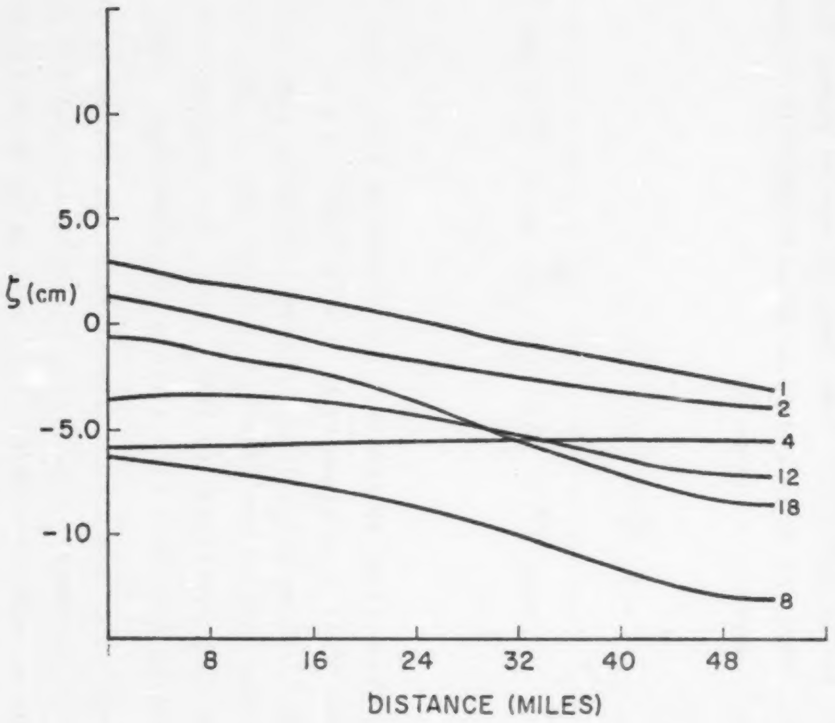

Figure 42. Surface displacement as a function of time along a line across the lake at Cleveland.

The basic equations are those presented in Section 7.1. It is assumed that the wind is spatially uniform and varies as a step function with time. By means of Laplace transforms, an analytic (but quite complex) solution can be obtained. The method of solution and the solution itself can be simplified by using a substitute kernel technique, an approximation shown to be generally valid for the range of parameters representative of large lakes.

Results are discussed here for two simple cases, (1) an infinitely long lake of width L and depth h, and (2) a square basin of length L and depth h. For an infinitely long lake, it can be shown, for the rigid-lid model, that the surface displacement decays with a time scale $t_1 = 1/f\mu^2$, where μ^2 is given by

$$\mu^2 = \sqrt{\frac{E_v}{2}} \left[\frac{\sinh \frac{2\pi h}{d} - \sin \frac{2\pi h}{d}}{\cosh \frac{2\pi h}{d} + \cos \frac{2\pi h}{d} - \sqrt{\frac{E}{2}} \sinh \frac{2\pi h}{d} + \sin \frac{2\pi h}{d}} \right] \tag{57}$$

where d is the Ekman layer thickness. For a shallow lake, where $h/d \ll 1$, the time scale t_1 is given by $t_1 = 4\pi^2 h^2/5fd^2$ and is proportional to h^2/d^2 or $1/E_v$, i.e., a viscous diffusion time (Greenspan, 1968). For a deep lake, where $h/d \gg 1$, the decay time is given by $t_1 = 2\pi h/fd$ and is proportional to $1/\sqrt{E_v}$, i.e., the usual spin-up time for a rotating container with a rigid lid (Greenspan, 1968).

For an infinitely long lake with a free surface, the motion is more complex. Various asymptotic time scales can be identified and depend on the parameter β, where $\beta = gh/L^2f^2$, as well as on the Ekman number. In the limit as $\beta \to \infty$ (the rigid-lid approximation), these times are t_1, a diffusion or spin-up time depending on the value of h/d, and $t_2 = 2L/\sqrt{gh}$, the period of oscillation of surface gravity waves. In this limit, the amplitude of the solution corresponding to gravity waves goes to zero so that these solutions are absent from the rigid-lid results. As $\beta \to 0$, the dominant times are $t_3 = 2\pi/f$, an inertial period (Proudman, 1952), and $t_4 = fL^2/\pi^2\mu^2 gh$, a flux time scale. This latter time scale arises from the fact that the lake surface is displaced by the wind stress and it takes a certain amount of time, given by t_4, to move fluid from one side of the lake to the other under the action of a wind stress or induced pressure gradient. In a deep lake, this mass motion occurs through the Ekman layers.

For intermediate values of β corresponding to real lakes, the time scales can be calculated from simple analytic formulas but cannot be easily interpreted, being combinations of the above times. In general, the solution consists of (a) a decaying part which has a decay time varying from t_1 to t_4 as β goes from ∞ to 0, and (b) an imposed decaying oscillatory part with a decay time of the order of t_1 and a period of oscillation varying from t_2 to t_3 as β goes from ∞ to 0. As $\beta \to \infty$, the free-surface model approaches the rigid-lid model. For $\beta \to \infty$ and $E_v << 1$, the results correspond to those for the spin-up of a rotating container with a rigid-lid [Greenspan, 1968]. The rigid-lid and free-surface results for $E_v = 1.0$ and $E = .025$ are shown in Figs. 43 and 44 respectively. These results are for a lake with width L = 300 km, h = 10m, and $\tau = 1$ dyne/cm^2. Analytical results for the rigid-lid case show that the surface displacement is given by

$$\frac{g\zeta}{fU_R L} = 0.65\left(\frac{x}{L} - \frac{1}{2}\right)(1-e^{-2.4ft}) \tag{58}$$

for $E_v = 1.0$ and

$$\frac{g\zeta}{fU_R L} = 8.4\left(\frac{x}{L} - \frac{1}{2}\right)(1-e^{-.13ft}) \tag{59}$$

for $E_v = .025$, where U_R is a reference velocity taken to be 10 cm/sec. These results are shown in Figs. 43 and 44 and the agreement with the numerical results is seen to be fairly good.

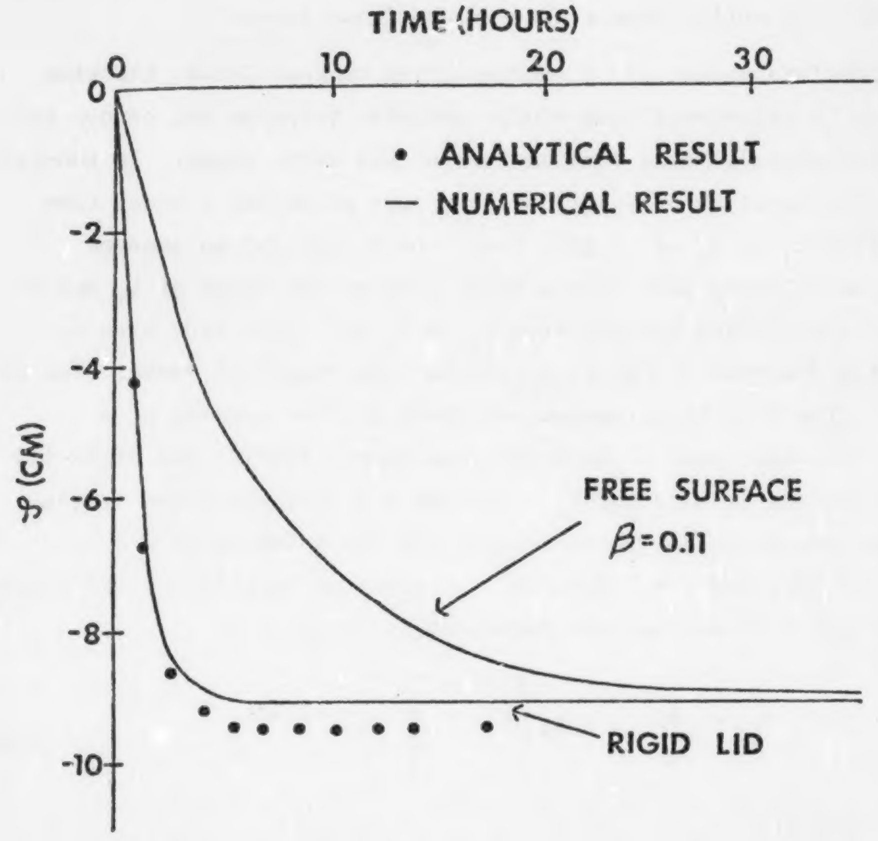

Figure 43. Surface displacement at x = 0 as a function of time for an infinitely long lake with L = 300 km, H = 10 m, $E_v = 1.0$, $\tau = 1$ dyne/cm^2.

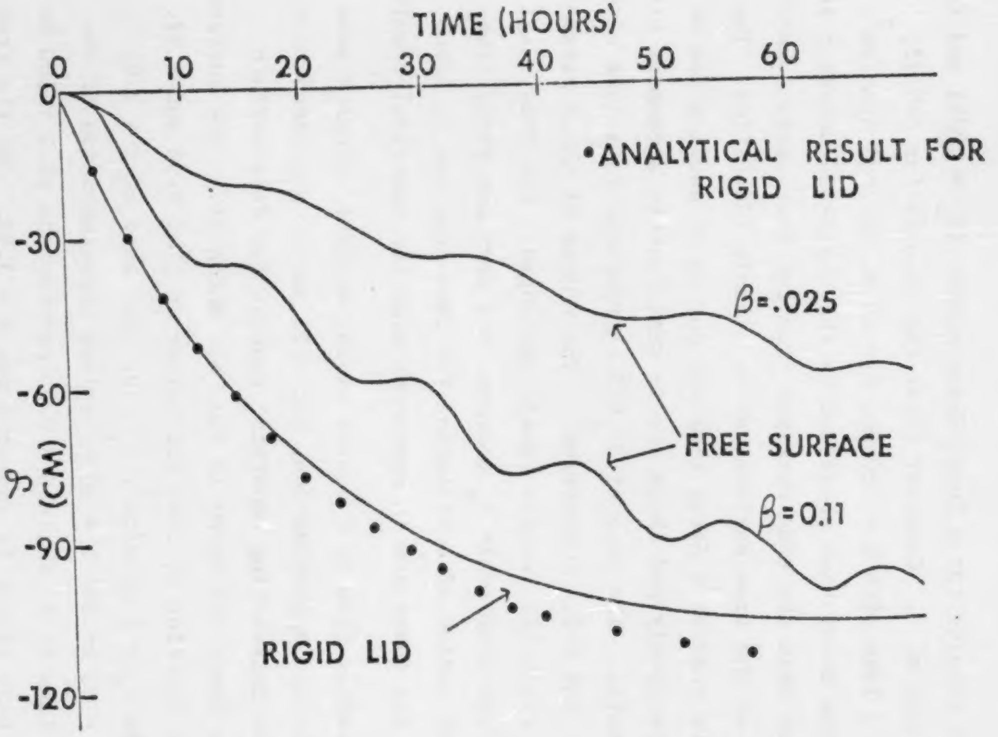

Figure 44. Surface displacement at x = 0 as a function of time for an infinitely long lake with E_v = .025 and τ = 1 dyne/cm^2 for different values of β.

From Figure 43 (for $E_v = 1.0$), it can also be seen that the decay time for this case as predicted by the rigid-lid model is much shorter (by about a factor of 4) than that predicted by the free surface model. However, no oscillations of the free-surface are evident due to the large viscous damping in the lake. The dominant time scale for the free-surface case can be shown to be of the order of $t_1 = 1.6$. In contrast with this, the decay time of the rigid-lid solution obtained from Eq. (70) is 0.42.

Fig. 44 shows the results for a lower Ekman number ($E_v = .025$) and for two different values of β. Consider first the results for $\beta=0.11$, corresponding to a lake with L = 200 km, h = 10 m, and $\tau=1$ dyne/cm^2. It is evident that the decay time predicted by the rigid-lid solution is once again shorter than the time obtained from the free surface model. The oscillations of the free surface can be clearly identified. The analytical results predict a decay time and period of oscillation of 11.5 and 4.5 respectively and these are in satisfactory agreement with the numerical results. The case of $\beta=.025$ corresponds to a lake with L=630 km, h=10 m, and $\tau=0.475$ dynes/cm^2. The choice of these parameters ensures that the rigid-lid results remain unchanged. For this small value of β, the flux time scale t_4 becomes the dominant decay time. The decay time and period of oscillation for this case are 31.4 and 5.7 respectively and these are in agreement with the numerical results.

For the time-dependent flow in a square basin, analytic results were found in the rigid-lid approximation, but will not be discussed here. Representative and interesting numerical results for free-surface flows in a square basin are shown in Fig. 45, which gives the surface displacement as a function of time for values of β of 0.98 and 3.92. The wind stress is $\tau_x = 1$ dyne/cm^2, $\tau_y = 0$. The case of $\beta = 3.92$ corresponds to L = 50 km and h = 10 m, values representative of the Western basin in Lake Erie, while $\beta = 0.98$ corresponds to L = 100 km and h = 10 m. A beat effect is apparent for $\beta = 3.92$. For the free inviscid oscillations in a lake, it can be shown (Lamb 1932, Goldsborough 1931, Corkan and Doodson 1952) that two sets of waves are present,

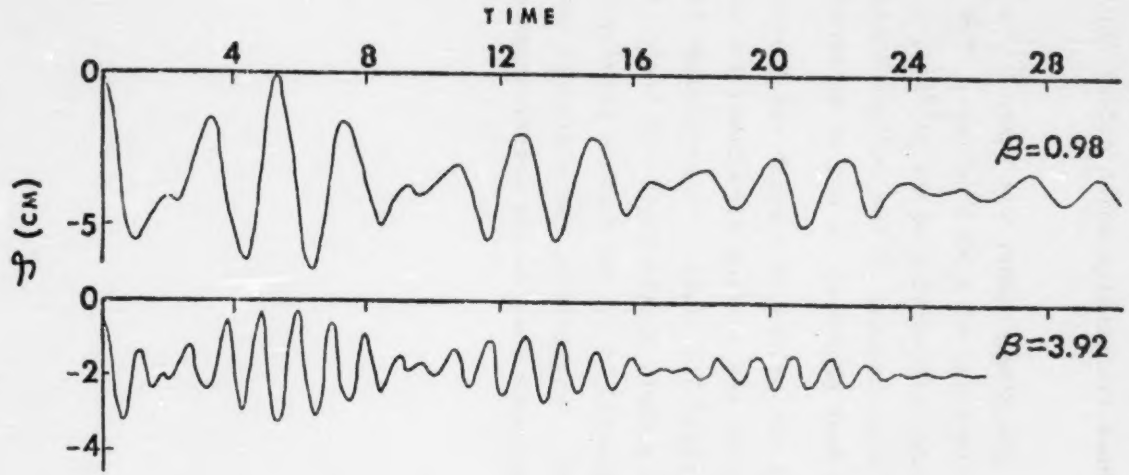

Figure 45. Surface displacement at $x = .05$, $y = .05$ as a function of time for a square basin with $E_v = .025$, $\tau_x = 1$ dyne/cm^2, $\tau_y = 0$.

one rotating in a clockwise direction and the other rotating in a counter-clockwise direction. The frequencies of these waves depend on the depth and horizontal dimensions of the basin. For the present case, the two opposing waves have frequencies which differ by only a small amount.

For these calculations, the Ekman number was taken to be 0.025 with a corresponding eddy diffusivity of $A_v=2.5\ cm^2/sec$. For these same conditions but with an eddy diffusivity of $25\ cm^2/sec$, a value more representative of Lake Erie, damping of the surface displacement is more evident and the beat phenomena is not as apparent.

It can be seen, at least for values of β which are typical of the Great Lakes, that the results for the surface elevation ζ are quite different from those of $\beta\to\infty$, the rigid-lid limit. In particular it can be seen from the analytic results that, in the rigid-lid limit, both the t_2 and t_4 time scales are eliminated, i.e., no surface gravity waves or piling up of water is permitted. Furthermore, the rigid-lid results predict a much faster rate of approach towards the steady-state compared to the free-surface results.

SECTION VIII

TIME-DEPENDENT, VARIABLE DENSITY MODELS

Various models which include the effects of time dependence and variable density have been developed by us and some of them are discussed in this section. The basic assumptions used in all of these models are: (a) The Boussinesq approximation is valid. This assumes that density variations are small and can be neglected except in the gravity term. The coupling between the momentum and energy equations is retained. A consequence of the Boussinesq approximation is that the energy equation reduces to a balance between convection and turbulent diffusion. (b) Eddy coefficients are used to account for the turbulent diffusion effects in both the momentum and energy equations. The horizontal eddy coefficients are assumed constant but the vertical eddy coefficients may vary depending on the temperature gradient and other parameters. (c) The pressure is assumed to vary hydrostatically. In the problems discussed here, variations in the vertical velocity are small enough that the neglected terms in the vertical momentum equation are small compared to the gravity term. A consequence of this approximation is that the order of the system of equations is reduced as is the computational effort required for solution. (d) The rigid-lid approximation is valid, i.e., $w(z=0)=0$. This approximation is used to eliminate surface gravity waves and the small time scales associated with them. The exclusion of these smaller time scales greatly increases the maximum time step possible in the numerical computations. When surface gravity waves are permitted, simple stability theory indicates that the allowable time step is limited by the Courant-Friedrichs-Levy condition, i.e., $\Delta t_f \leq \Delta x/\sqrt{gh}$, where Δx is the grid size, g is the gravitational constant, and h is the depth. With the rigid-lid approximation, the limiting time is no longer Δt_f but is given generally either by $\Delta t_r = \Delta x/u$, where u is a typical fluid velocity, or by $\Delta t_r = \Delta x/u_i$, where u_i is the speed of an internal wave given by $u_i = \sqrt{\Delta\rho g h/\rho}$

and $\Delta\rho$ is the density difference across the wave interface. In either case, Δt_r is generally much greater than Δt_f with the ratio $\Delta t_r/\Delta t_f$ usually being on the order of 10 to 100. In the rigid-lid approximation, only the high frequency surface variations associated with gravity waves are neglected. Internal variations with time are approximately correct while the steady-state results are calculated correctly and are the same as for the free-surface case.

Variable bottom topography is accounted for in the present numerical model by a stretching of the vertical coordinate proportional to the local depth, as was done in Section VII. This transformation ensures that in the shallow areas there is no loss of accuracy in the computations due to lack of vertical resolution, a significant factor in near-shore calculations. However, the transformation is not conformal and the transformed diffusion terms involve cross-derivatives of the spatial coordinates. For simplicity, the further approximation is generally made that the diffusion terms containing derivatives of the depth are negligible with respect to those diffusion terms containing only the depth. This approximation, which greatly simplifies the diffusion terms, is used in meteorological problems when topographic variations are included (Phillips 1957, Smagorinsky, et al 1965).

The main applications of these models have been to river discharges and thermal plumes from power plants flowing into large lakes (Paul adn Lick 1973 a,b, 1974). Representative results of our calculations are shown in Section 8.1 for the particular case of the thermal discharge from the Point Beach power plant on Lake Michigan including realistic geometry, buoyancy effects, wind stresses, and cross flows in the lake. The same basic model has been applied to lake circulation problems and representative results of these calculations are shown in Section 8.2. Further extensions and applications of these models are presently being made.

8.1 RIVER DISCHARGES AND THERMAL PLUMES

A great deal of work has been done recently trying to model the hydrodynamics of a thermal plume from a power plant (see Policastro and Tokar

(1972) for a recent summary and comparison of existing models and field data) and the similar problem of the discharge from a river. Most of these investigations are by means of integral methods or rather simple numerical models. Work similar to ours, i.e., three-dimensional numerical models, has been done by Waldrop and Farmer (1974 a,b). However, their model has a free surface (and therefore small limiting time steps $\Delta t_f \leq \Delta x/\sqrt{gh}$), no vertical stretching of the coordinates, and inaccurate representation of the time behavior (because of approximations made to expedite convergence).

Calculations have been made by us of simple river-lake flows with parameters typical of the Cuyahoga River entering Lake Erie (Paul and Lick 1973 a,b, 1974) and of the discharge from the Point Beach power plant on Lake Michigan. Representative results of these latter calculations are discussed here. Two cases are presented. These are the discharge into a quiescent lake and the discharge into a lake with a cross-flow and a surface wind present. The relevant parameters, based on field measurements taken at the site of the outfall (Frigo, Frye, and Tokar, 1974), are as follows: flow rate, 24.7 m^3/sec; outfall width, 10.8 m; outfall depth, 4.2m; ambient lake temperature, 8.3°C; discharge temperature, 17.5°C; maximum discharge velocity, 0.9 m/sec. The bottom topography is shown in Fig. 46. The outfall extends into the lake and the discharge forms a 60° angle with the shore.

In presenting the basic equations, it is convenient to introduce the following dimensionless variables:

$$u^* = \frac{u}{u_0} \quad , \quad v^* = \frac{v}{u_0} \quad , \quad w^* = \frac{wb_0}{u_0 h_0}$$

$$x^* = \frac{x}{b_0} \quad , \quad y^* = \frac{y}{b_0} \quad , \quad z^* = \frac{z}{h_0} \quad , \quad t^* = \frac{A_H t}{b_0^2}$$

$$p^* = \frac{p\ Re}{\rho g h_0 Fr^2} \quad , \quad \rho^* = \frac{\rho - \rho_0}{\rho_0} \; ; \quad T^* = \frac{T - T_a}{T_a}$$

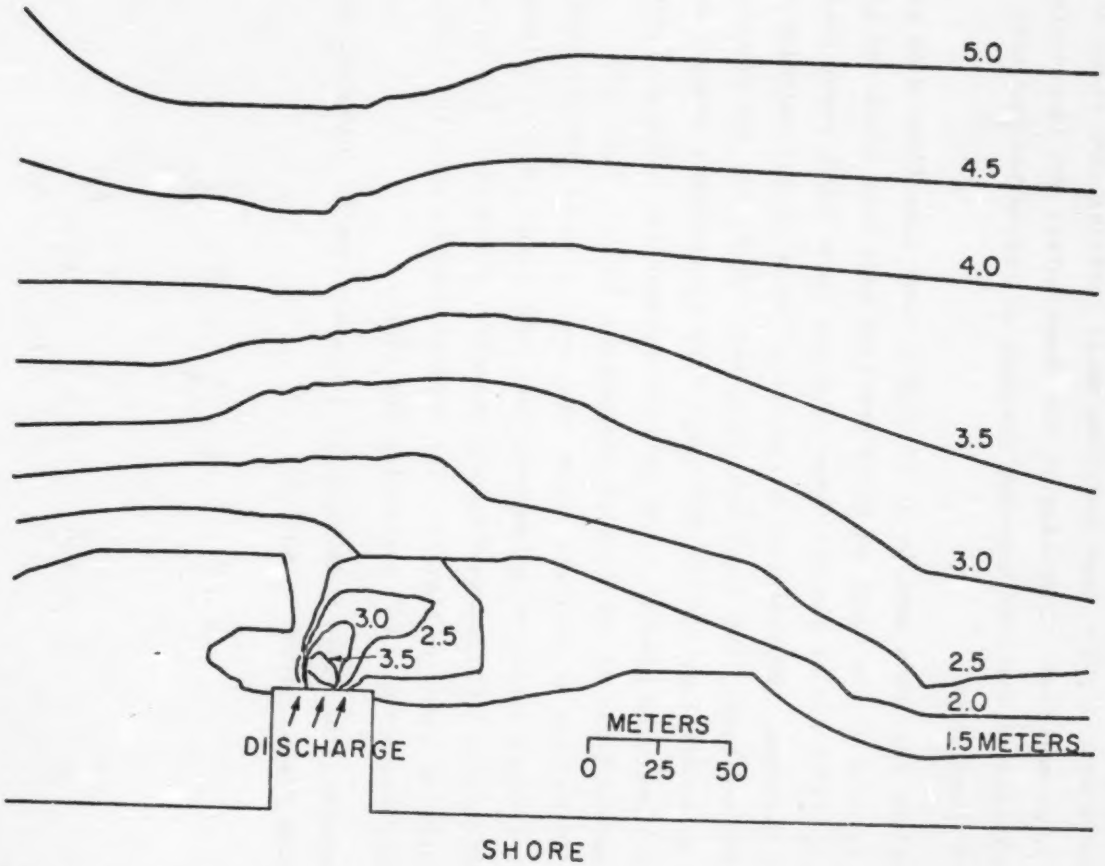
5.0
4.5
4.0
3.5
3.0
2.5
2.0
1.5 METERS
3.0
2.5
3.5
DISCHARGE
METERS
0 25 50
SHORE

Figure 46. Bottom topography for the Point Beach power plant.

$$\gamma = \frac{A_v}{A_H}\ , \quad R_o = \frac{f b_0^{\,2}}{A_H}\ , \quad Re = \frac{u_0 b_0}{A_H}$$

$$Pr = \frac{A_H}{K_H} \qquad \beta = \frac{K_v}{K_H}$$

$$Fr = \frac{u_0}{\sqrt{g h_0}}\ , \quad u_0 = u(x=0,\ y=0,\ z=0)$$

$$\sigma = -\frac{z}{h}\ , \quad \Omega = \frac{1}{h}\left[w - \sigma\left(u\,\frac{\partial h}{\partial x} + v\,\frac{\partial h}{\partial y}\right)\right] = \frac{d\sigma}{dt}$$

where b_0 and h_0 are the width and depth respectively of the discharge, ρ_0 is the density of the lake water and T_a is the air temperature. In the following, only non-dimensional variables will be used unless otherwise explicitly noted. Therefore, in order to simplify the notation, the asterisks on these non-dimensional variables will be dropped. The resulting system of transformed equations is then:

$$\frac{1}{h}\frac{\partial (hu)}{\partial x} + \frac{1}{h}\frac{\partial (hv)}{\partial y} + \frac{\partial \Omega}{\partial \sigma} = 0 \tag{60}$$

$$\frac{\partial u}{\partial t} + Re\left[\frac{1}{h}\frac{\partial (hu^2)}{\partial x} + \frac{1}{h}\frac{\partial (huv)}{\partial y} + \frac{\partial (\Omega u)}{\partial \sigma}\right] - R_o\, v = -\frac{\partial p}{\partial x}$$

$$-\frac{Re}{Fr^2}\left[\frac{\partial}{\partial x}\left(h\int_o^{\sigma} \Delta\rho\, d\sigma\right) - \sigma\,\frac{\partial h}{\partial x}\,\Delta\rho\right] + \frac{1}{h}\left[\frac{\partial}{\partial x}\left(\frac{h\partial u}{\partial x}\right) + \frac{\partial}{\partial y}\left(\frac{h\partial u}{\partial y}\right)\right]$$

$$+\left(\frac{b_0}{h_0}\right)^2 \frac{1}{h^2}\,\frac{\partial}{\partial \sigma}\left(\gamma\,\frac{\partial u}{\partial \sigma}\right) \tag{61}$$

$$\frac{\partial v}{\partial t} + Re\left[\frac{1}{h}\,\frac{\partial (huv)}{\partial x} + \frac{1}{h}\,\frac{\partial (hv^2)}{\partial y} + \frac{\partial (\Omega v)}{\partial \sigma}\right] + R_o\, u = -\,\frac{\partial p}{\partial y}$$

$$-\,\frac{Re}{Fr^2}\left[\frac{\partial}{\partial y}\left(h\int_0^{\sigma}\Delta\rho\, d\sigma\right) - \sigma\,\frac{\partial h}{\partial y}\,\Delta\rho\right] + \frac{1}{h}\left[\frac{\partial}{\partial x}\left(\frac{h\partial v}{\partial x}\right) + \frac{\partial}{\partial y}\left(\frac{h\partial v}{\partial y}\right)\right]$$

$$+\left(\frac{b_0}{h_0}\right)^2\,\frac{1}{h^2}\,\frac{\partial}{\partial \sigma}\left(\gamma\,\frac{\partial v}{\partial \sigma}\right) \qquad (62)$$

$$Pr\,\frac{\partial T}{\partial t} + Pr\,Re\left[\frac{1}{h}\,\frac{\partial (huT)}{\partial x} + \frac{1}{h}\,\frac{\partial (hvT)}{\partial y} + \frac{\partial (\Omega T)}{\partial \sigma}\right] =$$

$$\frac{1}{h}\left[\frac{\partial}{\partial x}\left(h\,\frac{\partial T}{\partial x}\right) + \frac{\partial}{\partial y}\left(\frac{h\partial T}{\partial y}\right)\right] + \left(\frac{b_0}{h_0}\right)^2\,\frac{1}{h^2}\,\frac{\partial}{\partial \sigma}\left(\beta\,\frac{\partial T}{\partial \sigma}\right)$$

$$(63)$$

$$\frac{1}{h}\,\frac{\partial p}{\partial \sigma} = \frac{Re}{Fr^2}\,(1+\rho) \qquad (64)$$

$$\rho = \rho\,(T)$$

The rigid-lid condition is difficult to apply in a numerical solution of the above system of equations. To alleviate this difficulty, an additional equation for the pressure which contains the rigid-lid condition can be derived. This is accomplished by taking the divergence of the vertically integrated horizontal momentum equations and using the vertically integrated continuity and hydrostatic pressure equations. The resulting equation then has the general form

$$\frac{\partial}{\partial x}\left(\frac{h\partial P_s}{\partial x}\right) + \frac{\partial}{\partial y}\left(\frac{h\ P_s}{\partial y}\right) = F(u,v,w,T) \qquad (65)$$

The term P_s is the integration constant resulting from the vertical integration of the hydrostatic pressure equation and is the surface pressure, i.e., the pressure at $z = 0$. This surface pressure can be interpreted as a pressure due to a height of water above or below the surface $z = 0$. In this way, surface displacements (neglecting the transient motion due to gravity waves) can be calculated.

In the above equation, the time derivative of the vertical velocity at the surface appears. The rigid-lid condition implies that this term should be zero. However, due to numerical errors, some non-zero values of this quantity are generally obtained. It can be shown that this indicates that the continuity equation is not satisfied exactly. These errors can accumulate with time if not accounted for properly. A corrective procedure due to Hirt and Harlow (1967) is used to eliminate these accumulative errors.

The boundary conditions are as follows. The inlet velocity and temperature profiles are specified. The inlet velocity profile is a smoothed average of that measured at the outfall while the inlet temperature was taken as the constant value measured. The bottom and the shore are taken as no-slip, impermeable, insulated surfaces. A heat transfer condition proportional to the temperature difference (surface temperature minus equilibrium temperature) and a wind-dependent stress are imposed at the surface. The surface heat transfer condition is calculated from the work of Edinger and Geyer (1965) while the stress acting on the water surface due to the wind is calculated by the formulae developed by Wilson (1960). The equation of state is obtained by a least squares curve fit of density vs. temperature data.

Normal derivative pressure boundary conditions are derived from the appropriate vertically integrated momentum equation. The outer x and y boundaries for the numerical calculations must be taken at some finite distance. The boundary conditions used here are that the normal derivatives of the velocities and the temperature are zero.

The values for the eddy coefficients were chosen as follows. From outfall measurements, the distance is determined that it takes the velocity to decay to one-half of the inlet value. A reasonable value for the horizontal coefficient is picked using previous experience. The ratio of the horizontal to vertical coefficient is then chosen so that it gives the same velocity decay as for the two-dimensional boundary layer jet with bottom friction. The vertical eddy coefficient is taken as dependent on the local vertical temperature gradient (see Eqs. (15) and (16)). The dependence on temperature is the same as that suggested by Munk and Anderson (1948) and, for the present case, is given by

$$A_v = \alpha - \beta \frac{\partial T}{\partial z} \tag{66}$$

where α and β are constants depending on the local conditions. The constant α is equal to the vertical eddy diffusivity A_v under neutral stability conditions and was taken to be 50 cm^2/sec while β was assumed to be 200 cm^3/°C sec.

The equations are put into appropriate finite difference form in both space and time. The horizontal velocities are defined at integral nodal points, the vertical velocity is defined at half-integral nodal points, the temperature is defined at half-integral nodal points in the horizontal and integral nodal points in the vertical, and the surface pressure is defined at half-integral nodal points in the horizontal. In the derivation of the finite difference equations, variables are sometimes required at points where they are not defined. In these circumstances, the undefined quantity is taken as the simple average of the neighboring values.

The finite difference approximations to the equations are derived by integrating the equations over nodal cells. Either the mid-point or trapezoidal integration rule is used to evaluate these integrals. Part of the rationale behind the arrangement of the variables is to provide cells which lend themselves to easy use of the integration rules.

The Euler explicit time scheme, where the time derivative is written as a simple forward time difference and the rest of the equation is evaluated with the previously calculated values, is used exclusively in the present model. The three time level explicit time scheme used by Paul and Lick (1973b) has been found to be not as stable as the Euler explicit scheme. Even the use of the filtering procedure suggested by Bryan (1969) for the three time level scheme did not provide enough stability when inertia dominated flows were calculated.

At each time step, the Poisson equation in the surface pressure has to be solved. For this purpose, the alternating-direction-implicit (ADI) method (Varga 1962, Wachspress 1966) is used and was found to be particularly efficient.

After the temperatures are calculated by the explicit time scheme, they are checked to see if static stability is satisfied, i.e., if the temperatures decrease monotonically downward (assuming that density increases with increasing temperature). When a static instability is encountered, infinite mixing is assumed which just averages the temperature over any unstable region.

The above procedure is carried out until the desired solution is obtained. In both cases discussed below, a variable grid was used with the grid size varying from about 2 m to about 100 m.

For the first case of the discharge into a quiescent basin, representative results of the calculations are shown in Figs. 47 to 49. Figs. 47 and 48 show the horizontal velocities at the surface and at a depth of 2.1 m respectively while Fig. 49 shows the surface temperature distribution. As the flow is discharged from the outfall, it is forced towards the surface by the decreasing depth (seen in Fig. 46) as well as by buoyancy. The large Froude number (Fr = 4.2) indicates that at least initially buoyancy effects are not dominant. The higher surface velocities on the left of the outfall centerline are due to the fact that the depth decreases more rapidly in that region. After about

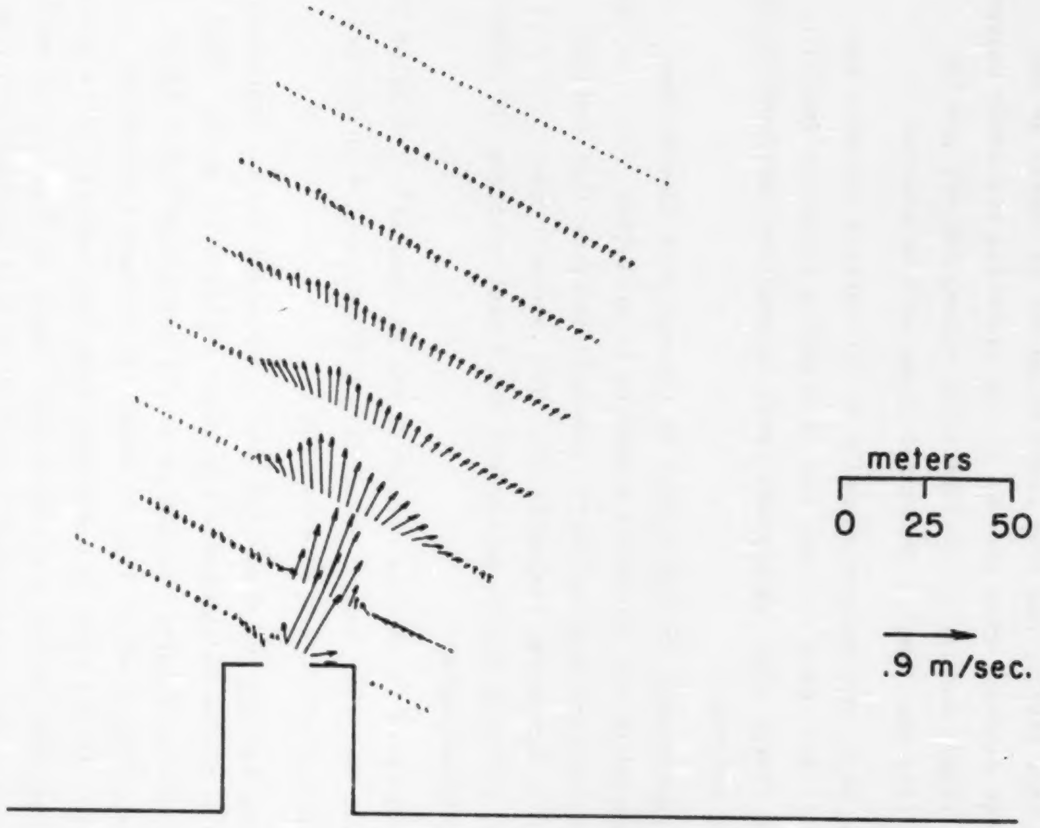

Figure 47. Surface velocities. No wind, no crossflow.

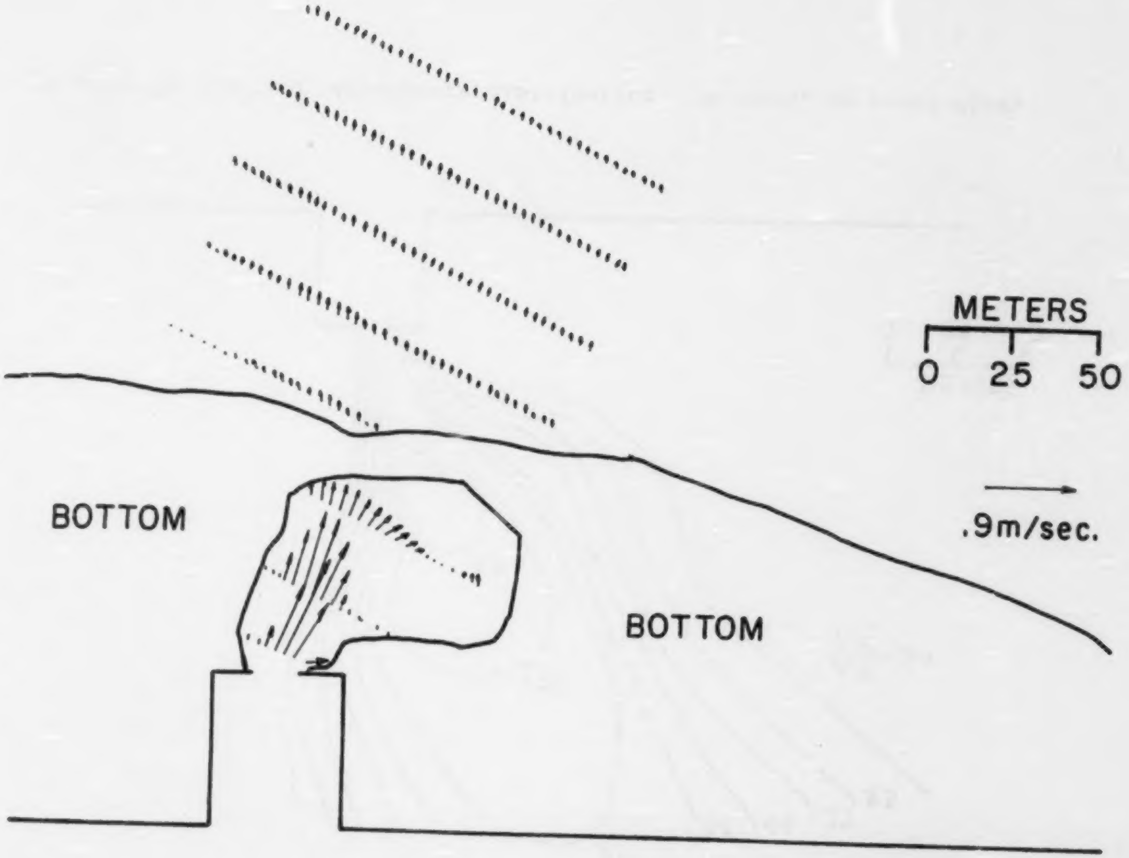
METERS
0
25
50
.9m/sec.
BOTTOM
BOTTOM

Figure 48. Velocities at a depth of 2.1 m. No wind, no crossflow.

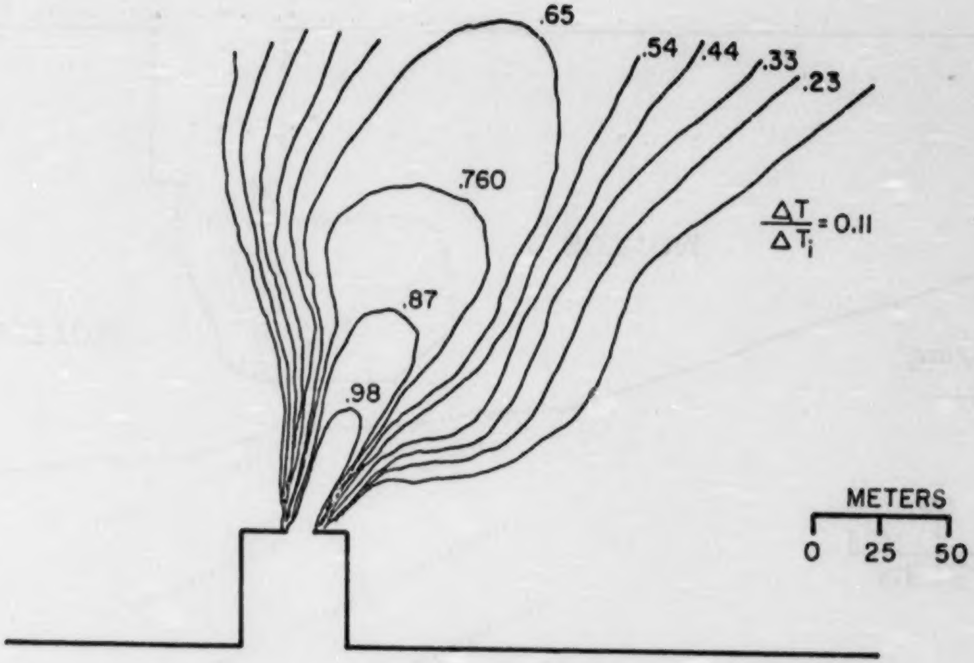

Figure 49. Surface temperature distribution. No wind, no cross-flow.

75 m from the outfall, the depth begins to increase. After this point, the velocities at the 2.1 m depth remain small, with most of the flow occurring near the surface.

A second calculation was made for a case when a cross-flow (current of 9.1 cm/sec) and an off-shore wind (approximately 5 m/sec) were present. Representative results of the calculations are shown in Figs. 50 and 51. Fig. 50 shows the surface velocities and it can be seen that the discharge is swept in the direction of the cross-flow. This is even more evident in Fig. 51 which shows the surface temperatures. It can be seen (compare Fig. 49) that the temperatures are displaced in the direction of the cross-flow and are also displaced towards shore.

A comparison of the calculated results with field observations is shown in Figs. 52 to 55. Figs. 52 and 53 are for the first case above and show the temperature decay along the centerline and the isotherm area for various temperatures. It can be seen that there is good agreement between the predicted results and field observations. Similar results are shown for the second case discussed above in Figs. 54 and 55. Again good agreement between the predicted and observed values is evident. The calculations are presently being extended to include more of the flow field.

Additional field data is available (Frigo, Frye, and Tokar, 1974) from which one can determine more details of the flow field. However, the flow, due to its turbulent nature (see Csanady (1973) for a general description of the turbulent diffusion and nature of plumes), is highly variable both in space and time. Continuous field measurements over a sufficiently long period of time to average out these variations must be made before more general comparisons can be made between our calculations and observations. This has not been done yet. However, the above calculated results, although limited, seem more than adequate at this point.

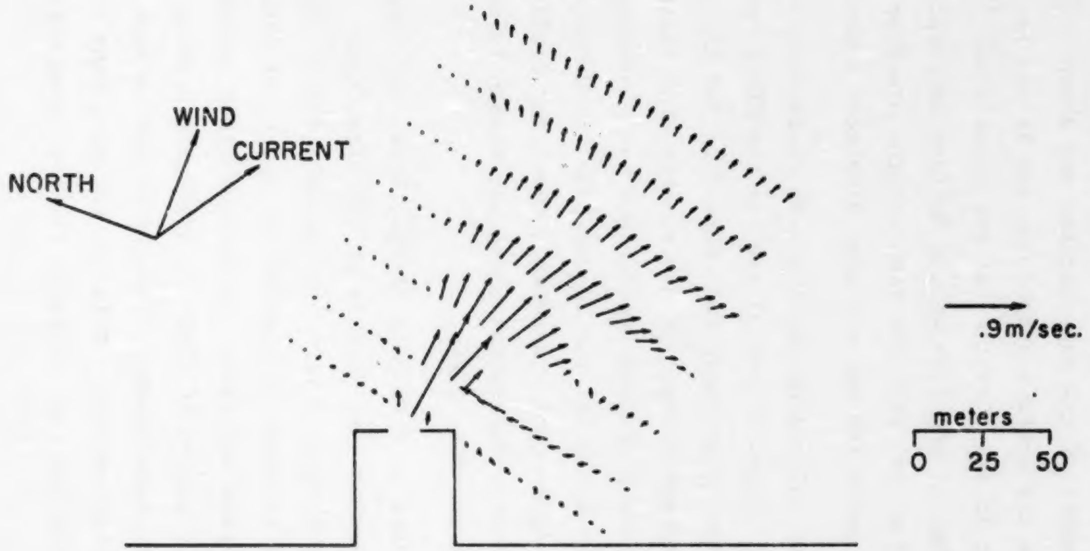

Figure 50. Surface velocities. With wind and cross-flow.

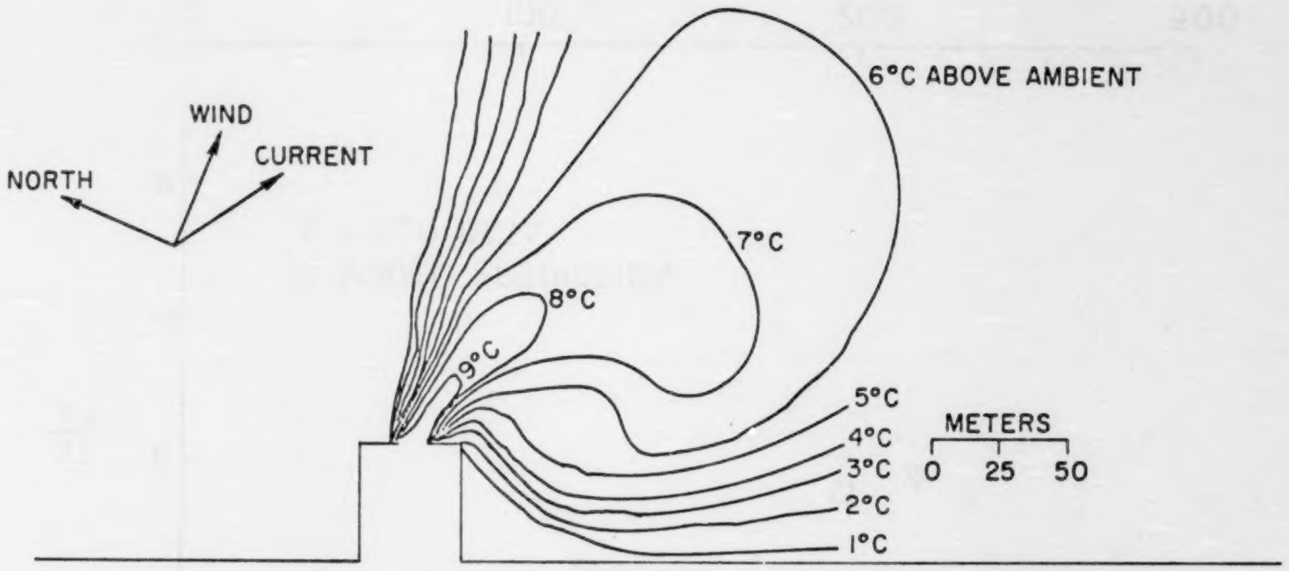

Figure 51. Surface temperatures. With wind and cross-flow.

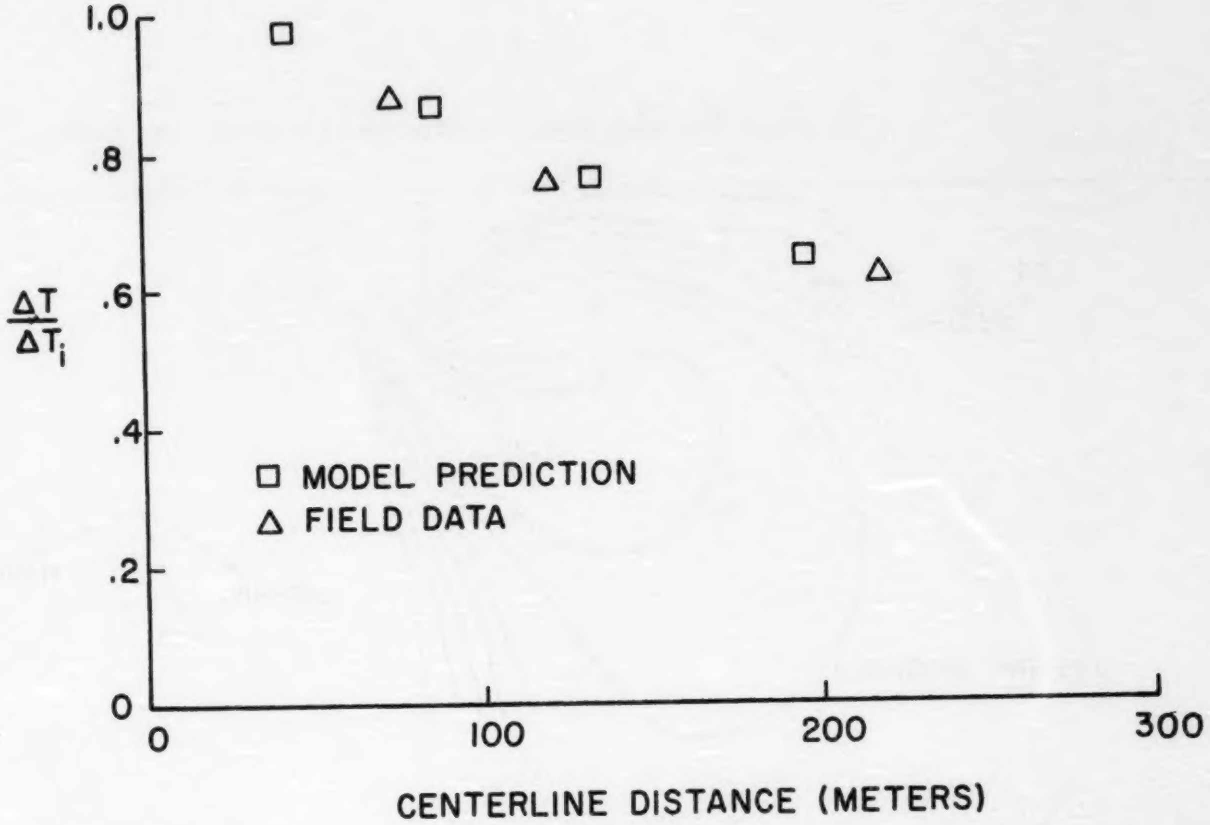

Figure 52. Surface temperature decay along centerline. No wind, no cross-flow.

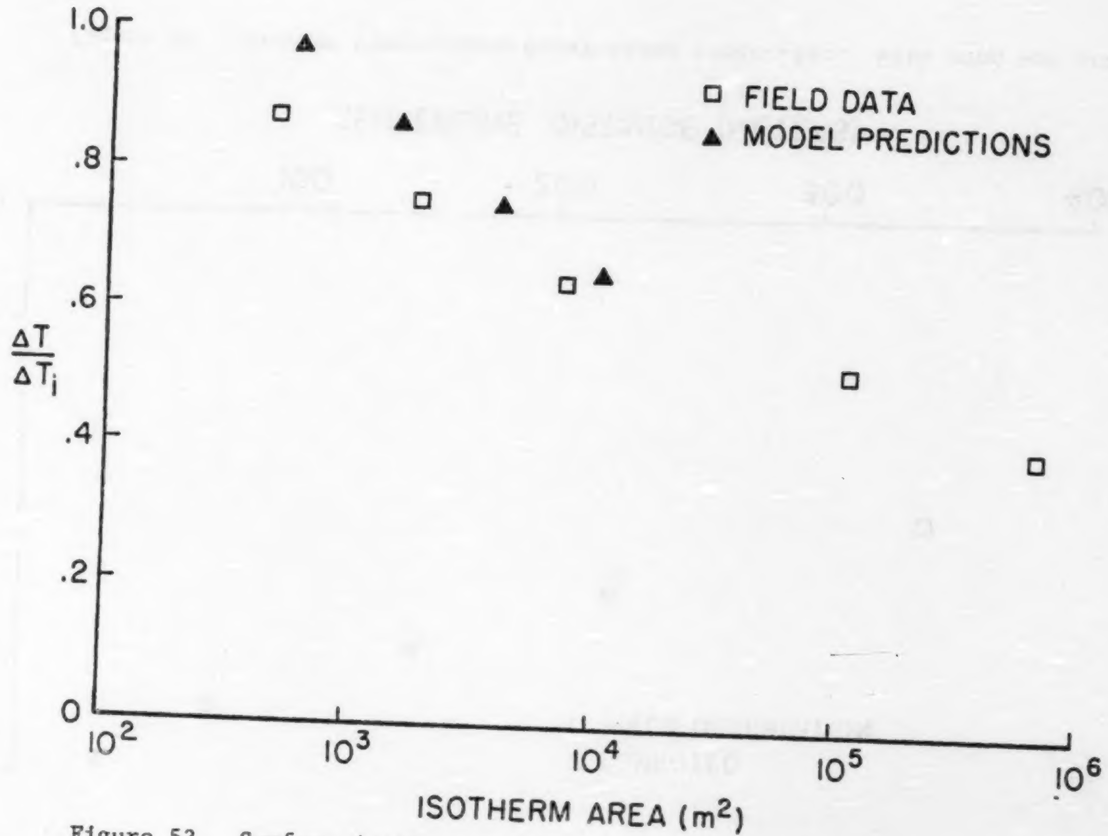

Figure 53. Surface isotherm areas. No wind, no cross-flow.

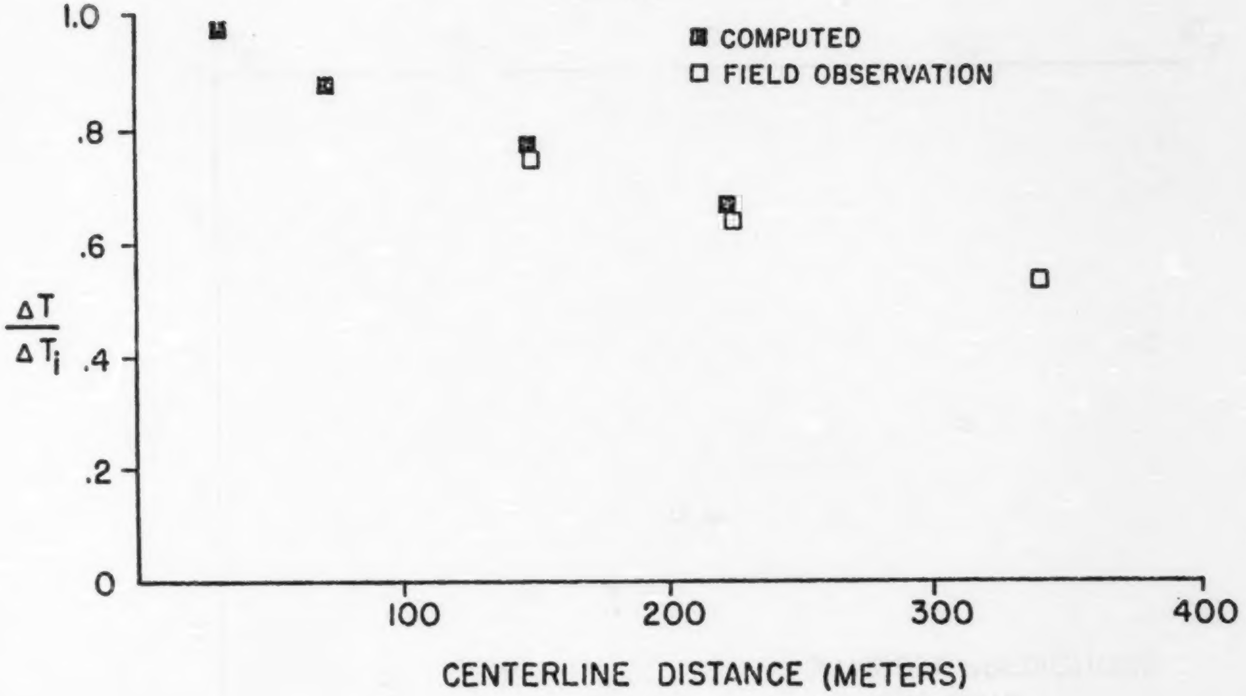

Figure 54. Surface temperature decay along centerline. With wind and cross-flow.

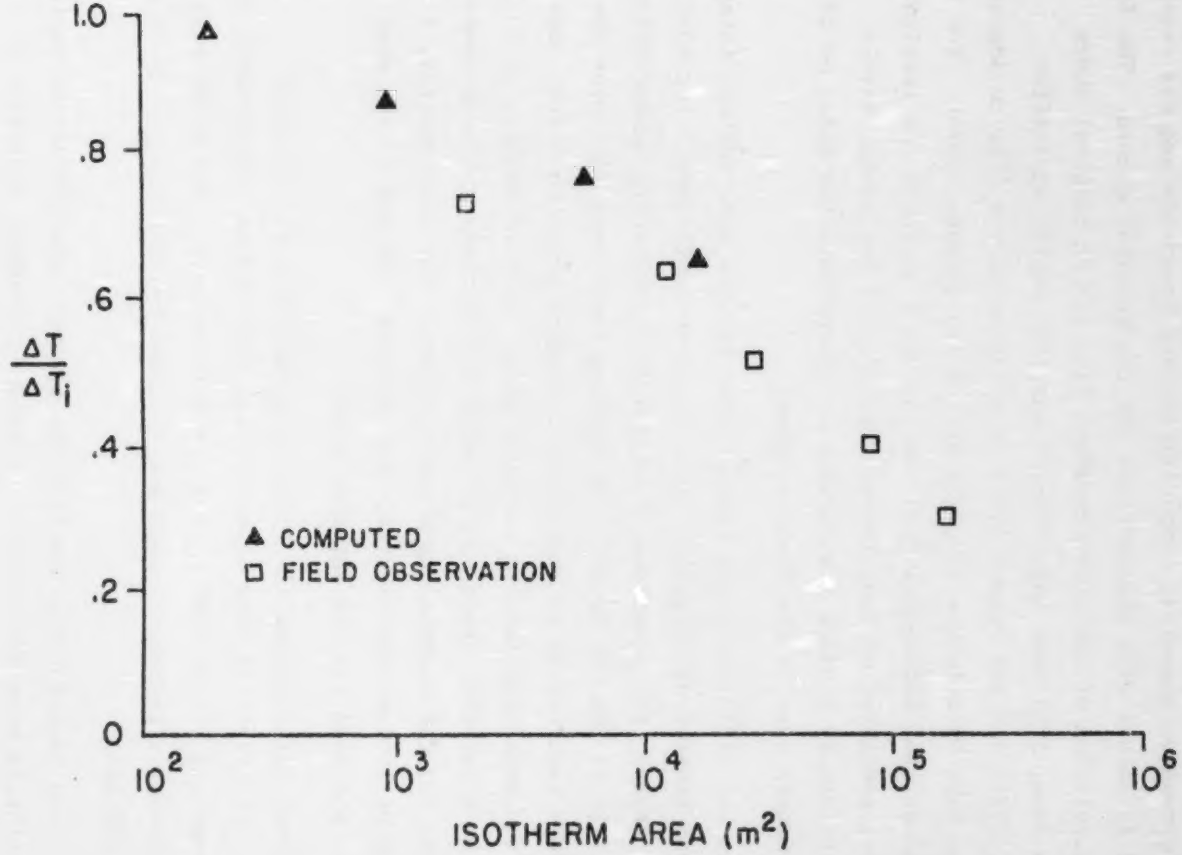

Figure 55. Surface isotherm areas. With wind and cross-flow.

8.2 LAKE CIRCULATION MODELS

The most extensive work on three-dimensional, variable density models for lakes is that due to Simons (1974, 1975), who used a free-surface model. Extensive numerical computations have been made and the results compared in detail with observations for two physical events. The first was a calculation of the time-dependent flow during tropical storm Agnes in June, 1972 when Lake Ontario was only weakly stratified (Simons, 1974) and the second was a calculation of the flow in August, 1972 when Lake Ontario was strongly stratified (Simons, 1975). For these calculations, the horizontal grid spacing was 5 km while the vertical resolution consisted of four layers separated by horizontal levels at 10, 20, and 40 m below the surface to approximate the location of current meters used in the field studies.

For numerical efficiency, the calculations for the external and internal modes were treated differently. This was done as follows. For each of the four layers, the equations of motion were written in conservative form similar to Eqs. 60 to 64. By summing these equations over the four layers (equivalent to vertically averaging over the depth), one obtains the equations for the external mode. In this manner, it is found that much larger time steps can be taken for the internal mode computations than those for the external mode computations. For Lake Ontario, a time step of 100 sec was used for the external mode and a time step of 15 min was used for the internal mode.

In the first calculation, the flow was essentially at constant density. The vertical eddy viscosity was taken to be proportional to the wind stress and of the form $A_v = A_{vo} + K\tau/\rho$ where A_{vo} and K are constants. Good agreement with measurements was obtained by taking $A_{vo} = 25\ \text{cm}^2/\text{sec}$ and K = 100 sec.

In the second calculation, the flow was strongly stratified and variable density effects were appreciable. However, turbulent diffusion of momentum was treated in the same manner as for the first (constant density) calculation with no dependence of the eddy viscosity on temperature gradient. Turbulent diffusion of heat was not included in the calculations but was determined by a comparison of the predicted and observed results. In general, the predictions of surface water levels and currents were quite good. Stratification was shown to have an appreciable effect on the temporal variations of currents. Phenomena such as internal waves were not simulated in a satisfactory manner because of the choice of eddy coefficients. Temperature predictions showed general agreement with large scale averaged observations. However, because of the neglect of turbulent heat transfer, the detailed temperature distribution was not given adequately.

From the differences in the calculated and observed temperature distributions, a lake-wide diffusive heat flux was calculated. From this, an effective eddy conductivity was determined. For this event, effective eddy conductivities were about 1 cm^2/sec. For an earlier period during Storm Agnes, effective eddy conductivities were determined to be approximately 2 to 4 cm^2/sec, indicating the effect of higher wind stresses on producing turbulence.

The rigid-lid model described in Section 8.1 has been used by us to calculate the circulation in simple basins and in Lake Erie, especially in the near-shore including a description of the flow in Cleveland Harbor. More extensive reports on these calculations are forthcoming and they will not be discussed here. Numerical experiments are presently being performed in an attempt to understand the formation and decay of a thermocline in a large lake and the accompanying modification to the dispersion of a contaminant because of this stratification. Some representative results of the flow in the Central Basin of Lake Erie are discussed below.

For this Central Basin calculation, for convenience, the geometry was approximated and the Central Basin was taken to be 60 miles wide and 100 miles long. The actual bottom topography was used except near shore where a constant 6 ft. depth was assumed. The temperature was assumed initially to be 75° F in the top 9.15 m and 55°F in the layer below that. A variable eddy viscosity was assumed of the form described by Eq. (66)

with $\alpha = 16.8$ cm^2/sec and $\beta = 84.0$ cm^3/°C sec. Horizontal mixing was neglected since this is only important in narrow layers (less than 2 km wide) near shore. A constant wind of 5.4 m/sec from the South was assumed.

Representative results of the calculations after approximately 14 hours are shown in Figs. 56 to 59. Fig. 56 shows the horizontal velocities at the surface, a generally uniform flow to the right of the wind and along the longitudinal axis of the lake as might be expected. Variations near shore are due to local topography and depth variations.

Fig. 57 shows the velocities of a vertical and longitudinal plane approximately in the center of the basin. The circulation consists of one large cell in contrast to the two counter-rotating cells obtained when a two-layer model is assumed (see Section 6.4 and Figs. 24 to 28). In the two-layer model, it is assumed that there is no flow between the epilimnion and hypolimnion while in the present case there is considerable flow vertically at all depths. The two-layer model is valid in the limit as the turbulent mixing and convection between the two layers becomes negligible.

This turbulent mixing depends nonlinearly on the temperature gradient. In the present calculation, this temperature gradient is small in the upper half of the basin but much larger in the lower half of the basin as can be seen in Figs. 58 and 59, which show the temperatures in vertical planes through the center of the basin. Table 2 shows the correspondence between the temperatures and the letters designating constant temperature lines in Figs. 58 to 61.

The strong stratification is apparent and reduces vertical mixing appreciably. This stratification depends of course on the initial conditions assumed but is strongly affected by the variable eddy coefficients. For a constant eddy viscosity and conductivity of 16.8 cm^2/sec equal to A_v in neutral stability, the same calculation produces the temperature variations shown in Figs. 60 and 61. The smaller temperature gradients and stronger mixing in this case are evident. Although the temperature variations are strongly affected, the velocities are not greatly modified. Qualitatively, the velocity variations are the same as for variable eddy coefficients. Smaller vertical velocities are

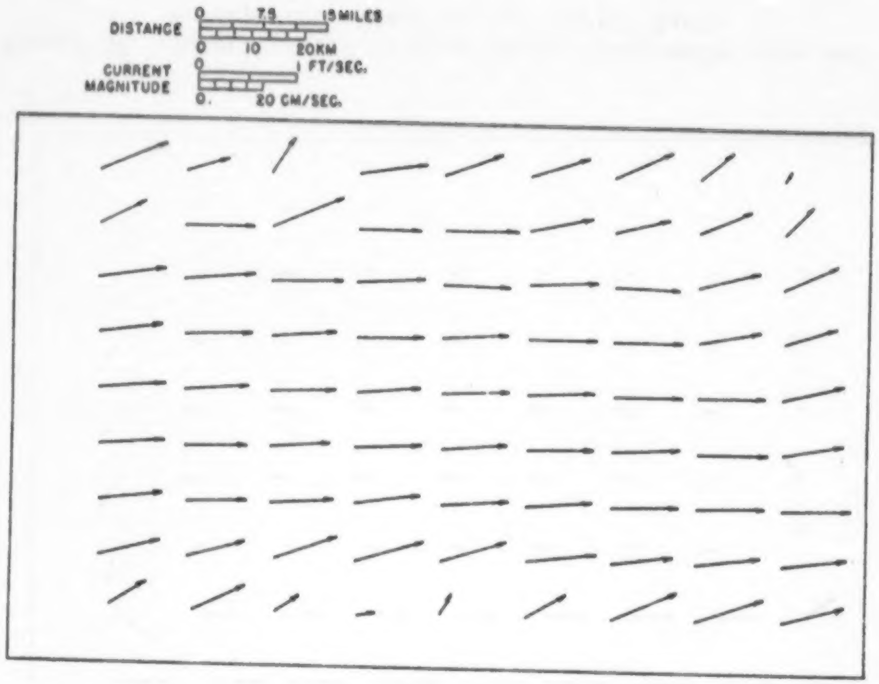

Figure 56. Horizontal velocities at the surface. Wind direction, East. Wind magnitude, 5.2 m/sec. Friction depth, 18.2 m.

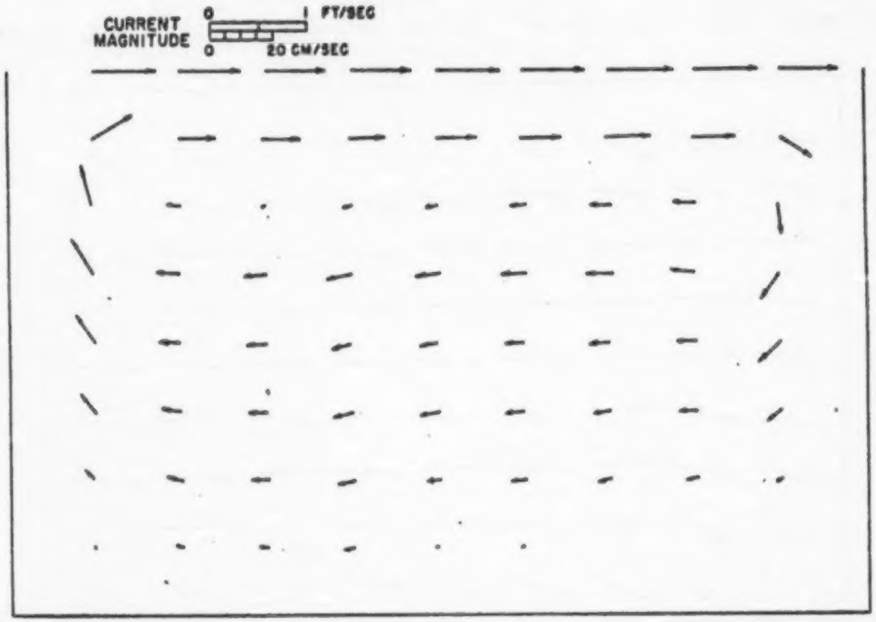

Figure 57. Velocities in vertical plane along major axis and through the center of the Central Basin.

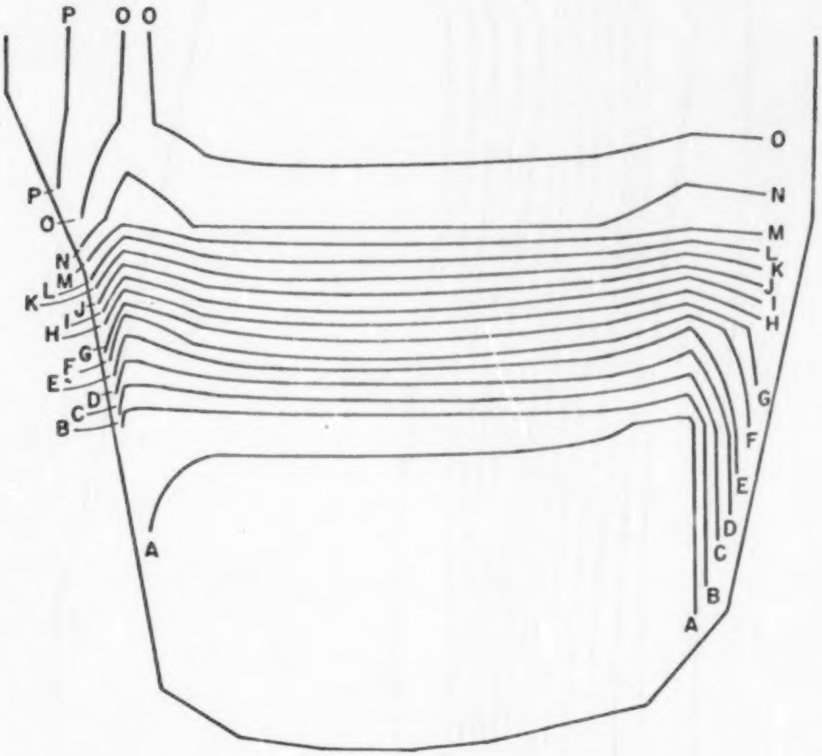

Figure 58. Temperatures in vertical plane along minor axis and through the center of the Central Basin.

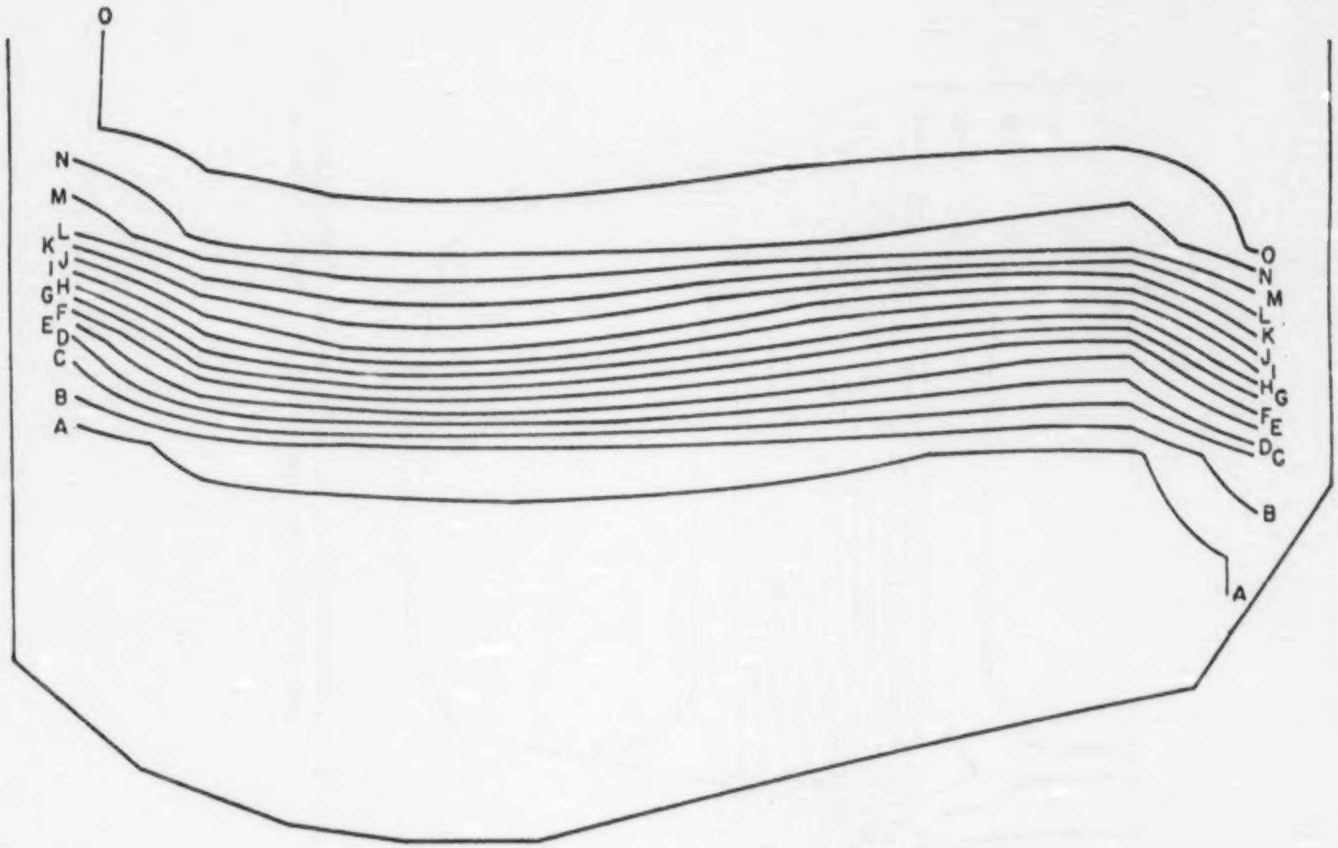

Figure 59. Températures in vertical plane along major axis and through the center of the Central Basin.

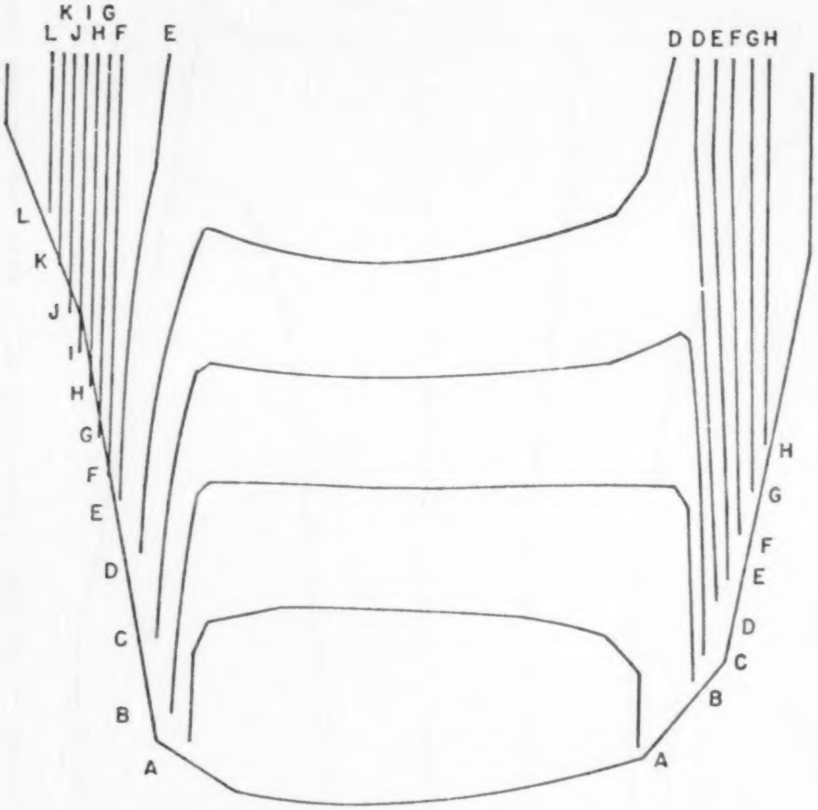

Figure 60. Temperatures in vertical plane along minor axis and through the center of the Central Basin. Constant eddy coefficients.

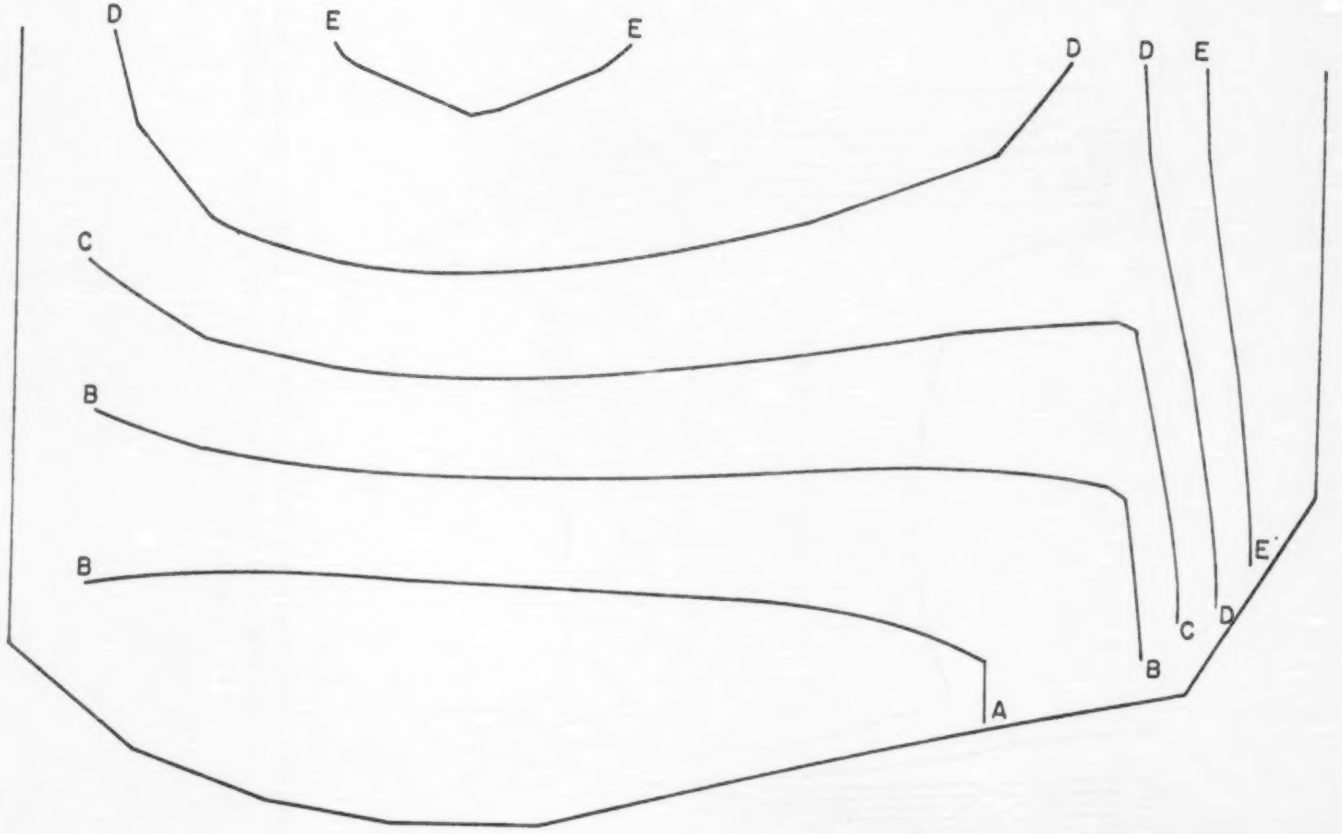

Figure 61. Temperatures in vertical plane along major axis and through the center of the Central Basin. Constant eddy coefficients.

Table 2. LABELS FOR CONSTANT TEMPERATURE LINES

Contour Label	Contour Value °C
A	14.1
B	14.7
C	15.4
D	16.0
E	16.6
F	17.3
G	17.9
H	18.6
I	19.2
J	19.8
K	20.5
L	21.1
M	21.8
N	22.4
O	23.0
P	23.7

noticeable with the maximum decrease on the order of 20%.

Strong horizontal temperature stratification occurs, especially near shore, due to the fact that surface near-shore waters only mix with near-surface waters while off-shore the surface waters mix with cooler bottom waters. The asymmetry in the temperature profiles is due to convection with downwelling occurring on the North shore and upwelling occurring on the South shore.

More work is presently being done to investigate the transition from a well-mixed flow to a strongly stratified flow. In particular, the near-shore areas where upwelling and downwelling are important are being investigated in detail.

SECTION IX

REFERENCES

Allender, J.H. 1975. Numerical Simulation of Circulation and Advection-Diffusion Processes in Saginaw Bay, Michigan. Ph.D. Thesis. University of Michigan, Ann Arbor.

Berdahl, P. 1968. Oceanic Rossby Waves, A Numerical Rigid-Lid Model. Lawrence Radiation Laboratory, University of California, Livermore. Report ITD-4500, UC-34.

Bonham-Carter, G., J.H. Thomas and D. Lockner. 1973. A Numerical Model of Steady Wind-Driven Currents in Lake Ontario and The Rochester Embayment Based on Shallow-Lake Theory. University of Rochester, Rochester, N.Y.

Bonham-Carter, G. and J.H. Thomas. 1973. Numerical Calculation of Steady Wind-Driven Currents in Lake Ontario and the Rochester Embayment. Proc. 16th Conference on Great Lakes Research. International Association for Great Lakes Research. p. 640-662.

Boyce, F.M. 1974. Some Aspects of Great Lakes Physics of Importance to Biological and Chemical Processes. J. Fish. Res. Bd. Can. 31:689-730.

Browning, G., H. Kreiss, and J. Oliger. 1973. Mesh Refinement. Math. Comp. 27:29-39.

Bryan, K. 1969. A Numerical Method for the Study of the World Ocean. Comp. Phys., Vol. 4.

Casey, D.J. 1965. Lake Ontario Environmental Summary. U.S. Environmental Protection Agency, Region V, Chicago.

Chen, J.H. and K. Miyakoda. 1974. A Nested Grid Computation for the Barotropic Free Surface Atmosphere. Mon. Weather Rev. 102:181-190.

Corkan, R.H. and A.T. Doodson. 1952. Free Tidal Oscillations in a Rotating Square Sea. Proceedings Royal Society, Ser. A:215.

Crowley, W.P. 1968. A Global Numerical Ocean Model, Part I. J. Comp. Phys., Vol.3.

Csanady, G.T. 1973. Turbulent Diffusion in the Environment. D. Reidel Publishing Company, Boston.

Donelan, M.A., F.C. Elder and P.F. Hamblin. 1974. Wind Stress from Water Set-up. Proceedings 17th Conference on Great Lakes Research, International Assocation for Great Lakes Research. p. 778-788.

Douglas, J. 1955. On the Numerical Integration of $\partial^2 u/\partial x^2 + \partial^2 u/\partial y^2 = \partial u/\partial t$ by Implicit Methods. J. Soc. Indus. App. Math. 3:42-65.

Edinger, J.E. and J.C. Geyer. 1965. Heat Exchange in the Environment. Edison Electric Institute, New York. Publication No. 65-902.

Freeman, N.G., A.M. Hale and M.B. Danard. 1972. A Modified Sigma Equations Approach to the Numerical Modeling of Great Lakes Hydrodynamics. J. Geophys. Res. 77:1050-1060.

Frigo, A., D. Frye, and J.V. Tokar. 1974. Field Investigations of Heated Discharges from Nuclear Power Plants on Lake Michigan. Argonne National Laboratories, Argonne, Illinois. Report ANL/ES-32.

Galloway, F.M. and S.J. Vakil. 1975. Criteria for the Use of Vertical Averaging in Great Lakes Dispersion Models. Abstract. Proceedings 18th Conference on Great Lakes Research.

Gedney, R.T. and W. Lick. 1970. Numerical Calculations of the Steady State, Wind Driven Currents in Lake Erie. Proceedings 13th Conference on Great Lakes Research, International Association for Great Lakes Research. p. 829-838.

Gedney, R.T. and W. Lick. 1971. Numerical Calculations of the Wind-Driven Currents in Lake Erie. Case Western Reserve University, Cleveland, Ohio.

Gedney, R. and W. Lick. 1972. Wind-Driven Currents in Lake Erie. J. Geophys. Res. 77:2714-2723.

Gedney, R.T., W. Lick, and F.B. Molls. 1972. Effect of Eddy Diffusivity on Wind-Driven Currents in a Two-Layer Stratified Lake. National Aeronautics and Space Administration. TN D-6841.

Gedney, R.T., W. Lick and F.B. Molls. 1973. Effect of Bottom Topography, Eddy Diffusivity, and Wind Variation of Circulation in a Two-Layer Stratified Lake. National Aeronautics and Space Administration, TND-7235.

Gedney, R.T., W. Lick, and F.B. Molls. 1973. A Simplified Stratified Lake Model for Determining Effects of Wind Variation and Eddy Diffusivity. Proceedings 16th Conference on Great Lakes Research. International Association for Great Lakes Research. p. 710-722.

Goldsborough, G.R. 1931. The Tidal Oscillations in Rectangular Basins. Proceedings Royal Society, Ser. A:132.

Greenspan, H.P. 1968. The Theory of Rotating Fluids. Cambridge University Press, London.

Hamblin, P.F. 1969. Hydraulic and Wind-Induced Circulation in a Model of Great Lake. Proceedings 12th Conference on Great Lake Research. International Association for Great Lakes Research.

Hamblin, P.F. 1971. An Investigation of Horizontal Diffusion in Lake Ontario. Proceedings 14th Conference Great Lakes Research. International Association for Great Lakes Research. p. 570-577.

Haq, A. and W. Lick. 1975. On the Time-Dependent Flow in a Lake. J. Geophys. Res. 80:431-437.

Haq, A. W. Lick, and Y.P. Sheng. 1975. The Time-Dependent Flow in Large Lakes with Application to Lake Erie. Case Western Reserve University, Cleveland, Ohio.

Henry, A.J. 1902. Wind Velocity and Fluctuations of Water Level of Lake Erie. Bulletin. U.S. Weather Bureau,

Hirt, C.W. and F.H. Harlow. 1967. A General Corrective Procedure for the Numerical Solution of Initial-Value Problems. J. Comp. Phys., Vol. 2.

Janowitz, G.S. 1970. The Coastal Boundary Layers of a Lake when Horizontal and Vertical Ekman Numbers are of Different Orders of Magnitude. Tellus, Vol. 22.

Janowitz, G.S. 1972. The Effect of Finite Vertical Ekman Number on the Coastal Boundary Layers of a Lake. Tellus, Vol. 24.

Koh, R.C.Y. and Y.P. Chang. 1973. Mathematical Model for Barged Ocean Disposal of Wastes. U.S. Environmental Protection Agency, Corvallis, Oregon. EPA-660/2-73-029.

Lamb, H. 1932. Hydrodynamics. Dover Publications.

Matsuno, T. 1966. Numerical Integrations of the Primitive Equations by a Simulated Backward Difference Method. J. Met. Soc. (Japan) 2:76-84.

Munk, W. H. and E.P. Anderson. 1948. Notes on the Theory of the Thermocline. J. Mar. Res. 1:276-295.

Okubo, A. 1971. Oceanic Diffusion Diagrams. Deep-Sea Res. 18:789-802.

Olsen, F.C.W. 1950. The Currents of Western Lake Erie. Ph.D. Thesis, Ohio State University, Columbus.

Oort, A.H. and A. Taylon. 1969. On the Kinetic Energy Spectrum Near the Ground. Mon. Weather Rev. 97:523-636.

Orlob, C.T. 1959. Eddy Diffusion in Homogeneous Turbulence. J. Hyd. Div. Proceedings ASCE, HY9:75-101.

Paskausky, D.F. 1971. Weather Circulation in Lake Ontario. Proceedings 14th Conference on Great Lakes Research. International Association for Great Lakes Research. p. 593-606.

Paskausky, D.F. 1973. Two Dimensional Prediction of Storm Surge on Lake Erie, Appendix 2g. In: Preliminary Safety Analysis Report, Perry Nuclear Power Plant. Cleveland Electric Illuminating Company, Perry, Ohio.

Paul, J.F. and J. Prahl. 1971. Investigations of a Constant Temperature Rectangular Jet. Case Western Reserve University, Cleveland, Ohio.

Paul, J.F. and W. Lick. 1973a. A Numerical Model for a Three-Dimensional, Variable-Density Jet. Proceedings 16th Conference on Great Lakes Research. International Association Great Lakes Research. p. 818-830.

Paul, J.F. and W. Lick. 1973b. A Numerical Model for a Three-Dimensional, Variable-Density Jet. Technical Report. Case Western Reserve University, Cleveland, Ohio.

Paul, J.F. and W. Lick. 1974. A Numerical Model of Thermal Plumes and River Discharges. Proceedings 17th Conference on Great Lakes Research. International Association for Great Lakes Research. p. 445-455.

Paul, J.F. 1975. A Note on the Vertically-Averaged Equations of Motion. Case Western Reserve University, Cleveland, Ohio.

Peaceman, D.W. and H.H. Rachford. 1955. The Numerical Solution of Parabolic and Elliptic Differential Equations. J. Soc. Ind. App. Math. 3:28-41.

Phillips, N.A. 1957. A Coordinate System Having Some Special Advantages for Numerical Forcasting. J. Meteor., Vol. 14.

Platzman, G.W. 1963. The Dynamic Prediction of Wind Tides on Lake Erie. Meteor. Mono. 4:26.

Policastro, A.J., and J.V. Tokar. 1972. Heated-Effluent Dispersion in Large Lakes: State-of-the-Art of Analytical Modeling, Part I. Argonne National Laboratory, Argonne, Illinois. Report ANL/ES-11.

Proudman, J. 1953. Dynamical Oceanography. John Wiley and Sons, Inc.

Rao, D.B. and T.S. Murty. 1970. Calculations of the Steady State Wind-Driven Circulation in Lake Ontario. Arch. Meteor. Geophys. Biochim. A19:195-210.

Reid, R.O. and B.R. Bodine. 1968. Numerical Model for Storm Surges in Galveston Bay. J. Waterways Harbors. (Div. ASCE) 94:33-57.

Richtmyer, R.D. and K.W. Morton. 1967. Difference Methods for Initial-Value Problems. Interscience Publishers.

Roache, P.J. 1972. Computational Fluid Dynamics. Hermosa Publishers, Albuquerque.

Sheng, Y.P. and W. Lick. 1973. Wind-Driven Currents in a Partially Ice Covered Lake. Proceedings 16th Conference on Great Lakes Research. International Association for Great Lakes Research. p. 1001-1008.

Sheng, Y.P. and W. Lick. 1975. The Wind-Driven Currents and Contaminant Dispersion in the Near-Shore of Large Lakes. Case Western Reserve University, Cleveland.

Simons, T.J. 1971. Development of Numerical Models of Lake Ontario. Proceedings 14th Conference on Great Lakes Research. International Association for Great Lakes Research. p. 655-669.

Simons, T.J. 1972. Development of Numerical Models of Lake Ontario. Proceedings 15th Conference on Great Lakes Reserach. International Association of Great Lakes Reserach. p. 655-672.

Simons, T.J. 1974. Verification of Numerical Models of Lake Ontario, Part I: Circulation in Spring, Early Summer. J. Phys. Ocean. 4:507-523.

Simons, T.J. 1975. Verification of Numerical Models of Lake Ontario, Part II: Stratified Circulations and Temperature Changes. J. Phys. Ocean. 5:98-110.

Simons, T.J. 1976. Continuous Dynamical Calculations of Water Transports in Lake Erie in 1970. J. Fish. Res. Bd. Can. To be published January 1976.

Smagorinsky, J., G. Manabe and J.L. Holloway. 1965. Numerical Results from a Nine-Level General Circulation Model of the Atmosphere. Mon. Weather Rev. 93:1965.

Smith, G.D. 1965. Numerical Solution of Partial Differential Equations. Oxford University Press.

Stommel, H. 1949. Horizontal Diffusion Due to Oceanic Turbulence. J. Mar. Res. 8:199-225.

Sundaram, T.R. and R.G. Rehm. 1970. Formation and Maintenance of Thermoclines in Stratified Lakes Including the Effects of Power-Plant Thermal Discharges. AIAA Paper No. 70-238.

Varga, R.S. 1962. Matrix Iterative Analysis. Prentice-Hall, Inc.

Wachspress, E.L. 1966. Iterative Solution of Elliptic Systems. Prenctice-Hall Inc.

Waldrop, W.R. and R.C. Farmer. 1974a. Three-Dimensional Computation of Buoyant Plumes. J. Geophys. Res. 79:1269-1276.

Waldrop, W.R. and R.C. Farmer. 1974b. Thermal Plumes from Industrial Cooling Water. Proc. 1974 Heat Transfer and Fluid Mechanics Institute. Stanford University Press, Stanford.

Welander, P. 1957. Wind Action on a Shallow Sea. Tellus 9:47-52.

Welander, P. 1961. Numerical Prediction of Storm Surges. Advances in Geophysics, Vol. 8. Academic Press, New York.

Welander, P. 1968. Wind Driven Circulation in One and Two Layer Oceans of Variable Depth. Tellus 20:1.

Wilson, B.W. 1960. Note on Surface Wind Stress Over Water on Low and High Speeds. J. Geophys. Res. 65:3377-3382.

Witten, A.J. and J.H. Thomas. 1975. Calculation of Steady Wind-Driven Currents in Lake Ontario with a Spatially Variable Eddy Viscosity. Abstracts. Proceedings 19th Conference on Great Lakes Research, International Association for Great Lakes Research.

Wurtell, M.G., J. Paegle and A. Sielecki. 1971. The Use of Open Boundary Conditions with the Storm-Surge Equations. Mon. Weather Rev. 99:537-544.

SECTION X

PUBLICATIONS

1. Gedney, R. and W. Lick. 1970. Numerical Calculations of the Steady-State, Wind Driven Currents in Lake Erie. Proceedings 13th Conference on Great Lakes Reserach. International Association for Great Lakes Research. p. 829-838.

2. Gedney, R.T. and W. Lick. 1971. Numerical Calculations of the Wind-Driven Currents in Lake Erie. Case Western Reserve University, Cleveland.

3. Gedney, R.T. and W. Lick. 1972. Wind-Driven Currents in Lake Erie. J. Geophys. Res. 77:2714-2723.

4. Gedney, R.T., W. Lick, and F.B. Molls. 1972. Effect of Eddy Diffusivity on Wind-Driven Currents in a Two-Layer Stratified Lake. National Aeronautics and Space Administration, TN-D 6841.

5. Gedney, R.T., W. Lick and F.B. Molls. 1973a. Effect of Bottom Topography, Eddy Diffusivity, and Wind Variation on Circulation in a Two-Layer Stratified Lake. National Aeronautics and Space Administration. TND-7235.

6. Gedney, R.T., W. Lick and F.B. Molls. 1973b. A Simplified Stratified Lake Model for Determining Effects of Wind Variation and Eddy Diffusivity. Proceedings 16th Conference on Great Lakes Research. International Association for Great Lakes Research. p. 710-722.

7. Haq, A. and W. Lick. 1975. On the Time-Dependent Flow in a Lake. J. Geophys. Res. 80:431-437.

8. Haq, A., W. Lick, and Y.P. Sheng. 1975. The Time-Dependent Flow in Large Lakes with Application to Lake Erie. Case Western Reserve University, Cleveland.

9. Kuhlman, J.M. 1974. Laboratory Modeling of Surface Thermal Plumes. Ph.D. Thesis, Case Western Reserve University, Cleveland.

10. Lick, W. 1976. Numerical Modeling of Lake Currents. Ann. Rev. Earth and Planetary Sci. Vol. 4. To be published.

11. Lick, W., J. Paul, and Y.P. Sheng. 1975. The Dispersion of Contaminants in the Near-Shore Region. In: Mathematical Modeling of Biochemical Processes in Aquatic Ecosystems (R. Canale, Editor). Ann Arbor Science, Ann Arbor.

12. Paul, J.F. and J. Prahl. 1971. Investigations of a Constant Temperature Rectangular Jet. Case Western Reserve University, Cleveland.

13. Paul, J.F. and W. Lick. 1973a. A Numerical Model for a Three-Dimensional, Variable-Density Jet. Proceedings 16th Conference on Great Lakes Research. International Association for Great Lakes Research. p. 818-830.

14. Paul, J.F. and W. Lick. 1973b. A Numerical Model for a Three-Dimensional, Variable-Density Jet. Case Western Reserve University, Cleveland. Technical Report.

15. Paul, J.F. and W. Lick. 1974. A Numerical Model for Thermal Plumes and River Discharges. Proceedings 17th Conference on Great Lakes Research. International Association for Great Lakes Research. p. 445-455.

16. Paul, J.F. 1975. A Note on the Vertically-Averaged Equations of Motion. Case Western Reserve University, Cleveland.

17. Sheng, Y.P. and W. Lick. 1973. Wind-Driven Currents in a Partially Ice Covered Lake. Proceedings 16th Conference on Great Lakes Research. International Association for Great Lakes Research. p. 1001-1008.

18. Sheng, Y.P. and W. Lick. 1975. The Wind-Driven Currents and Contaminant Dispersion in the Near-Shore of Large Lakes. Case Western Reserve University, Cleveland.